$^{40}Ar/^{39}Ar$ Dating of the Labrador Sea Volcanics and their Relation to Sea-Floor Spreading

by

Richard J. E. Parrott

Submitted in partial fulfillment of the requirements for the degree of Master of Science at Dalhousie University.

February, 1976.

Examining Committee

DALHOUSIE UNIVERSITY

Date February, 1976

Author Richard J. E. Parrott

Title $^{40}Ar/^{39}Ar$ Dating of the Labrador Sea Volcanics and their Relation to Sea-Floor Spreading

Department or School Geology

Degree M. Sc. Convocation Spring Year 1976

Permission is herewith granted to Dalhousie University to circulate and to have copied for non-commercial purposes, at its discretion, the above title upon the request of individuals or institutions.

Signature of Author

Table of Contents

Page

List of Figures

List of Tables

Page

Abstract

Stepwise degassing experiments were performed on eight whole-rock basalt samples from Svartenhuk Peninsula (West Greenland), from Cape Dyer (Baffin Island), and from D.S.D.P. site 112 just off mid-Labrador Sea ridge structure. In addition, experiments were performed on two whole-rock trachytes from Svartenhuk Peninsula (West Greenland) and on three whole-rock lamprophyres from Ubekendt Ejland (West Greenland).

Gas released throughout the heating range was often characterized by either negative or anomalously high apparent ages. Computation of isochron ages indicated that these effects were due to the presence of initial gas, that is, argon with $^{40}Ar/^{36}Ar$ ratios which differ from the atmospheric value. The best data from Svartenhuk Peninsula yields ages of 57.9± 2.6 my, 58.1 ± 3.8 my and 59.8 ± 3.8 my (2σ errors). Furthermore, the remaining basalts from Svartenhuk Peninsula, Baffin Island and the mid-Labrador Sea ridge yield ages which are indistinguishable from the above (at the 95% confidence limit). However, the best ages of the lamprophyres from Ubekendt Ejland (i.e. 30.6 ± 6.4 my and 32.8 ± 6.8 my, 2σ errors) are significantly different. These rocks were originally thought to have only shortly postdated the other volcanics.

These new results, along with existing data for other areas in the Brito-Arctic volcanic province indicate that volcanism in all regions occurred contemporaneously and was of relatively short duration (say from 60-58 my ago). The present data have in addition confirmed the

relationship of the Davis Strait volcanics to the spreading history of the Labrador Sea. Spreading about the mid-Labrador Sea ridge started ∿ 80 my ago and ceased about 60 my ago. At this time there was extensive volcanism in the Brito-Arctic province and spreading in the Labrador Sea recommenced, this time about the Ran Ridge. This second and final phase lasted until 47 my ago.

Symbols and Abbreviations

*	radiogenic
Atm	atmospheric
I	initial
NCa	neutron induced from calcium
NK	neutron induced from potassium
RR	removed by neutron reaction
ε	energy
Δt, ΔT	duration of irradiation
$\phi(\varepsilon)$	neutron flux at energy ε
$\sigma(\varepsilon)$	neutron capture cross-section at energy ε
t	time since irradiation
t_s	age of standard
t_u	age of unknown
my	million years
$J =$	$\dfrac{e^{\lambda t_s} - 1}{{}^{40}Ar^*/{}^{39}Ar^{NK}}$
λ_β	probability that ^{40}K will decay into $^{40}Ca^*$ in unit time
λ_e	probability that ^{40}K will decay into $^{40}Ar^*$ in unit time
λ_e'	probability that ^{40}K will decay into $^{40}Ar^*$ in unit time (no γ emission)
λ	total decay constant for ^{40}K
λ'	total decay constant for ^{37}Ar
$A =$	$^{40}Ar/^{39}Ar$
$B =$	$^{36}Ar/^{39}Ar$

D = $^{37}Ar^{C}/^{39}Ar$

c (superscript) corrected for decay

F = $^{40}Ar^{*}/^{39}Ar^{NK}$

a = $^{39}Ar^{NCa}/^{37}Ar^{NCa}$

b = $^{36}Ar^{NCa}/^{37}Ar^{NCa}$

c = $^{40}Ar^{NK}/^{39}Ar^{NK}$

x = $^{40}Ar^{Atm}/^{36}Ar^{Atm}$ = 295.5

σ_F^2 = variance of F

σ_F = one standard deviation of F

ΔF = estimated error in F

Acknowledgements

Thanks are due to Dr. D. B. Clarke and to the National Science Foundation from whom samples were obtained. I would also like to thank W. Clay for technical assistance and computing assistance and M. A. Annand for the typing of this thesis. More people were instrumental in the completion of this thesis. Besides discussions with some of the people mentioned previously, invaluable discussions were made with Dr. P. H. Reynolds and V. Stukas without whom this work would probably not have been completed. Finally, I would like to thank my wife who put up with me while I completed my research. Financial support was provided by a Dalhousie Graduate Student Award.

Chapter I: Volcanic Regimes

The Labrador Sea and Baffin Bay

The Labrador Sea and Baffin Bay have been of interest to scientists for more than a decade, but with the upcoming energy shortage they have received additional study as potential sources of hydrocarbons. Baffin Bay is located north of the Arctic circle, bordered by Greenland to the east, Baffin Island to the west, Ellesmere Island to the north and Davis Strait to the south (see Figures 1.1 a,b). The Labrador Sea lies to the south of Baffin Bay, bordered by Davis Strait to the north, Labrador to the west and the Atlantic Ocean to the south and east (see Figures 1.1 b,c).

The mainland of Canada and Greenland is mostly Precambrian in age with only sparse remains of Phanerozoic rocks; among these are extensive volcanics which occur on both sides of Davis Strait. It is these volcanics which constitute the main portion of this study. By determining the age relationships of these rocks it is intended to clarify the timing of the spreading history of the Labrador Sea and Baffin Bay. A discussion of the volcanics themselves and their relationship to spreading follows.

Volcanics of Davis Strait

(a) Baffin Island: Flat-lying basalts occur along a 90 km. coastal strip between Cape Dyer and Cape Searle on eastern Baffin Island (Figure 1.2). All outcrops lie within 10 km. of a straight-line drawn

Figure 1.1.a,b,c. Index map for the Labrador Sea, Baffin Bay area also showing the location of DSDP site 112.

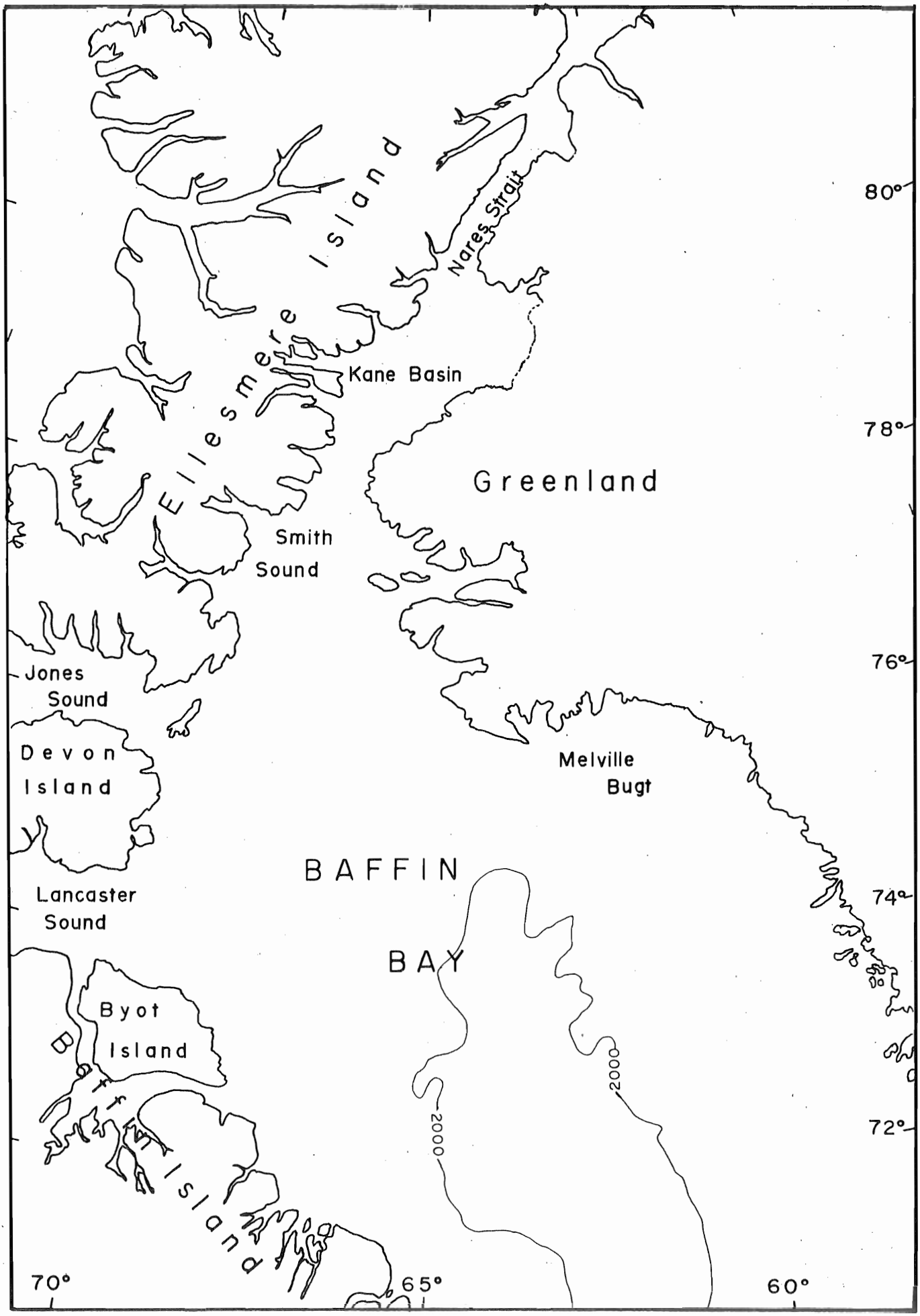
Ellesmere Island
Nares Strait
Kane Basin
Greenland
Smith Sound
Jones Sound
Devon Island
Melville Bugt
BAFFIN BAY
Lancaster Sound
Byot Island
Bathurst Island
2000
2000
80°
78°
76°
74°
72°
70°
65°
60°

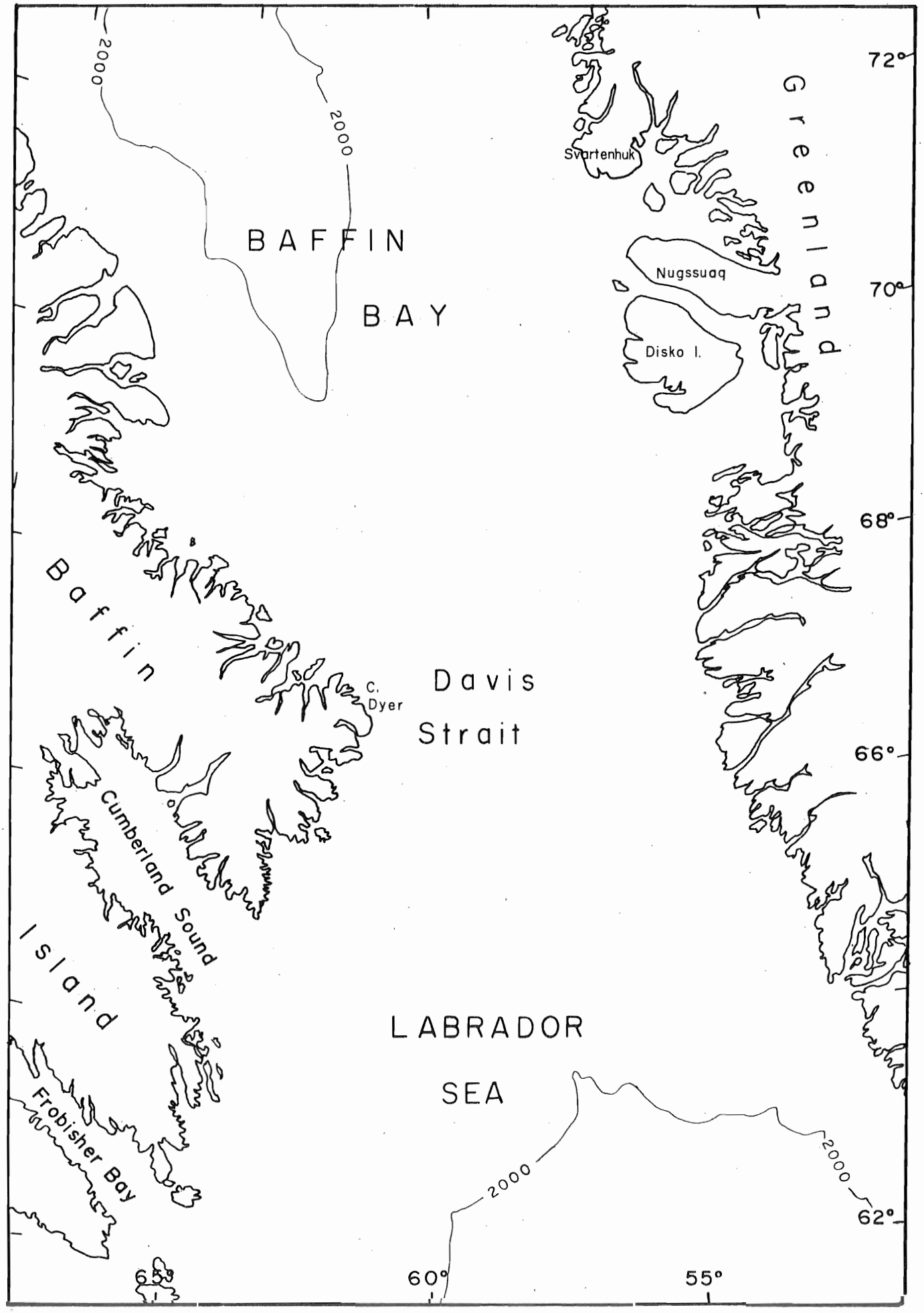
2000
2000
BAFFIN
BAY
Svartenhuk
Greenland
Nugssuaq
Disko I.
72°
70°
68°
66°
62°
Baffin
Island
C.
Dyer
Davis
Strait
Cumberland Sound
Frobisher Bay
LABRADOR
SEA
2000
2000
65°
60°
55°

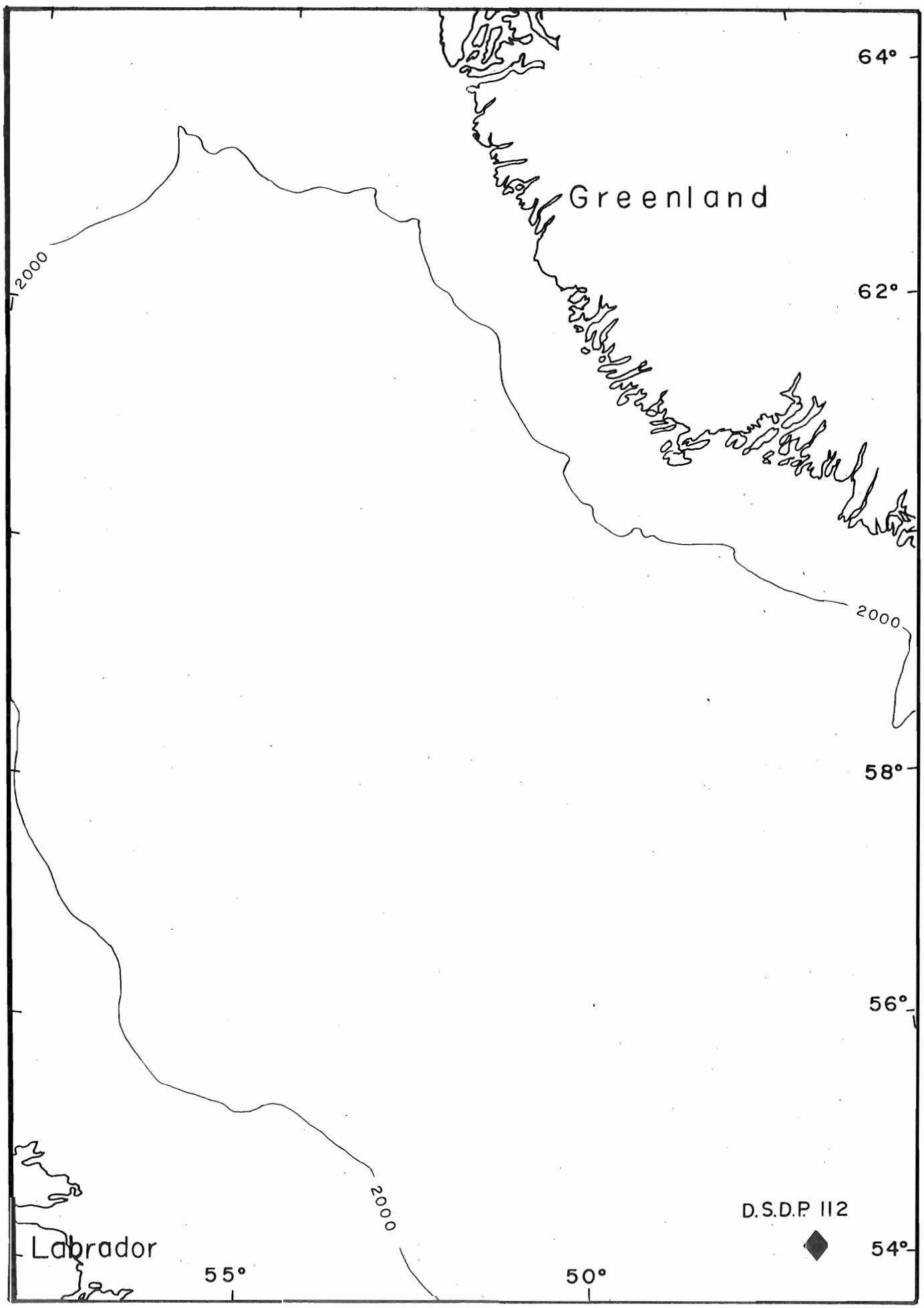
Greenland
64°
62°
2000
2000
58°
56°
2000
D.S.D.P. 112
54°
Labrador
55°
50°

Figure 1.2. Outcrops of Tertiary basalts and sediments between Cape Dyer and Cape Searle, Baffin Island, N.W.T.

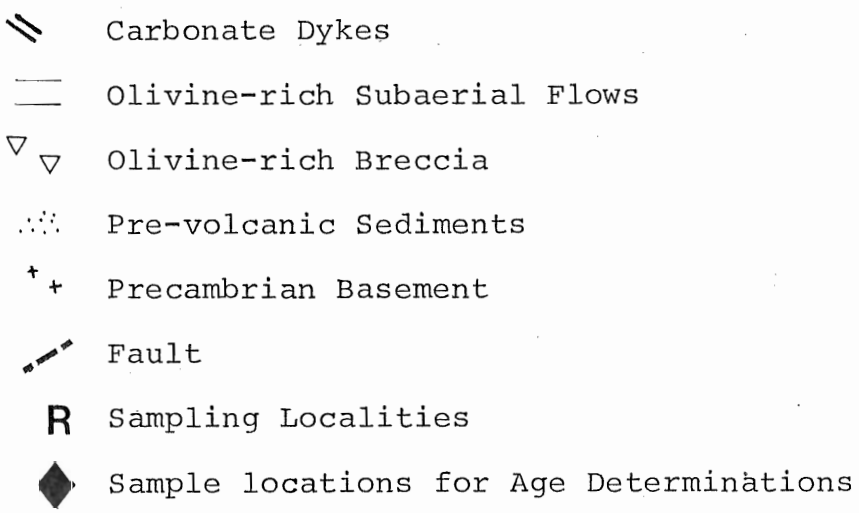

between the two capes. All of the outcrops are smaller than 15 $km.^2$ and most are smaller than 10 $km.^2$. The major geological units exposed are the Precambrian basement of the Churchill Province, minor early Tertiary terrestrial sediments, intermittently occurring volcanic breccias and a sequence of picritic basalt flows.

Sutherland (1853) published the first report on the rocks of Baffin Island, however more recent work has been continued by Wilson and Clarke (1965), Clarke and Upton (1971), Clarke (1967, 1968a,b, 1970) and O'Nions and Clarke (1972).

Lying on top of the 1700 my basement (Wanless et al., 1966) in many localities are sediments which underlie the volcanics. They consist of unconsolidated white quartz sands, impure sandstones, shales, minor coal and conglomerate. Current crossbedding, lack of marine fossils and abundance of plant fossils suggest that these are of terrestrial origin. A fossil flora has been allocated to the Lower Paleocene (a partial time-scale is given in Table 1.1 for reference). In addition these flora strongly resemble those of the Upper Atanikerdluk series of western Greenland.

Overlying the terrestrial sediments are basalt breccias which can be divided into two types on the basis of colour (i.e. either black or orange). Both contain hyaloclastite, basalt fragments and massive basaltic blocks. Many of the breccias contain long thin non-brecciated entrail pahoehoe in sideromelane. In the orange breccia the crystalline blocks are smaller than in the black breccia. The colour difference appears to be due to a greater hydration of the glass (palagonization) and oxidation of the iron in more finely divided orange material. A few

TABLE 1.1

Subdivisions of the Tertiary and Cretaceous

	Series		Representative European Stages	Age 10^6 yrs
	Pleistocene		Irvingtonian Villafranchian	3.5
	Pliocene		Piacenzian-Astian	8.0
		Upper	Pannonian Sarmatian	11.0
	Miocene	Middle	Vindobonian	19.0
		Lower	Burdigalian Aquitanian	27.0
		Upper	Chatian	30.0
	Oligocene	Middle	Rupelian	32.0
TERTIARY		Lower	Sannoisian Ludian	38.0
		Upper	Bartonian	45.0
	Eocene	Middle	Lutellian	49.0
		Lower	Ypresian	53.0
		Upper	Sparnacian Thanetian	59.0
	Paleocene			
		Lower	Montian(Danian)	65.0 ± 3.0
			Maestrichian	70.0
			Campanian	76.0
		Senonian		
			Santonian	82.0
CRETACEOUS	Upper			
			Conacian	88.0
		Turonian		94.0
		Cenomanian		100.0
	Lower			137.0 ± 5.0
	Jurassic			

Modified after Casey (1964), Funnell (1964), Evernden and Evernden (1970) and Rast (1971)

orange breccias are horizontally stratified and show graded bedding. The most striking feature however, is the development of giant cross-bedding. Fuller (1931) and Jones (1966) have indicated that this is due to subaqueous eruption. The crossbeds dip in a southwesterly direction indicating that perhaps the source of the volcanics is towards the northeast. One sample obtained for the present study was from a piece of black breccia and another was from a piece of a basaltic block found in orange breccia from outcrops E and I respectively (Figure 1.2).

These breccias are overlain by picritic and olivine-rich flows which have an average thickness of 3.5 m. Each flow usually has four divisions (a) a lower basalt chill, (b) a lower massive zone constituting 60% of the flow, (c) an upper vesicular zone constituting 40% of the flow and (d) the upper few centimetres of the flow showing ropy pahoehoe structures and containing much glass. Correlation from flow to flow is difficult because individual flows pinch out after a short distance. Absence of glacial features indicates that a complete succession is present and that it has a maximum thickness of 500 m. This indicates, in comparison with other Tertiary volcanic provinces in the North Atlantic, that the period of volcanic activity was relatively short. The final sample from Baffin Island comes from the top of a large flow at outcrop A (Figure 1.2).

The extent of volcanic rocks offshore is uncertain. Hood and Bower (1973) on the basis of aeromagnetic profiles, plotted an extensive area supposedly underlain by basalts. Grant (1975) on the basis

of seismic profiling has mapped a much smaller area. During October 1974 as part of the Arctic '74, Phase IV cruise (in which the author participated), the C.S.S. Hudson drilled in this area but did not obtain the expected number of basalt cores. It is quite possible that the marine extension of the terrestrial volcanics is as patchy or as discontinuous as it is on land.

(b) West Greenland: Flat-lying and gently westward dipping basalts cover an area 370 km. long from Disko Island to Svartenhuk Peninsula (Figure 1.3). The maximum width of these volcanics is 125 km. and, including recently discovered offshore extensions, covers an area of roughly 55,000 km^2.

Some of the earliest investigations in this area were reported by Giesecke (1823, 1910) and Rink (1853). Some more recent general papers are by Munck and Noe-Nygaard (1957), Rosenkrantz and Pulvertaft (1969), Brooks (1973) and Noe-Nygaard (1974). Other works have concentrated on specific areas: e.g. Pulvertaft and Clarke (1966), Clarke (1968 a, b, 1970), O'Nions and Clarke (1972) (Svartenhuk Peninsula); Clarke (1973) (the late stage igneous rocks of Ubekendt Ejland). Svartenhuk and Ubekendt are the two areas which figure most prominently in the present study, since it was samples from these areas which were dated. The seaward extension of the volcanic province of western Greenland has been discussed by Park et al. (1971), Keen et al. (1972), Ross and Henderson (1973), Keen and Clarke (1974) and Clarke (1975).

The volcanism in western Greenland is confined to an area marked by Cretaceous subsidence with subsequent alternations of marine and

Figure 1.3. Distribution of Cretaceous and Tertiary rocks in West Greenland.

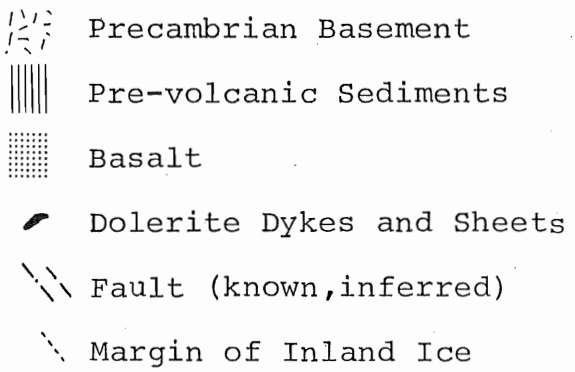

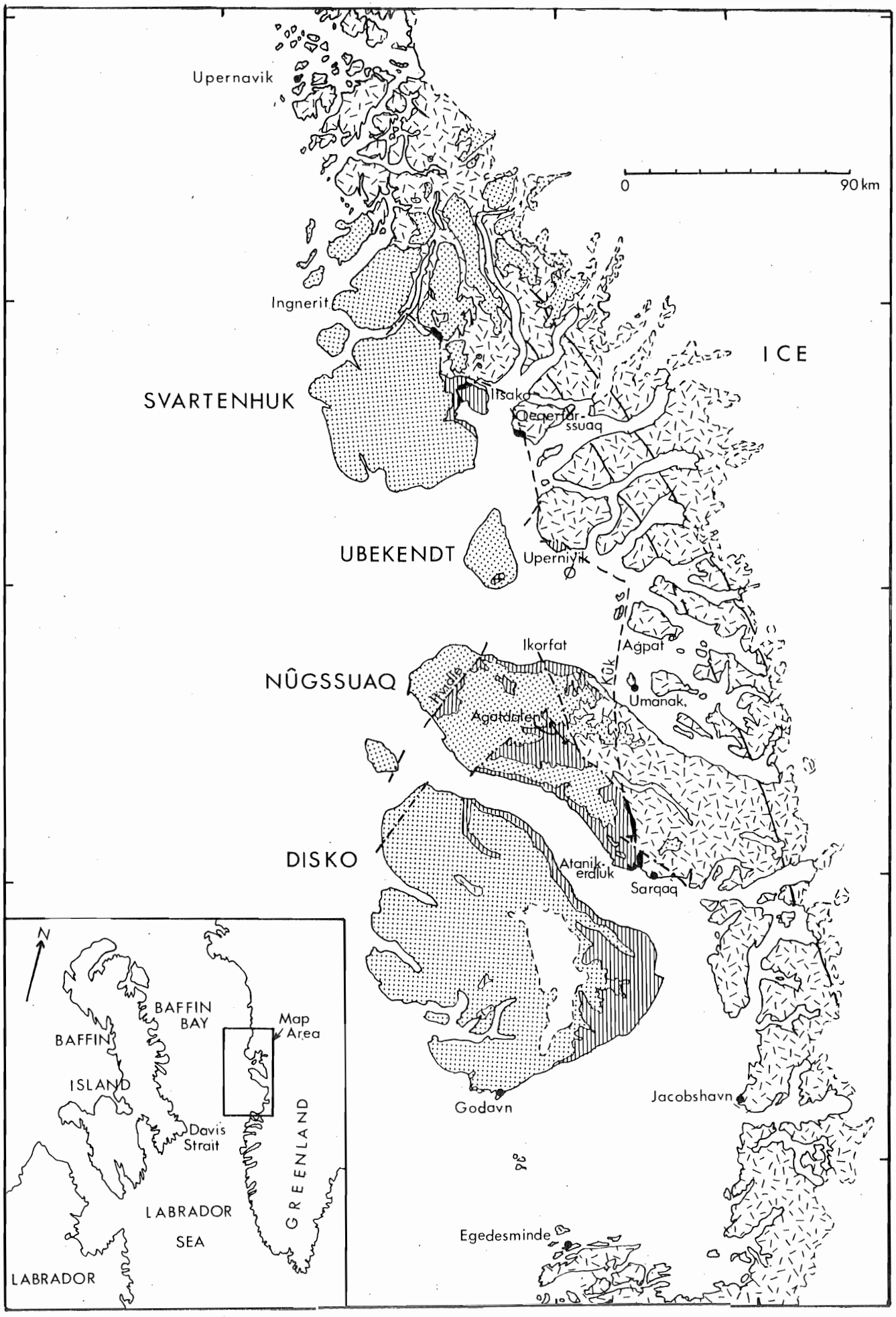
Upernavik
0
90 km
Ingnerit
ICE
SVARTENHUK
Itsako
Qeqertar-
ssuaq
UBEKENDT
Upernivik
Ikorfat
Agpat
NÛGSSUAQ
Kûk
Umanak
Agatdalen
DISKO
Atanik-
erdluk
Sarqaq
Godavn
Jacobshavn
Egedesminde
N
BAFFIN
BAY
Map
Area
BAFFIN
ISLAND
Davis
Strait
GREENLAND
LABRADOR
SEA
LABRADOR

limnic-fluvatile sedimentation. Rosenkrantz and Pulvertaft (1969) have indicated that the earliest sedimentary units are late Cretaceous in age; a more accurate dating is not possible until more paleontologic evidence is available. In late Turonian time (88-94 my, see Table 1.1) a marine sea carrying North American fauna transgressed outer Svartenhuk and during the Conacian (82-88 my, see Table 1.1) reached Nugssuaq. In the early Tertiary the sea must have joined that covering western Europe since European affinities become noticeable. The first indications of volcanic activity are intercalations of tuff in Danian (59-65 my, see Table 1.1) sedimentary strata. These were followed by massive outpourings of subaqueous volcanic breccias characterized by glass and fragmented pillows. These in turn were followed by a uniform sequence of olivine tholeiites which have the same composition as the breccias. The breccias, with the exception of minor tuffs, are the basal unit and lie discordantly on Upper Turonian to Lower Cenomanian sediments. Giant cross-bedding indicates a source to the west. One sample has been obtained from this unit (Figure 1.4).

The early volcanism is dominated by olivine-rich basalts and picrites erupted from widely scattered, randomly oriented thin dykes. The flows tend to be 3-5 m thick and rarely exceed 15 m. The scarcity of weathered tops indicates intense volcanic activity and rapid accumulation. No samples have been obtained from this unit.

In some parts of the province there is a pronounced break in the volcanic activity after the eruption of olivine-rich basalts; in some areas this is marked by non-marine sediments while in other areas vol-

Figure 1.4. Distribution of Tertiary basalts on Svartenhuk Peninsula, West Greenland.

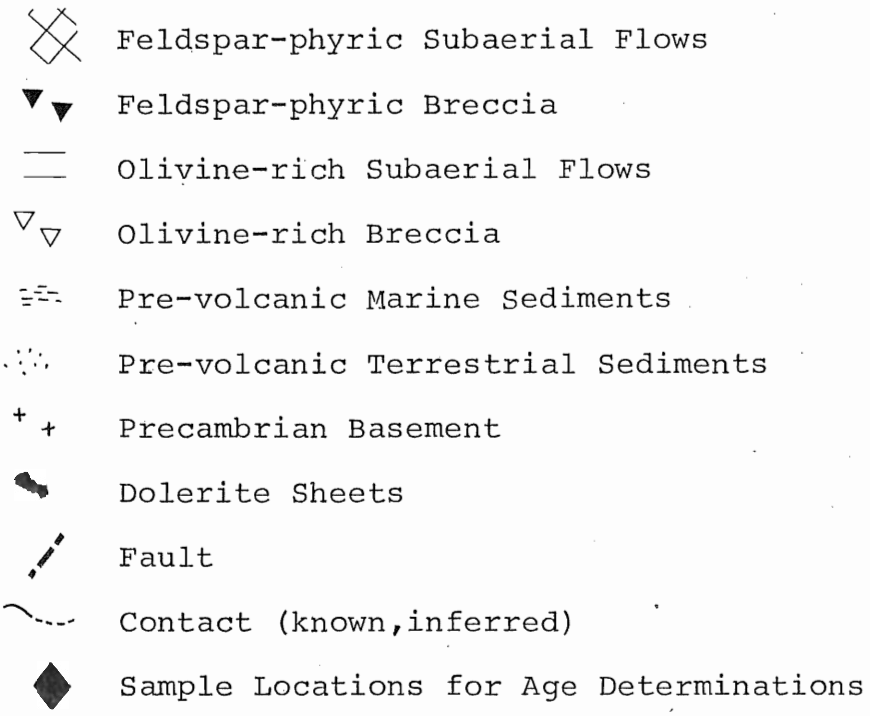

canic activity is continuous and the break is characterized by nearly aphyric brown weathering flows.

The lavas erupting at the top of the section are different from the previous eruptions in volume, morphology, petrography and chemistry. These flows erupted from central vents and by dykes. In contrast to the earlier flows, these may be traced for long distances, often in excess of 50 km. Weathered tops indicate long pauses between eruptions. These lavas, termed feldspar-phyric basalts, contain prominent phenocrysts of plagioclase and usually smaller amounts of augite and pseudomorphed olivine. Three more samples have been obtained from this unit (Figure 1.4). Ubekendt Ejland has not developed a thick sequence of these basalts; here, the last extrusives comprise a highly variable suite of rocks, including feldspar-phyric basalt, monchiquitic basalt, trachybasalt, biotite trachyte, rhyolite, pitchstone, ignimbrite, agglomerate and tuffs with a wide range of compositions forming at least two thick sequences along the coast (Clarke, 1973; see Figure 1.5).

Final stages of volcanic activity are represented by trachybasalt bodies on Svartenhuk Peninsula, at least one of which is a flow. The remaining two samples selected from Svartenhuk are from these bodies which are located at the head of Arfurtuarssuk (see Figure 1.4). The whole volcanic sequence has subsided and has tilted towards the southwest. Although numerous faults have a tendancy to repeat portions of the section, a complete sequence is available travelling from west to east along the south coast of Svartenhuk Peninsula (see Figure 1.4).

Of further interest is a swarm of perhaps a hundred NNW trending lamprophyre dykes which cut the late volcanics on Ubekendt Ejland.

Figure 1.5. Distibution of the last extrusives on the SE corner of Ubekendt Ejland.

LEGEND

1 Picrite Basalts

2 Aphyric and Feldspar-phyric Basalts

3 Pyroclastics

4 Olivine and Feldspar-phyric Basalts with Minor Rhyolites and Ignimbrites

5 Vent Agglomerates

Dykes, Mainly Vertical

Conjectured Boundaries

Sample Locations for Age Determinations

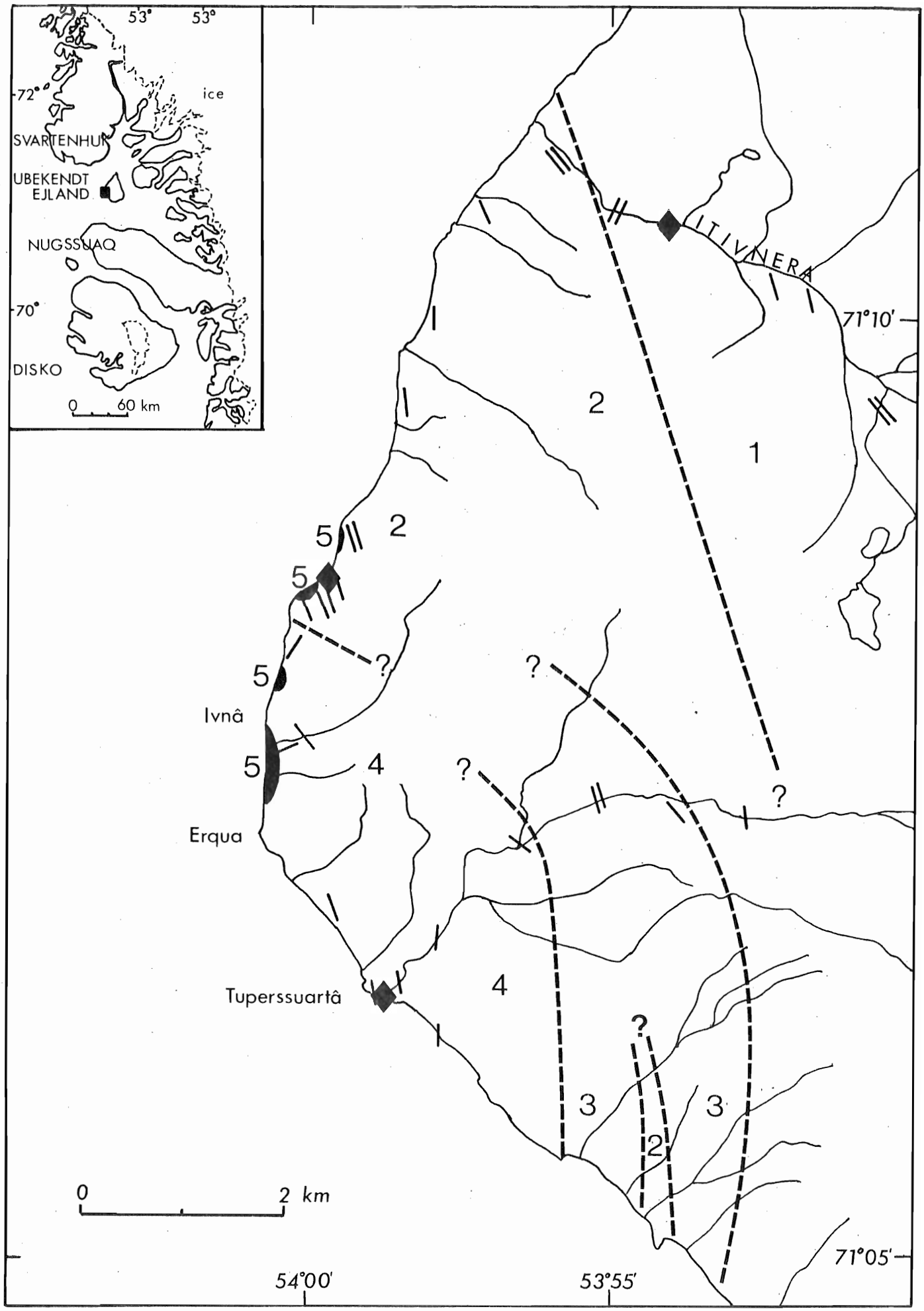
53°
53°
72°
ice
SVARTENHUK
UBEKENDT
EJLAND
NUGSSUAQ
70°
DISKO
0 60 km
ITIVNERA
71°10'
2
1
5
2
5
5
?
?
Ivnâ
5
4
?
?
?
Erqua
4
Tuperssuartâ
?
3
3
2
0 2 km
71°05'
54°00'
53°55'

These dykes were originally thought to only shortly post-date the other volcanics. Three of these dykes were sampled for age determinations (see Figure 1.5).

(c) Conclusions: Chemically, these basalts from Davis Strait are tholeiitic and, according to O'Nions and Clarke (1972), are, on the basis of the trace element distribution within them, indistinguishable from oceanic "abyssal" tholeiites. Petrogenetically they are primitive in the sense that MgO values are high and K_2O values are low. Clarke (1970) proposed that they are primary derivatives from the mantle. The chemical characteristics of the basalts changed with time and differences can be observed regionally. For example, the ratio of total iron to magnesium increases from oldest to youngest rocks. The concentrations of the lighter rare earth elements of the west Greenland rocks are enriched with respect to the heavier ones, to a greater extent than is the case for the Baffin Island basalts (O'Nions and Clarke, 1972). Among the mechanisms suggested by O'Nions and Clarke to account for these variations were (i) changes in eclogite fractionation and (ii) changes in the degree of partial melting of mantle peridotite.

Davis Strait and the Brito-Arctic Province

The Davis Strait volcanic province has long been recognized as a part of the Thulean Tertiary basalt province and as such should be considered in relation to the neighbouring volcanic areas.

Because of their similarity in age and field relations (see be-

low), East and West Greenland have been considered related. Brooks (1973) has compared the East Greenland tholeiitic basalts with the West Greenland feldspar-phyric basalts and noted their similarity. However, since the two provinces are separated by more than 700 km, there are considerable differences, i.e. East Greenland has not produced large volumes of picritic basalts and West Greenland does not show numerous syenitic or nepheline syenitic plutons. Age determinations from East Greenland by Beckinsale et al. (1970) indicate that the latest plateau basalts were extruded in the Upper Paleocene. Ages on amphibole separates show that the latest intrusives occurred about 50 my ago and it was suggested that the whole igneous history lasted only 15 my.

More closely related to East Greenland is the British Tertiary volcanic province. Extensive age determinations have been done and these have been compiled and expanded by Evans et al. (1973). A frequency distribution (after Evans et al., 1971) is shown in Figure 1.6. The range is quite extreme; however, some of the data can be safely ignored for reasons which will be discussed later along with K-Ar isochron data by Mellor and Mussett (1975). Nevertheless, the mode of the data is about 57 my which compares favourably with dates from East Greenland and Baffin Island (see below); however, no definite information regarding the beginning of volcanism is available. Data from the plateau lavas of the Faroes vary from 49 to 62 my (Tarling and Gale, 1968).

Until recently, limited age data were available from the Davis Strait volcanic province. Farrar (1966) made ten conventional K-Ar

Figure 1.6. Frequency distribution of some potassium-argon apparent ages from the British Tertiary igneous rocks (after Evans et al,1973)

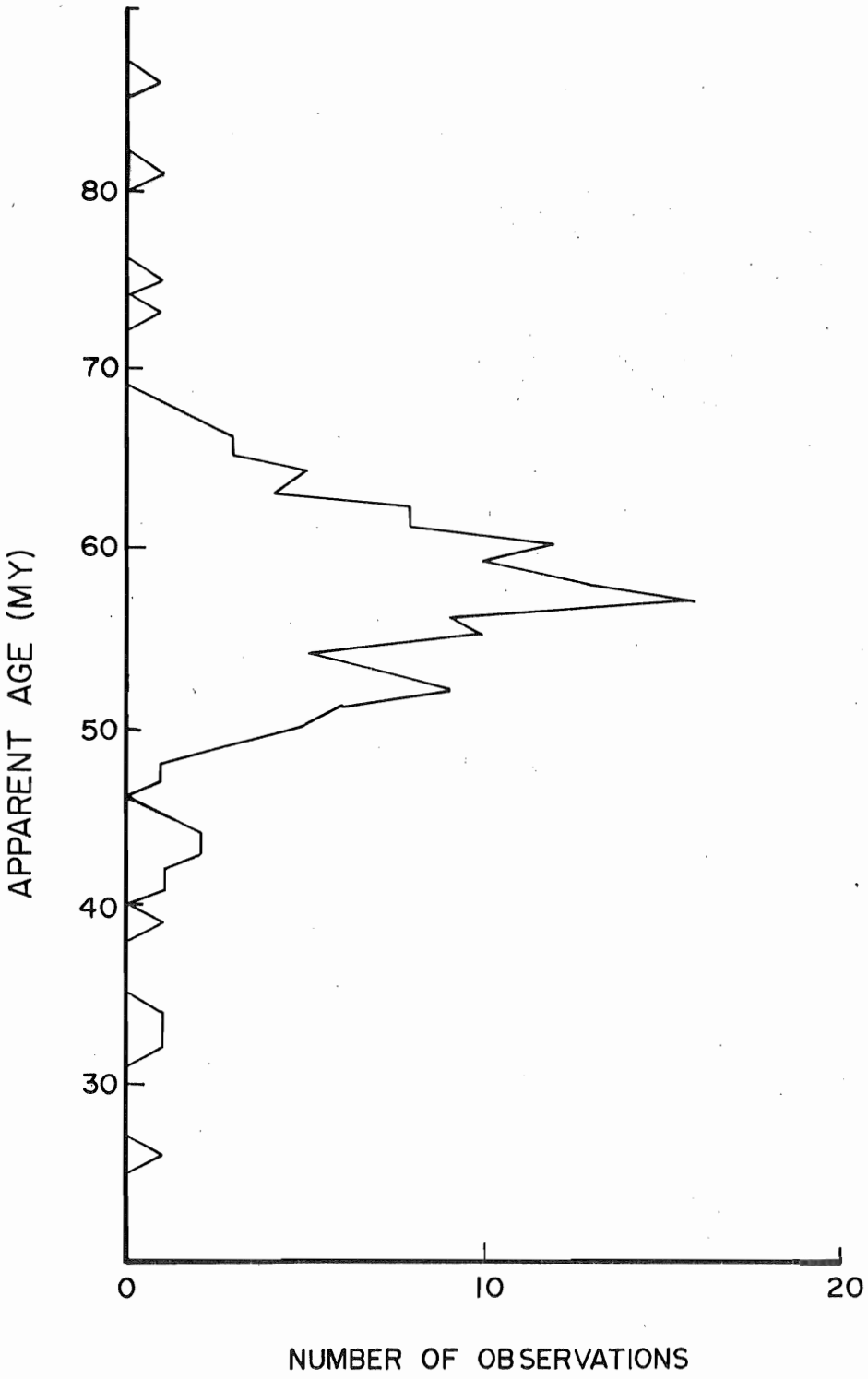
80
70
60
50
40
30
APPARENT AGE (MY)
0
10
20
NUMBER OF OBSERVATIONS

age determinations on samples obtained from D. B. Clarke from Baffin Island (see Table 1.2). As can be seen, the apparent ages range from 62.1 ± 8 my (1σ error) to values less than zero. Even ignoring the latter three values, it is unlikely, for reasons stated earlier, that the spread in data represent a real variation in age. The age most often quoted is the arithmetic mean of the first seven values, that is, an age of 57.0 my with a standard deviation of 1.1 my. Perhaps a more representative age would be obtained from the weighted mean of the first seven points, i.e. an age of 59.0 my with a weighted mean error of 3.7 my (1σ error). These data will be discussed further.

Beckinsale et al. (1974) have made two conventional K-Ar measurements and one Rb-Sr age determination on the central complex of Ubekendt Ejland (a late stage group of gabbroic and granitic plutons intruding the picritic lavas). Their results were 55.4 ± 1.5 my, 54.0 ± 1.5 my and 65.2 ± 3.8 my respectively (1σ errors).

Paleomagnetic studies by Athavale and Sharma (1975) on basalts from Disko Island revealed a normal polarity zone in a predominately reversed sequence. They have suggested an age of ≃ 63 my for this zone. The only other relevant age information is a commercial date of 70 ± 4my for a sample from Disko Island. This result may, however, be unreliable.

In contrast to the volcanic areas discussed above, the volcanic provinces of Iceland and Jan Mayen are extremely young, the oldest known Icelandic lava being ≃ 16 my old (Moorbath et al., 1968). It has been suggested (Morgan, 1972) that this volcanism is the surface expression of a mantle plume. The British and East Greenland volcanics are believed

TABLE 1.2

Conventional K-Ar Age Determinations from Baffin Island

(after Farrar (1966))

Sample Number	Age (± 1σ error)
I-133	62.1 ± 8 my
A-21	61.8 ± 2.8
FD-1	59.5 ± 14
A-9	58.1 ± 2.6
I-130	56.9 ± 4.6
FD-1	56.6 ± 11
A-21	50.0 ± 8
A-9	41.1 ± 4.1
-	< 0
-	< 0

to be the earliest expressions of that hot spot, expressions which occurred at a time before the continents had broken up. If this is true, then perhaps the volcanics associated with Davis Strait were also caused by an early Tertiary hot spot.

Davis Strait: An Ancient Hot Spot?

While the similarities among the various volcanics of Davis Strait have already been discussed, other chemical characteristics may be observed. Along the Reykjanes Ridge and in Iceland, geochemical studies indicate that systematic variations exist in the concentrations of rare-earth and minor elements in recently erupted basalts. Schilling (1973) has identified these as characteristics of volcanic rocks derived in part from a plume beneath a hot spot, the mantle being inhomogeneous in his view. Similar chemical variations found for the basalts of Davis Strait (Keen and Clarke, 1974; Clarke, 1975) indicate that these basalts are also plume derived. It should be noted however, that some people (e.g. O'Hara, 1973) are in disagreement with Schilling's views. Also of interest is the fact that the chemical variations would locate the mantle plume well to the north of Davis Strait, the location of the excess elevation of the crust (see below).

Seismological evidence indicates that the mantle is inhomogenous beneath a modern hot spot (e.g. Hawaii) (Kanasewich et al., 1973). This possibility has not been considered in the mechanisms put forward by O'Nions and Clarke (1972) for the geochemical variations of the Davis Strait basalts. Seismologically, Davis Strait appears similar to

Iceland with anomalously thick crust; however, mantle velocities are higher, a fact which may be accounted for by the higher temperatures existing beneath Iceland at this time.

The sea floor of Davis Strait is much shallower than the deeper parts of Baffin Bay and the Labrador Sea. Hyndman (1973) used this elevation as a means of dating the termination of spreading in the Labrador Sea, under the assumption that this elevation is plume derived. He showed that spreading ceased about 48 my ago, a result comparable to ones obtained in other studies (e.g. Le Pichon et al., 1971). However, this would not have been so without compensation for the excess elevation attributed to the hot spot. In Baffin Bay, if the age of the crust is calculated without compensation for the hot spot, an unreasonably low value of 15 my is obtained.

Hyndman (1975) observed that the oceanic basement areas at the margins of the Labrador Sea have anomalously great depths (up to 10 km) compared to the central basin. The former oceanic crust presumably formed before 60 my ago (the assumed approximate age of initiation of the hot spot), has normal depth and does not shoal toward Davis Strait. The ocean crust formed after the supposed initiation of the hot spot does shoal toward Davis Strait. It is not expected that these basins, which are suitable for petroleum exploration, would exist if formed during the hot spot activity or if no hot spot formed at all. Hyndman also observed that these structures should also be present in Baffin Bay. Perhaps they are represented for example, by the Melville Bugt graben structure (C. Keen et al., 1972; Keen et al., 1972 ; Hyndman

et al., 1973; Ross and Henderson, 1973). Vogt and Avery (1974) point out that there is a sharp step in the basement depth south of the Rockall-Hatton bank off Ireland. The step has an age of 50 my with the younger sea floor being anomalously shallow. The area was the continuation of the eastern and southern sides of the Labrador Sea, prior to the most recent phase of opening of the north Atlantic. Thus the older sea floor was probably produced as a part of the first phase of opening of the Labrador Sea and so has normal depth.

In summary, the facts would indicate that the volcanics of Davis Strait are probably hot spot derivatives. In order to make proper comparisons with other areas of the Thulean Tertiary province it is necessary not only to study the petrology and the geochemistry of the basalts but also the geochronology. It is the purpose of this study to determine the timing and duration of the Davis Strait volcanics and their relation to the evolution of the Labrador Sea and Baffin Bay.

Chapter II: The Argon-40/Argon-39 Method

Introduction

The occurrence of radioactivity was first discovered in 1896 by the French physicist Becquerel. The process was subsequently found by other investigators to be a spontaneous breakdown or decay of unstable atoms. Of the naturally occurring elements the majority have stable nuclei. The one of immediate interest is an isotope of potassium, ^{40}K. In order to use any decay scheme for estimating the geological age of a rock or mineral it is necessary to measure the concentrations of the parent and the radiogenic daughter elements.

Potassium-40 Decay

Potassium is one of the more abundant elements in the lithosphere and occurs in almost all rocks to some degree; hence the potassium-argon method can be used, in principle, in almost any geological environment. Potassium is made up of three known naturally occurring isotopes with mass numbers 39, 40 and 41 (Table 2.1). The least abundant of these is potassium-40 which decays to two daughter products: Calcium-40 and Argon-40.

The radioactivity of potassium is unusual. It decays by β-decay (i.e. by losing an electron from its nucleus) into ^{40}Ca about 89% of the time, that is:

$$^{40}K \rightarrow {}^{40}Ca + \beta^-$$

Since calcium is also a very common element in the lithosphere and since

TABLE 2.1

Isotopic Abundances of K, Ar, and Ca

Element	Isotopic	Abundance (atom %)
Potassium	^{39}K	93.080
	^{40}K	0.119 *
	^{41}K	6.911
Argon	^{36}Ar	0.337
	^{37}Ar	--
	^{38}Ar	0.063
	^{39}Ar	-- *
	^{40}Ar	99.600 *
Calcium	^{40}Ca	96.97
	^{41}Ca	--
	^{42}Ca	0.64
	^{43}Ca	0.145
	^{44}Ca	2.06
	^{45}Ca	-- *
	^{46}Ca	0.0033
	^{47}Ca	--
	^{48}Ca	0.185

* Radioactive

-- Not naturally occuring

^{40}Ca in particular comprises the majority of all Calcium (Table 2.1), this minute contribution of Calcium is negligible and therefore it is virtually impossible to detect radiogenic ^{40}Ca from non-radiogenic ^{40}Ca.

However, ^{40}K also decays by electron capture (i.e. by adding an electron to the nucleus) into ^{40}Ar about 10% of the time, that is:

$$^{40}K + e^{-} \rightarrow {}^{40}Ar + \gamma$$

Argon is one of the lesser abundant elements on the earth and even though ^{40}Ar comprises the majority of all argon (Table 2.1) it is not usually difficult to detect ^{40}Ar contributed by the decay of ^{40}K.

In addition there are two weak interactions. The first is by electron capture to the ground state of ^{40}Ar with no γ-emission. The second is by positron emission to the ground state of ^{40}Ar. These two transitions have generally been ignored and the significance of this will be discussed later. The decay scheme is summarized in Figure 2.1.

The Equation of Decay

Rutherford (1900) showed that radioactive decay followed an exponential law. The fundamental equation is:

$$\frac{dP}{dt} = -P\lambda \qquad (2.1)$$

where P = number of parent atoms and λ is a constant unique to the particular radioactive element in question. It is called the decay constant and represents the probability that any given atom will decay in a unit time.

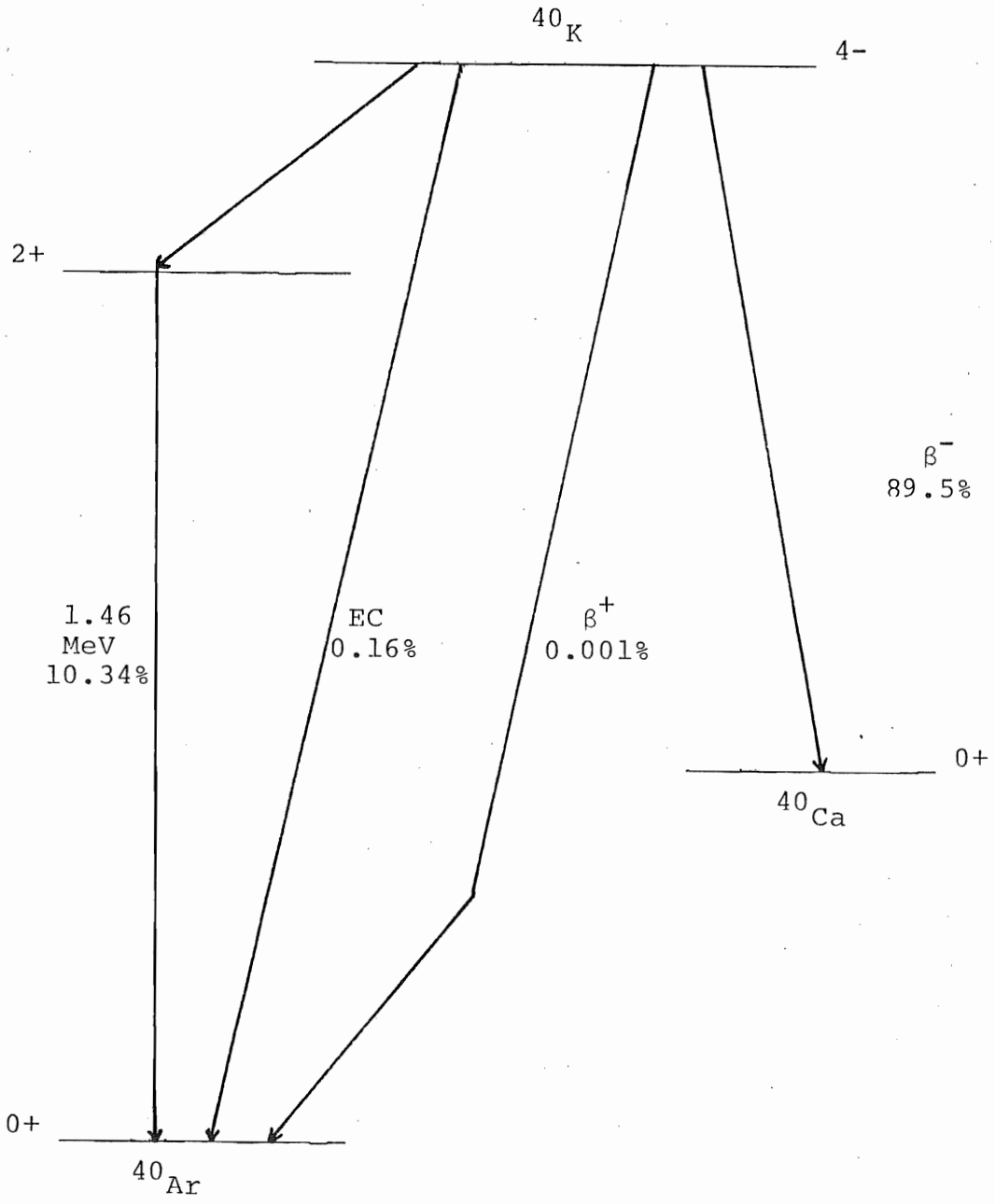

Figure 2.1 The Decay Scheme of ^{40}K

Rearrangement and integration of equation (2.1) gives

$$P = P_0 \, e^{-\lambda t} \tag{2.2}$$

where P_0 is the number of parent atoms when time t = 0, P is the number of atoms at time t = t. Rearrangement will also give an equation for the time based on the abundance of the parent atoms at time t = 0 and at time t = t, i.e.:

$$t = \frac{1}{\lambda} \ln \frac{P_0}{P} \tag{2.3}$$

By conservation of mass:

$$P_0 = P + D \tag{2.4}$$

where D = the number of daughter elements at time t = t. By substituting equation (2.4) into equation (2.3) one obtains the fundamental equation of geochronology, that is:

$$t = \frac{1}{\lambda} \ln \left(1 + \frac{D}{P} \right) \tag{2.5}$$

In our particular case ^{40}K is the parent atom and the daughters are $^{40}Ca^*$ and $^{40}Ar^*$ (* means radiogenic). Then, if we define:

λ_e = probability that ^{40}K will decay into $^{40}Ar^*$ in unit time

λ_β = probability that ^{40}K will decay into $^{40}Ca^*$ in unit time

or
$$\lambda_e + \lambda_\beta = \lambda \tag{2.6}$$

Substituting for the known daughters and parent in equation (2.5) we get:

$$t = \frac{1}{\lambda} \ln \left(1 + \frac{^{40}Ca^* + {}^{40}Ar^*}{^{40}K} \right) \tag{2.7}$$

By using equation (2.6), equation (2.7) becomes

$$t = \frac{1}{\lambda} \ln \left(1 + \frac{\lambda}{\lambda_e} \frac{^{40}Ar^*}{^{40}K} \right) \tag{2.8}$$

Figure 2.2. Effect on K-Ar age of errors in λ_β and λ_e. (After Aldrich and Wetherill, 1958)

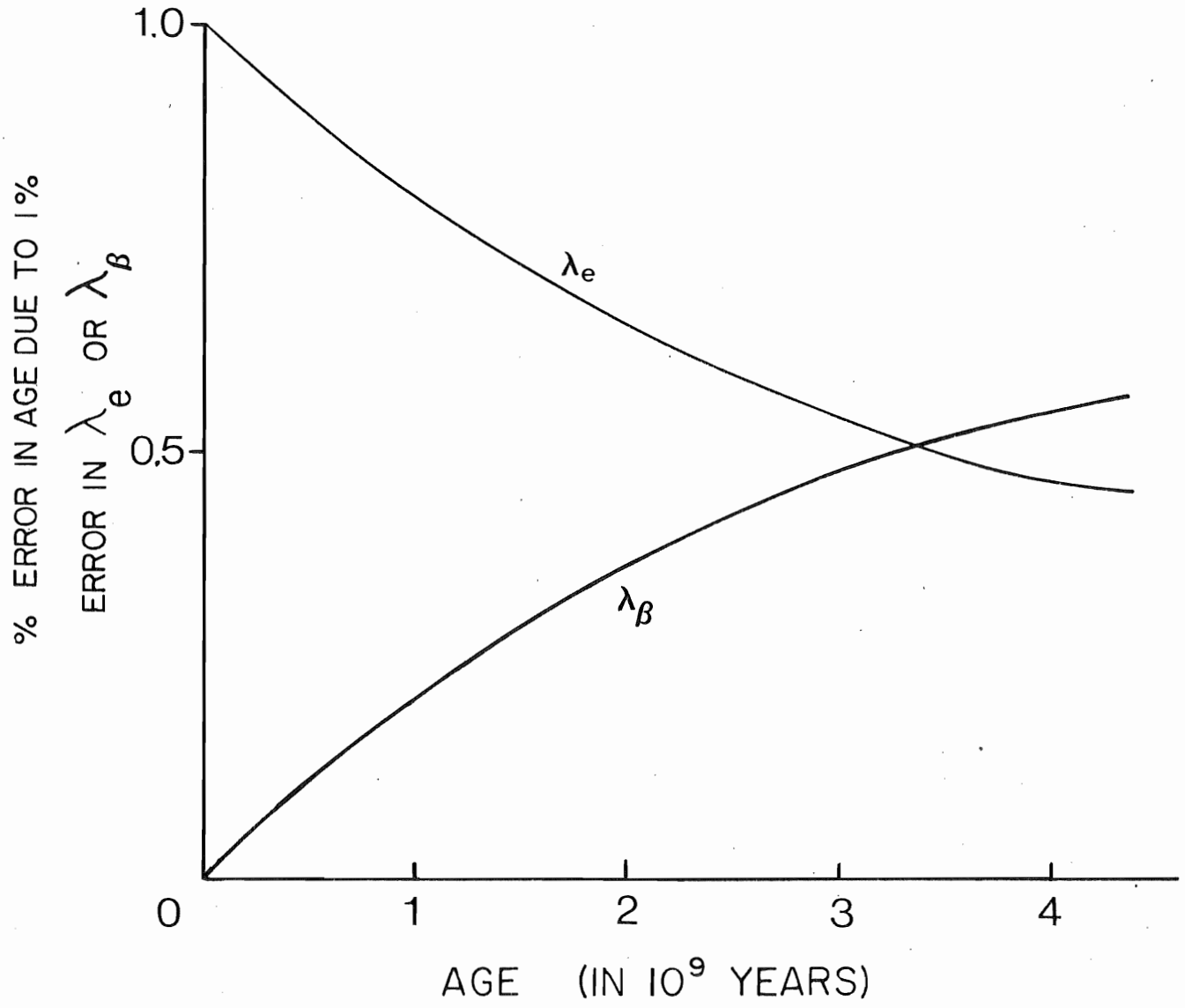
1.0
0.5
0
1
2
3
4
λ_e
λ_β
% ERROR IN AGE DUE TO 1% ERROR IN λ_e OR λ_β
AGE (IN 10^9 YEARS)

TABLE 2.2

Determinations of the Specific Beta and Gamma Activities of Natural Potassium

	Investigators	Activity β^-/g.sec.	γ/g.sec.
A.	Sawyer and Wiedenbeck (1949)	28.3 ± 1.0	
	Houtermans, Haxel and Heintz (1950)	27.1 ± 1.5	3.1 ± 0.3
	Good (1951)	27.1 ± 0.6	
	Burch (1953)		3.37 ± 0.09
	Kono (1955)	29.2 ± 1.0	
	Backenstoss and Goebel (1955)		3.50 ± 0.14
	Suttle and Libby (1955)	29.6 ± 0.7	2.96 ± 0.3
	McNair, Glover and Silson (1950)		3.33 ± 0.15
	Wetherill (1957)		3.39 ± 0.12
	Kelly, Beard, and Peters (1959)	27.3 ± 0.5	
B.	Egelkraut and Leutz (1960)	28.3 ± 0.15	3.35 ± 0.15
	Saha and Gupta (19t0)	28.8 ± 0.90	3.22 ± 0.15
	Glendenim (1961)	28.2 ± 0.03	
	Brinkman, Aten and Veenbour (1965)	29.2 ± 0.5	
	Leutz, Schulz and Wenninger (1965)	28.26± 0.05	3.25 ± 0.07
	deRyter, Aten, van Dulmen KrolKoning and Zuidema (1966)		3.25 ± 0.06

If we now define:

$$R = \frac{\lambda_e}{\lambda_\beta}$$

then equation (2.8) becomes

$$t = \frac{1}{\lambda} \ln \left(1 + \frac{1 + R}{R} \frac{^{40}Ar^*}{^{40}K} \right) \qquad (2.9)$$

R is known as the "branching ratio".

Equation (2.9) can be rearranged as follows:

$$^{40}Ar^* = \frac{R}{1 + R} \, ^{40}K \left(e^{\lambda t} - 1 \right) \qquad (2.10)$$

Its uses will be seen later.

The decay constants used in this study are:

$$\lambda_\beta = 4.72 \times 10^{-10} \text{ yrs.}^{-1}$$

$$\lambda_e = 5.84 \times 10^{-11} \text{ yrs.}^{-1}$$

$$\lambda = 5.304 \times 10^{-10} \text{ yrs.}^{-1}$$

as determined by Smith (1964).

The half-life of ^{40}K is thus:

$$t_{1/2} = 0.693/\lambda$$

$$= 1.31 \times 10^9 \text{ yrs.}$$

As with all experimental constants there is an inherent uncertainty. Originally, potassium decay constants were determined by producing concordant potassium-argon and uranium-lead ages for co-genetic minerals. After 1956 this method was superceded by careful direct counting measurements, in particular work done by Wetherill et al. (1956) is often quoted. In a review by Aldrich and Wetherill (1958) they suggested a value of $4.72 \times 10^{-10} \text{yr}^{-1}$ for λ_β, and $5.85 \times 10^{-11} \text{yr}^{-1}$

for λ_e. These are considered to have uncertainties of about ± 2% and ± 5% respectively although scatter between experimenters is often greater. The effect of errors in λ_β and λ_e on the potassium-argon ages is shown in Figure 2.2. Smith (1964) discusses the most accurate physical measurements up to 1961 but recommends the use of values used most often for the sake of uniformity. Beckinsale and Gale (1969) re-evaluated the various beta and gamma activities of natural potassium. These are compiled in Table 2.2. Only those determinations with experimental errors less than about 4% were considered. The data were divided into two groups, group B comprising the more reliable determinations as indicated by the small range of values. The dependance of the partial decay constants on the associated activities is

$$\lambda_i = \frac{dn_i}{dt} \frac{AY}{fN} \text{ yr}^{-1}$$

where f is the atomic abundance of ^{40}K in natural potassium; A is the atomic weight of potassium (= 39.102 on the ^{12}C scale); N is Avogadro's number (= 6.02252×10^{-23} atoms per mole on the ^{12}C scale); Y is the number of seconds in a mean solar year (= 3.15569×10^{7} sec; Weast and Selby, 1966).

The weighted means for the group B activities are

$$\frac{dn_{\beta^-}}{dt} = 28.27 \pm 0.05 \text{ d.p.s.g.}^{-1}\text{K}$$

and

$$\frac{dn_\lambda}{dt} = 3.26 \pm 0.02 \text{ d.p.s.g.}^{-1}\text{K}$$

which yields partial decay constants of

$$\lambda_{\beta} = (4.905 \pm 0.009) \times 10^{-10} yr^{-1}$$

$$\lambda_{e} = (0.566 \pm 0.0035) \times 10^{-10} yr^{-1}$$

These are dependent on the atomic abundance of ^{40}K. Variation from the value (1.19×10^{-4}) reported by Nier (1950) for the atomic abundance of ^{40}K is not just a function of experimental errors, but also of geological fractionation.

Good values for the weaker interactions have also been determined. A weighted mean value for the ratio of positron decay to negatron decay obtained by various investigators (Tilley and Madansky, 1959; Eigelkemeir, Flynn and Glendenim, 1962; Leutz, Schulz and Wenninger, 1965) yields

$$\frac{d\beta^{+}}{dt} = (3.25 \pm 0.37) \times 10^{-4} d.p.s.g.^{-1}K$$

The value for the electron capture to the ground state is harder to obtain

$$\frac{d\lambda_{e}'}{dt} = (5.0 \pm 1.0) \times 10^{-2} d.p.s.g^{-1}K$$

The resulting decay constants are summarized in Table 2.3 and are compared with those given by Smith (1964).

If the constants recommended by Beckinsale and Gale (1969) are adopted instead of those most often used, the result would be an adjustment in age of about +2% at 5 my changing to about -2% at 4500 my. This is summarized in Figure 2.3. In this particular study there would be an adjustment of about 1 my.

TABLE 2.3

The decay constants of ^{40}K and related parameters

Quantity	Smith (1964)	Beckinsale and Gale (1969)
λ_β	$4.72 \times 10^{-10}\ yr^{-1}$	$(4.905 \pm 0.009) \times 10^{-10} yr^{-1}$
λ_e	$0.584 \times 10^{-10} yr^{-1}$	$(0.566 \pm 0.0035) \times 10^{-13} yr^{-1}$
$\lambda_{e'}$	-	$(8.67 \pm 1.74) \times 10^{-10} yr^{-1}$
λ	$5.304 \times 10^{-10} yr^{-1}$	$(5.480 \pm 0.010) \times 10^{-10} yr^{-1}$
Branching ratio		
$\frac{\lambda_e + \lambda_e'}{\lambda_{\beta^-}}$	0.124	0.117 ± 0.001
$T_{1/2} = \frac{\ln 2}{\lambda}$	$1.31 \times 10^9 yr$	$(1.265 \pm 0.002) \times 10^9 yr$

Figure 2.3. Multiplication factor for conversion from constants of Smith (1964) to those of Beckinsale and Gale (1969). After Armstrong (1974).

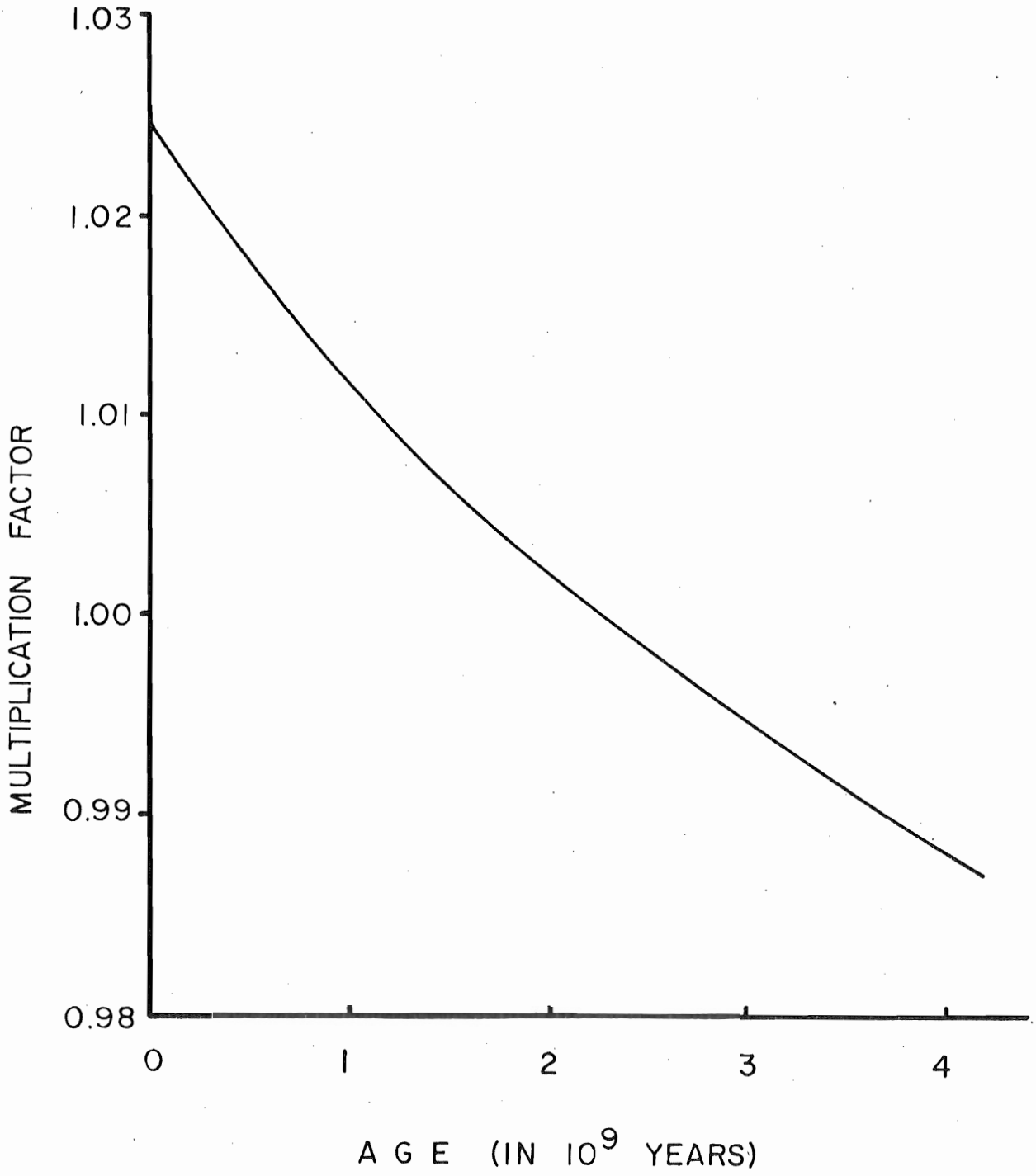
1.03
1.02
1.01
1.00
0.99
0.98
MULTIPLICATION FACTOR
0
1
2
3
4
AGE (IN 10^9 YEARS)

$^{40}Ar/^{39}Ar$ Dating

This method of potassium-argon age determinations was first described by Merrihue (1965) as applied to meteoritic material. First studies on terrestrial material were carried out at Cambridge University, England (Grasty and Mitchell, 1966). Although a further number of measurements on meteoritic material were reported (Turner, Miller and Grasty, 1966; Merrihue and Turner, 1966) the validity of this technique had never been established. Mitchell (1968b) did so conclusively for rocks having the ratio $K_2O/CaO > 0.1$. Later studies show the validity of this method for less potassium-rich rocks.

When a rock or mineral containing potassium is irradiated by thermal and fast neutrons, many reactions occur which lead to the production of isotopes of argon. One of these reactions is of the most interest. Let us assume for the moment that this is the only reaction that takes place, namely the production of ^{39}Ar from ^{39}K via:

$$^{39}K(n,p)^{39}Ar$$

^{39}Ar is unstable and will decay by negatron emission to ^{39}K with a half-life of 269 years.

After a sample has been irradiated, the amount of ^{39}Ar produced by fast neutrons of energy ε is:

$$^{39}Ar = {}^{39}K\Delta T\ \phi(\varepsilon)\sigma(\varepsilon) \qquad (2.11)$$

where ^{39}K is the number of potassium-39 atoms in the sample

^{39}Ar is the number of argon-39 atoms produced

$\phi(\varepsilon)$ is the neutron flux at energy ε

$\sigma(\varepsilon)$ is the neutron capture cross-section of $^{39}K(n,p)^{39}Ar$ at energy ε

ΔT is the irradiation time

The total ^{39}Ar production is found by integrating over all neutron energies, that is:

$$^{39}Ar = {}^{39}K\Delta T\int\phi(\varepsilon)\sigma(\varepsilon)d\varepsilon \tag{2.12}$$

It follows by dividing equation (2.10) by equation (2.12) that:

$$\frac{^{40}Ar}{^{39}Ar} = \frac{^{40}K}{^{39}K}\frac{R}{1+R}\frac{1}{\Delta T}\frac{(e^{\lambda t}-1)}{\phi(\varepsilon)\sigma(\varepsilon)d\varepsilon} \tag{2.13}$$

Let

$$J = \frac{^{39}K}{^{40}K}\frac{1+R}{R}\Delta T\int\phi(\varepsilon)\sigma(\varepsilon)d\varepsilon \tag{2.14}$$

then from equation (2.13) it follows that

$$J = \frac{e^{\lambda t}-1}{^{40}Ar/^{39}Ar} \tag{2.15}$$

Now if one were to apply the same neutron flux to a sample of known age t_s and to a sample of unknown age t_u, all arranged in precise locations in the reactor (to account for variations of neutron flux within the reactor), then for the two samples of ages t_s and t_u equation (2.10) becomes

$$^{40}Ar_s{}^* = \frac{R}{1+R}\,{}^{40}K_s(e^{\lambda t_s}-1) \tag{2.16}$$

and

$$^{40}Ar_u{}^* = \frac{R}{1+R}\,{}^{40}K_u(e^{\lambda t_u}-1) \tag{2.17}$$

Following the method outlined before, equation (2.16) can be written similarly to equation (2.15):

$$J_s = \frac{e^{\lambda t_s} - 1}{{}^{40}Ar_s*/{}^{39}Ar_s} \qquad (2.18)$$

and equation (2.17) becomes

$$J_u = \frac{e^{\lambda t_u} - 1}{{}^{40}Ar_u*/{}^{39}Ar_u}$$

or $$t_u = \frac{1}{\lambda} \ln \left(1 + J_u \frac{{}^{40}Ar_u*}{{}^{40}Ar_u}\right) \qquad (2.19)$$

Since in equation (2.14) J is only dependent on the neutron flux and that is constant by design, then

$$J_s = J_u$$

Equation (2.19) becomes

$$t_u = \frac{1}{\lambda} \ln \left(1 + J_s \frac{{}^{40}Ar_u*}{{}^{39}Ar_u}\right)$$

or $$t_u = \frac{1}{\lambda} \ln \left(1 + \frac{({}^{40}Ar*/{}^{39}Ar)_u}{({}^{40}Ar*/{}^{39}Ar)_s} (e^{\lambda t_s} - 1)\right) \qquad (2.20)$$

In reality there is usually a small but significant variation in the neutron flux present. J_s then becomes an average value determined by two or more samples of known age.

Correction for Atmospheric Argon

The important feature shown in equation (2.20) is that the result is expressed as a ratio of radiogenic ^{40}Ar and ^{39}Ar. Note that it is the ratio of radiogenic ^{40}Ar. There are three naturally occurring iso-

topes of argon as mentioned before: ^{40}Ar, ^{38}Ar and ^{36}Ar which occur in the atmosphere in the ratios $^{40}Ar/^{36}Ar = 295.5$ and $^{38}Ar/^{36}Ar = .187$ (Nier, 1950). The total amount of ^{40}Ar present is, in the simplest case, the sum of the radiogenic ^{40}Ar and the atmospheric ^{40}Ar. The amount of atmospheric argon is determined by monitoring ^{36}Ar which is assumed to be only atmospheric in origin. Thus

$$\frac{^{40}Ar^*}{^{39}Ar} = \frac{^{40}Ar}{^{39}Ar} - 295.5 \frac{^{36}Ar}{^{39}Ar} \qquad (2.21)$$

A situation now exists which is potentially dangerous, that is, the assumption that all ^{36}Ar is atmospheric and that all ^{40}Ar is either atmospheric or radiogenic. This will be discussed fully later.

Advantages of the $^{40}Ar/^{39}Ar$ Method

In conventional K - Ar dating, the potassium is measured by flame photometry, a method which has an error associated with it of around 2%. In addition, sampling errors are introduced by dividing a sample into portions. This is especially important in whole rock analyses of basaltic samples since the argon measurement is performed on fragments of rock as opposed to a finely ground powder. Argon errors are further increased by the necessary introduction of a calibrated Ar spike in order to determine absolute quantities of the gas.

It is quite evident from equation (2.20) that the only values to be determined are the argon ration $(^{40}Ar^*/^{39}Ar)_s$, $(^{40}Ar^*/^{39}Ar)_u$. The age of the "standard", t_s, and the decay constant λ, are assumed known.

The argon ratios can be measured quite accurately by using a mass spectrometer, and the errors are significantly lower than those mentioned above for conventional dating. If a standard is selected with care, the uncertainty in its age, as determined by the conventional method, can be very small. In our particular case where $t_s \simeq 400$ my and $t_u \simeq 60$ my, this uncertainty is reflected (percentage-wise) in the estimated error in the age of the unknown.

The most powerful use of the $^{40}Ar/^{39}Ar$ method is the stepwise degassing technique. Instead of heating the sample to fusion and analyzing all the argon gas released, the sample is heated in stages for fixed periods of time. The released gas is analyzed at each stage. This is repeated for successively higher temperatures until the melting point is reached. The data may be treated in different ways as discussed later.

Behaviour of Argon in a Mineral

The release of argon from a mineral sample which is being heated is a very complex process. It is assumed that the argon produced from the decay of ^{40}K and the argon produced from the irradiation of ^{39}K will be released at the same time from a given mineral crystal.

Brandt and Voronovsky (1967) showed that the recoil energy of radiogenic ^{40}Ar atoms, when ^{40}K decays is sufficient to produce a random distribution of ^{40}Ar in the mineral lattice. Similarly, Mitchell (1968a) showed that the recoil energy of ^{39}Ar produced by the $^{39}K(n,p)$ ^{39}Ar reaction was sufficient to produce a random distribution of ^{39}Ar in the mineral lattice. The energy for the ^{39}Ar recoil is many orders

of magnitude higher than the energy for ^{40}Ar recoil, and also may produce considerable lattice disorder. Mitchell set an upper limit of 10^{-4} mm for the range of ^{39}Ar atoms in a typical mica lattice. Hence, argon loss from irradiation effects is probably not significant unless extremely fine-grained samples are used. This is usually avoided for other reasons, such as higher atmospheric argon levels in finer grained samples(Keeling and Naughton, 1974).

Chapter III: Treatment of Data

Interfering Isotopes

For simplicity in earlier discussions it was assumed that there was only one reaction, $^{39}K(n,p)^{39}Ar$, which took place when a rock or mineral sample was irradiated with thermal and fast neutrons. However, numerous other reactions do take place. Of importance here are those that produce isotopes of argon, in particular ^{36}Ar, ^{39}Ar and ^{40}Ar (see Table 3.1). The production of ^{36}Ar will affect the atmospheric correction while the production of ^{39}Ar and ^{40}Ar will affect the calculation of the age directly.

In order to calculate the correction factors for these interference reactions, Mitchel (1968b), Brereton (1970), Berger and York (1970) Turner (1970) and Bottomly (1975, personal communication) analyzed argon from irradiated samples of "zero-age", calcium and potassium salts. By analyzing these salts it is possible to separate the effects of the various interfering, neutron induced reactions. There are only three principal sources of interference: K derived ^{40}Ar ($^{40}Ar^{NK}$) and Ca derived ^{36}Ar ($^{36}Ar^{NCa}$) and ^{39}Ar ($^{39}Ar^{NCa}$).

In order to correct for interference effects it is assumed that all ^{37}Ar is derived from calcium. The ^{37}Ar produced from potassium is ignored as it has been determined experimentally that it produces less than 0.05% of the ^{39}Ar volume produced from potassium. Argon isotopes produced from argon are also ignored as the ratio of argon atoms to potassium atoms is small.

TABLE 3.1

Effect of Neutron Irradiation: Production and Removal of Argon

Natural Isotope (Abundance)	Interaction	Product Isotope	Decay Scheme	Half-life	Final Isotope	Reference
Production of ^{36}Ar						
^{35}Cl (75.53%)	(n,γ)	^{36}Cl	β^-	3×10^5yrs	^{36}Ar	a,c
^{39}K (95.08%)	(n,α)	^{36}Cl	β^-	3×10^5yrs	^{36}Ar	a,c
^{40}Ca (96.97%)	(n,2α)	^{36}Ar	stable	--	^{36}Ar	b,c,e
Removal of ^{36}Ar						
^{36}Ar (0.337%)	(n,p)	^{36}Cl	β^-	3×10^5yrs	^{36}Ar	a,c
^{36}Ar (0.337%)	(n,α)	^{33}S	stable	--	^{33}S	a
^{36}Ar (0.337%)	(n,γ)	^{37}Ar	e_K	35.1 days	^{37}Cl	b,e
Production of ^{37}Ar						
^{36}Ar (0.337%)	(n,γ)	^{37}Ar	e_K	35.1 days	^{37}Cl	b,e
^{39}K (93.08%)	(n,nd)	^{37}Ar	e_K	35.1 days	^{37}Cl	e
^{40}Ca (96.97%)	(n,α)	^{37}Ar	e_K	35.1 days	^{37}Cl	a,e,c

continued on following page

TABLE 3.1 (continued)

Natural Isotope (Abundance)	Interaction	Product Isotope	Decay Scheme	Half-life	Final Isotope	Reference
Production of ^{38}Ar						
^{37}Cl (24.47%)	(n,γ)	^{38}Cl	β^-	37.3 min.	^{38}Ar	a,e,c
^{39}K (93.08%)	(n,d)	^{38}Ar	stable	--	^{38}Ar	e,c
^{40}Ar (99.60%)	(n,α)	^{38}Cl	β^-	37.3 min.	^{38}Ar	e
^{41}K (6.91%)	(n,nd)	^{38}Cl	β^-	37.3 min.	^{38}Ar	a,e
^{42}Ca (0.64%)	(n,nα)	^{38}Ar	stable	--	^{38}Ar	e
Removal of ^{38}Ar						
^{38}Ar (0.063%)	(n,p)	^{38}Cl	β^-	37.3 min.	^{38}Ar	b
^{38}Ar (0.063%)	(n,d)	^{37}Cl	stable	--	^{37}Cl	b
^{38}Ar (0.063%)	(n,γ)	^{39}Ar	β^-	269 yrs	K	b,e
Production of ^{39}Ar						
^{38}Ar (0.063%)	(n,γ)	^{39}Ar	β^-	269 yrs	^{39}K	b,e
^{39}K (93.08%)	(n,p)	^{39}Ar	β^-	269 yrs	^{39}K	b,e
^{40}Ar (99.60%)	(n,d)	^{39}Cl	β^-	55.5 min.		
		^{39}Ar	β^-	269 yrs	^{39}K	b,e,f

continued on following page

TABLE 3.1 (continued)

Natural Isotope (Abundance)	Interaction	Product Isotope	Decay Scheme	Half-life	Final Isotope	Reference
Production of ^{39}Ar (continued)						
^{40}K (0.0118%)	(n,d)	^{39}Ar	β^-	269 yrs	^{39}K	e
^{41}K (6.91%)	(n,^{3}He)	[^{39}Cl	β^-	55.5 min.]		
		^{39}Ar	β^-	269 yrs	^{39}K	b
^{42}Ca (0.64%)	(n,α)	^{39}Ar	β^-	269 yrs	^{39}K	c,e
^{43}Ca (0.145%)	(n,nα)	^{39}Ar	β^-	269 yrs	^{39}K	e
Production of ^{40}Ar						
^{40}K (0.0118%)	(n,p)	^{40}Ar	stable	--	^{40}Ar	c,e
^{41}K (6.91%)	(n,d)	^{40}Ar	stable	--	^{40}Ar	b,e
^{43}Ca (0.145%)	(n,α)	^{40}Ar	stable	--	^{40}Ar	c,e
^{44}Ca (2.06%)	(n,nα)	^{40}Ar	stable	--	^{40}Ar	e
Removal of ^{40}Ar						
^{40}Ar (99.60%)	(n,α)	^{37}S	β^-,γ	5.1 min.	^{37}Cl	a
^{40}Ar (99.60%)	(n,d)	[^{39}Cl	β^-	55.5 min.]		
		^{39}Ar	β^-	269 yrs.	^{39}K	b,e,f

continued on following page

TABLE 3.1 (continued)

Natural Isotope (Abundance)	Interaction	Product Isotope	Decay Scheme	Half-life	Final Isotope	Reference
Removal of ^{40}Ar (continued)						
^{40}Ar (99.60%)	(n,p)	^{40}Cl	β^-, γ	1.4 min.	^{40}Ar	b
^{40}Ar (99.60%)	(n,γ)	^{41}Ar	β^-, γ	1.83 hrs.	^{41}K	b
Other Reactions						
^{41}K (6.91%)	(n,p)	^{41}Ar	β^-, γ	1.83 hrs.	^{41}K	d
^{44}Ca (2.06%)	(n,α)	^{41}Ar	β^-, γ	1.83 hrs.	^{41}K	d

a. Stehn et al. (1964) (as reported in Stukas (1971))

b. Endt and van der Leun (1967)

c. Mitchell (1966)

d. Jessen et al. (1966)

e. Brereton (1970)

f. Weast (1970)

Measurement of the argon isotope ratios present in the respective salts allows one to calculate the correction factors required. These are applied to the argon isotope ratios for a given sample so that the ratio $(^{40}Ar^*/^{39}Ar^{NK})_{u,s}$ may be evaluated and inserted in equation (2.20). The expression for $^{40}Ar^*/^{39}Ar^{NK}$ is derived in Appendix A, the result is:

$$\frac{^{40}Ar^{K}}{^{39}Ar^{NK}} = \frac{\frac{^{40}Ar}{^{39}Ar} - \frac{^{36}Ar}{^{39}Ar}\, x + \frac{^{37}Ar}{^{39}Ar}\, fe^{\lambda' t}\,(bx + ac) - c}{1 - \frac{^{37}Ar}{^{39}Ar}\, fe^{\lambda t}\, a} \qquad (3.1)$$

where $a = \dfrac{^{39}Ar^{NCa}}{^{37}Ar^{NCa}}$

$b = \dfrac{^{36}Ar^{NCa}}{^{37}Ar^{NCa}}$

$c = \dfrac{^{40}Ar^{NK}}{^{39}Ar^{NK}}$

$\lambda' = \dfrac{\ln 2}{35.1}\ \text{days}^{-1}$ (decay constant for ^{37}Ar)

t is the time interval between irradiation and isotopic analysis of the sample

Δt is the duration of irradiation

$f = \lambda' \Delta t\ (1 - e^{-\lambda' \Delta t})^{-1}$

The values of a, b, and c that have been obtained by a few investigators are presented in Table 3.2. The values for our particular studies are the new ones determined by R. Bottomly (1975, personal communication) for the McMaster University reactor.

TABLE 3.2

Values of Constants for Interfering Isotopes

	a ($\times 10^{-4}$)	b ($\times 10^{-4}$)	c ($\times 10^{-2}$)
Bottomly (1975)	6.51 ± .31	2.54 ± .09	1.56 ± .04
Brereton (1970)	7.19 ± .24	2.47 ± .09	1.23 ± .24
Berger and York (1970)	8.5 ± .4	2.7 ± .3	3.1 ± .7
Turner (1970)	8.0 ± .5	--	--
Mitchell (1968)	30.1	8.8	0.64

"Excess" Argon

It was stated earlier that one of the basic assumptions of potassium-argon dating is that the rock or mineral sample was completely devoid of argon at the time of cooling. This is not always the case and "initial" argon is especially prevalent in volcanic rocks. Initial argon may be present in any of three ways:

i) incorporated

ii) inherited

iii) introduced

Dalrymple and Lanphere (1969) pointed out that the formation of igneous rocks is believed to involve partial or complete melting, a process which would release radiogenic ^{40}Ar. Also, metamorphism would be responsible for release of ^{40}Ar. The question is: what becomes of this gas? Studies on natural gases from wells and fumeroles have shown $^{40}Ar/^{36}Ar$ ratios in excess of 30,000 (Zartman et al., 1961). This would indicate that high ^{40}Ar partial pressures are present during crystallization of minerals, and so ^{40}Ar may be "incorporated" at time of formation.

Argon may be "inherited" from partially outgassed xenoliths or xenocrysts. Further complications arise during some metasomatic process when argon may be "introduced" into a sample, often accompanied by loss or redistribution of existing radiogenic ^{40}Ar.

The presence of extraneous initial ^{40}Ar has long been recognized as a possible cause of high age discrepancies. Conversely, low age discrepancies have been attributed to loss of ^{40}Ar, either by some later

thermal event or by chemical alteration of the potassium bearing phases. This is not necessarily the case. The addition of argon with a $^{40}Ar/^{36}Ar$ ratio less than that of atmospheric argon would be essentially the same as adding ^{36}Ar. Since there is no way of telling what this isotopic ratio is, normal adjustment for atmospheric argon would result in low ages. Thus it is advisable to utilize a method for age calculation which does not rely on ^{36}Ar as a direct correction for atmospheric ^{40}Ar. This will be discussed further later.

Initial argon ratios can be a problem. It is easy to see where ^{40}Ar may come from and thus produce high $^{40}Ar/^{36}Ar$ ratios ("excess argon") and thus high ages. But an excess of ^{36}Ar compared to ^{40}Ar is harder to explain. It is necessary to postulate $^{40}Ar/^{36}Ar$ ratios less than 295.5 in the mantle or perhaps a continuous fractionation process. Evidence for enrichment in ^{36}Ar is given by Dalrymple (1969) who found several historic lavas with ratios less than that of air, and by Cherdyntsev and Shitov (1967) who reported relative excesses of ^{36}Ar of 1 to 6% in gases from several Kamchatka volcanoes. This initial component of argon gas is joined by atmospheric argon which has a $^{40}Ar/^{36}Ar$ ratio of 295.5. It is of interest to see where this component comes from.

Studies by Evernden et al. (1960) and Evernden and Curtis (1965) indicated that much of the atmospheric argon is surface associated. McDougall (1966) found that whole rock samples had an order of magnitude less air argon than mineral separates and attributed it to surface absorption during and after crushing. Mussett and Dalrymple (1968) after an elaborate experiment concluded that negligible amounts of air argon

are acquired in the laboratory and any that is acquired can be removed by simple overnight bakeout at about 200°C.

Keeling and Naughton (1974) demonstrated that the amount of atmospheric argon uptake from crushing rock samples in air was in significant quantities for particle sizes less than 63μ. The amount was related to the surface area but was not held by simple adsorption as it existed even at elevated temperatures, thus it would appear to be due to some form of surface reaction or alteration.

Thus the sources of argon contamination can be summarized as:

(i) initial argon
(ii) surface associated atmospheric (adsorption)
(iii) surface associated atmospheric (surface alteration)
(iv) system associated atmospheric ("blank")

Our studies on the blank have shown that it increases with temperature, but since the temperature and pressure conditions vary from sample to sample, it is not possible to just subtract the blank. The blank has in some cases been observed to be in fact larger than the total gas released in the corresponding heating step of a sample. The implications of these observations will be discussed later.

Correlation Diagrams

As mentioned previously, the important feature of the $^{40}Ar/^{39}Ar$ method is stepwise degassing. The sample is heated at a number of temperature steps and the apparent age is calculated for each step. The apparent age is then plotted against temperature or against the fraction of ^{39}Ar released. The former representation is used in this study. Ideally, the apparent age curve should form a plateau at the

age of the sample, with the lower temperature steps often yielding ages that are too low. However, in many cases a plateau is never formed. This is possibly the result of the atmospheric correction which assumes an $^{40}Ar/^{36}Ar$ ratio of 295.5 when, as indicated earlier, initial argon is often present. An alternate method will be discussed which does not utilize the ^{36}Ar for an atmospheric correction.

The ^{40}Ar content of a mineral is the sum of many components given by:

$$^{40}Ar = {}^{40}Ar^{Atm} + {}^{40}Ar^{I} + {}^{40}Ar^{*} + {}^{40}Ar^{NK} + {}^{40}Ar^{NCa} - {}^{40}Ar^{RR}$$

and ^{36}Ar is given by:

$$^{36}Ar = {}^{36}Ar^{Atm} + {}^{36}Ar^{I} + {}^{36}Ar^{NCa} - {}^{36}Ar^{RR}$$

where the superscript I represents argon in the mineral lattice at the time of the closure of the system; the other components are as before. Dividing ^{40}Ar by ^{36}Ar yields

$$\frac{^{40}Ar}{^{36}Ar} = \frac{{}^{40}Ar^{Atm} + {}^{40}Ar^{I} + {}^{40}Ar^{NK} + {}^{40}Ar^{NCa} - {}^{40}Ar^{RR}}{^{36}Ar} + \frac{^{39}Ar^{NK}}{^{36}Ar}\left(\frac{^{40}Ar^{*}}{^{39}Ar^{NK}}\right) \qquad (3.2)$$

now the total ^{39}Ar measured is

$$^{39}Ar = {}^{39}Ar^{NK} + {}^{39}Ar^{NCa}$$

so equation (3.2) becomes

$$\frac{^{40}Ar}{^{36}Ar} = \frac{{}^{40}Ar^{Atm} + {}^{40}Ar^{I} + {}^{40}Ar^{NK} + {}^{40}Ar^{NCa} - {}^{40}Ar^{RR}}{^{36}Ar} + \frac{^{39}Ar + {}^{39}Ar^{NCa}}{^{36}Ar}\left(\frac{^{40}Ar^{*}}{^{39}Ar^{NK}}\right) \qquad (3.2)$$

by correcting for neutron induced interference isotopes, equation (3.2) becomes:

$$\frac{^{40}Ar^{C}}{^{36}Ar^{C}} = \frac{^{40}Ar^{Atm}}{^{36}Ar^{Atm}} + \frac{^{40}Ar^{I}}{^{36}Ar^{I}} + \frac{^{39}Ar^{C}}{^{36}Ar^{C}} \left(\frac{^{40}Ar^{*}}{^{39}Ar^{NK}}\right)$$

where the superscript C denotes the neutron induced corrected quantities.

This is the equation of a straight line with slope = $^{40}Ar^{*}/^{39}Ar^{NK}$ and intercept = $\frac{^{40}Ar^{Atm} + ^{40}Ar^{I}}{^{36}Ar^{Atm} + ^{36}Ar^{I}}$, the age is calculated in the usual manner. When presented graphically this is called an isochron diagram.

The $^{40}Ar^{C}/^{36}Ar^{C}$ ratios when plotted against the corresponding $^{39}Ar^{C}/^{36}Ar^{C}$ ratios obtained from each of the heating steps should reveal a "linear relationship". However, since the data are subject to experimental errors, this linear relationship has now changed to a relationship which is only linear within the limits of experimental error. It is possible that the data may show a deviation from the linear relationship even beyond that which could be attributed to experimental error. This excess scatter has been called "geological error" (McIntyre et al., 1966). It has been suggested by Brooks et al. (1972) that a line fitted to data with geological error should not be termed an isochron but an "errorchron".

Simple regression techniques of X on Y (X assumed to be error-free), Y on X (Y assumed to be error-free) or even the average of the two have long been recognized as unsuitable for isochron calculation (Murthy and Compston, 1965). It has been necessary to develop regression methods in which allowance is made for the errors of $^{39}Ar^{C}/^{36}Ar^{C}$ (X) and $^{40}Ar^{C}/^{36}Ar^{C}$ (Y) and can distinguish between isochrons and error-

chrons. A number of methods have been developed and are discussed in Appendix B.

The quantity of ^{36}Ar in many gas fractions is quite small, and its measurement is subject to large errors. This results in the errors in the ratios $^{40}Ar^{C}/^{36}Ar^{C}$ and $^{39}Ar^{C}/^{36}Ar^{C}$ being as high as 5 - 10%, and may be as much as 50%, even though ^{40}Ar and ^{39}Ar may be measured with an accuracy of 0.5% or less. Because the uncertainty in ^{36}Ar dominates, the errors in the ratios are highly and positively correlated. The effect of an error in ^{36}Ar is to move a given point along a ^{36}Ar "error-line" which passes through the point and the origin. The ^{36}Ar error-lines are nearly always subparallel to the isochron because the isochron intercept is near zero relative to the values on the ordinate and the abscissa. Thus the points tend to be shifted along the isochron and so have a minimal effect on the slope of the isochron. For this reason the use of a least-squares fit which considers the errors in the ratios as well as the degree of correlation as developed by York (1969) was used for isochron calculation.

Chapter IV: Experimental Procedure

System Description

The argon extraction system is shown schematically in Figure 4.1. The system is divided into three sections. The first section includes the extraction furnace; here a rock or mineral sample is placed in a tantalum crucible which in turn is placed inside a heating coil, also made of tantalum (M.P. 2977°C). The coil assembly is mounted on a flange and access to it is obtained by removing flange and coil assembly. A copper gasket is used to provide an air tight seal between flange and furnace housing. A water jacket surrounds the furnace housing, since temperatures often exceed 1000°C.

A cold finger was attached to the furnace housing in order to attract the gases given off when the sample is heated. This was done since it was found that the coil's life expectancy was substantially reduced when large volumes of gas were given off and allowed to remain in the furnace. The cold finger consits of activated charcoal in a glass tube which is immersed in liquid nitrogen.

The majority of the chemically reactive gases are removed in the second section by use of a titanium getter and a Copper-copper oxide oxidizer. These are heated to operating temperatures and are allowed to cool in two stages after the gas has been exposed to them. This section is connected to the extraction furnace by means of a ultra high vacuum valve ("extraction furnace value"). It is also connected by

Figure 4.1. Schematic diagram of the argon extraction system.

C_1, C_2	Cold Fingers
A_1, A_2, A_3	Air Sample Tubes
I.G.	Ion Gauge

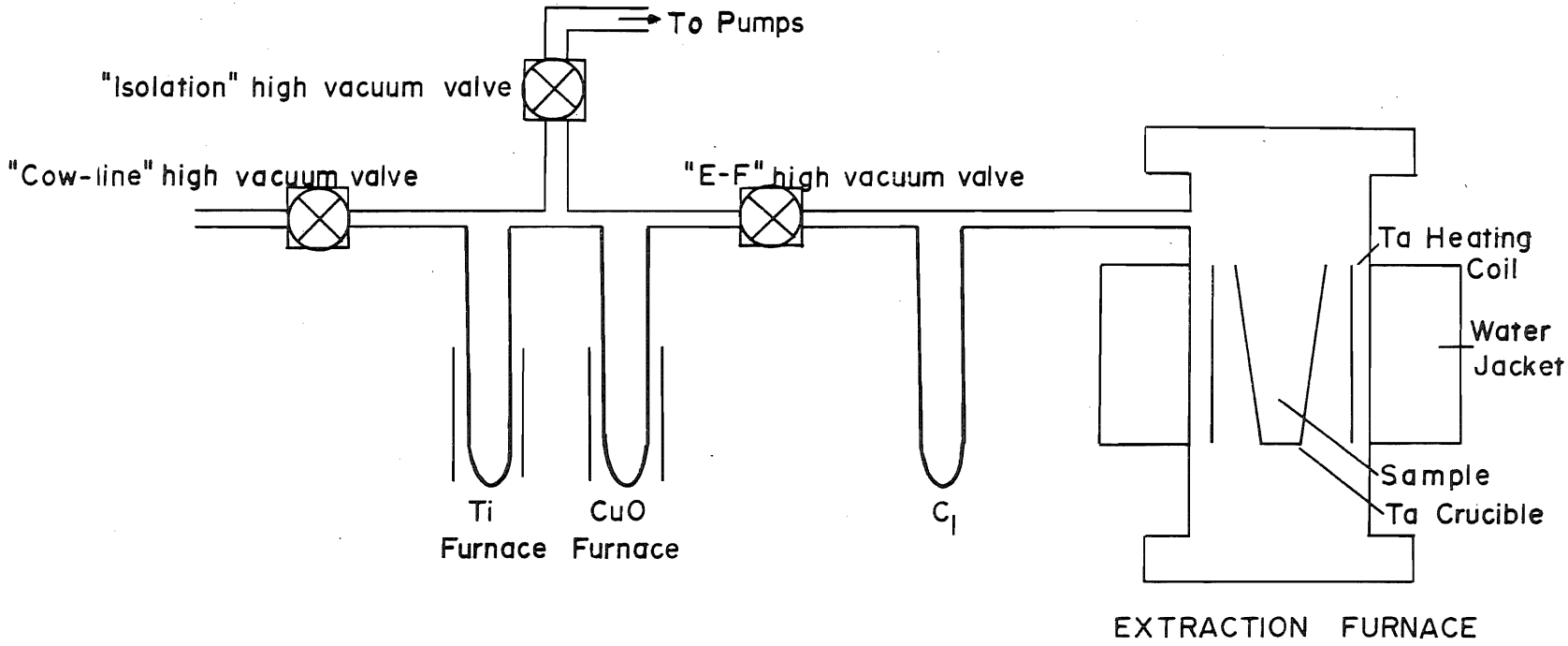

FIGURE 4.1. Schematic Diagram of Argon Extraction System

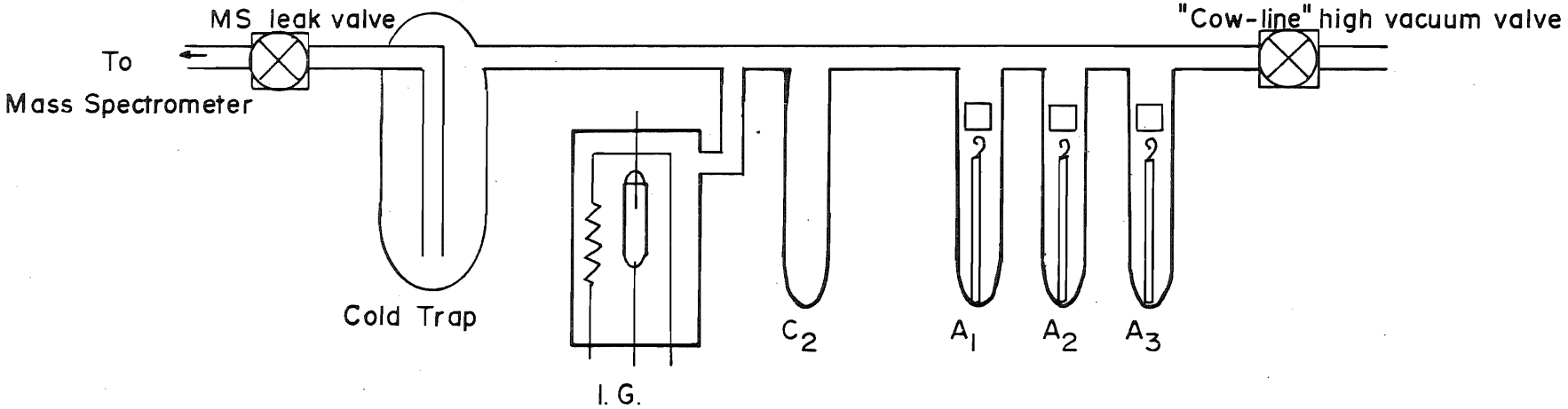

similar valves to the pumping system ("isolation valve") and the third section ("cow-line valve").

As indicated, the third section has been termed the "cow-line". After cleaning, the sample is concentrated in this section by means of a second cold finger. This section is isolated from the rest and further purification is done with a liquid nitrogen cold trap. The purified argon is then analyzed by a (somewhat modified) AEI MS10 mass spectrometer. The sample is let into the mass spectrometer by means of a graduated leak valve.

System pressure is also monitored in the cow-line by an ion gauge. Mass discrimination is monitored by analyzing air samples which are contained in breakable glass vials sealed inside the cow line.

Sample Description

In general, conventional K-Ar age determinations can only be done on fresh, unaltered rocks for which there is no evidence of argon loss. The $^{40}Ar/^{39}Ar$ method is not quite so limited, but it will be shown that care must be taken in choosing samples.

The samples for the present study were supplied by Dr. D. B. Clarke who collected them during the summers of 1966 and 1971. Two additional samples were obtained through the assistance of the National Science Foundation from D.S.D.P. hole 112 (Laughton et al., 1972).

The samples collected from Svartenhuk Peninsula, Baffin Island and Ubekendt Island have been discussed in Chapter I. In summary, four basaltic samples and two late stage trachytic samples were obtained from

Svartenhuk, three basaltic samples were obtained from Baffin Island and three samples from lamprophyre dykes were obtained from Ubekendt Ejland. Brief petrographic descriptions and some chemical analyses are presented in Appendix D.

In 1970 the Glomar Challenger undertook the drilling of a hole in the ocean floor approximately 20 km. east of a structure which is part of the mid-Labrador Sea Ridge (Location: 54° 01.0'N, 46° 36.24'W) at a depth of 3657 m. Before drilling was terminated three metres of basalt had been drilled, of which about half had been recovered. One sample was obtained from the top and one from the bottom of the recovered section.

A standard sample of known age was used as flux monitor. This sample, a biotite mica, No. 71-232, has an age (obtained by the conventional K-Ar method) of 370 ± 4 my (revised from Kublick, 1972).

Sample Preparation

Sample preparation was relatively simple. Samples were crushed using a steel piston and plate. The crushed sample was size sorted and only the -1 to 0 Ø mesh size was retained, since addition of atmospheric argon would be expected with smaller size fractions (Keeling and Naugton, 1974). Samples were then hand picked in order to ensure that any weathered surfaces were excluded, and then washed in acetone and distilled water. Preparatory to irradiation, samples were wrapped in aluminum foil which had been washed in acetone.

Irradiation Requirements

In order to prepare a sample for $^{40}Ar/^{39}Ar$ dating it is necessary to consider two important parameters: the sample size and the integrated neutron flux. The size of the sample is determined by the atmospheric argon background level, the potassium content and the approximate age of the sample. The size of the atmospheric argon background (i.e. the "blank") in the mass spectrometer and in the extraction/purification system will determine the volume of radiogenic ^{40}Ar that is measureable. Once this volume has been determined ($10^{-6}cm^3$ STP of $^{40}Ar^*$ in this laboratory) the sample size is determined by the age (obviously the older the sample the more $^{40}Ar^*$ is produced) and the potassium content (similarly the higher the potassium content the more $^{40}Ar^*$ is produced). This is illustrated in Figure 4.2.

The choice of an optimum integrated neutron flux requires that a number of conditions are met. The most important factors are: i) sufficient ^{39}Ar must be produced from ^{39}K so that an accurate age may be determined, ii) production of ^{39}Ar from ^{42}Ca (see Table 3.1) must be small compared to (i), iii) production of ^{36}Ar from ^{40}Ca (see Table 3.1) must be insufficient to cause significant errors in the atmospheric argon correction, iv) production of ^{40}Ar from ^{40}K (see Table 3.1) must be small compared to $^{40}Ar^*$. While Mitchell (1968b) has shown that problems do not arise if $K/Ca > 0.1$, typical basalts have $K/Ca \approx 0.5$. Turner (1971) has shown that if $K/Ca > 0.01$ a value can be found for the integrated neutron flux which will satisfy all these conditions (Figure 4.3).

Figure 4.2. Sample size required to yield 10^{-6} cm^3 STP of radiogenic ^{40}Ar. The figures on the curves refer to potassium content (after Turner, 1971).

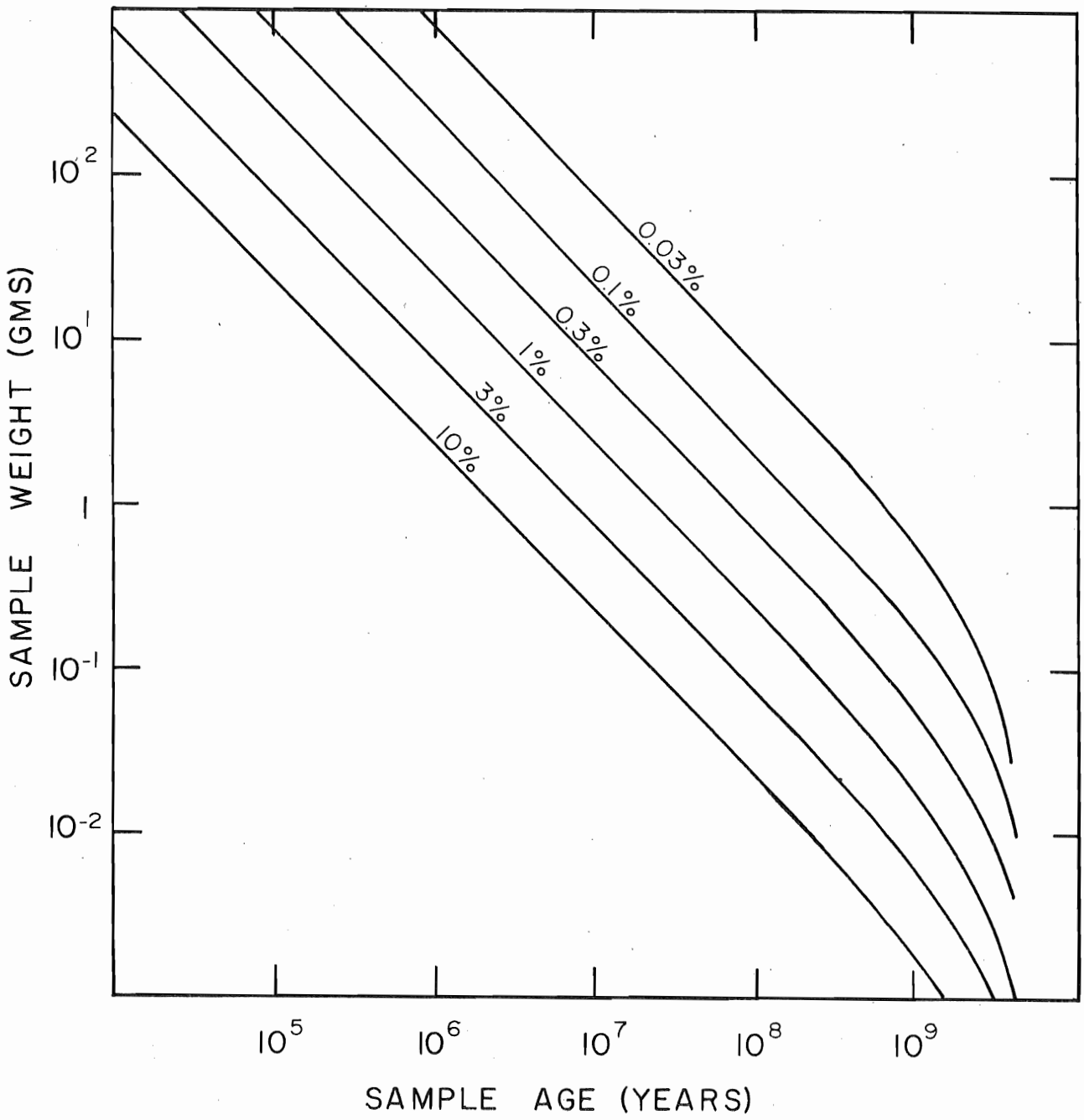
SAMPLE WEIGHT (GMS)
10^2
10^1
1
10^-1
10^-2
0.03%
0.1%
0.3%
1%
3%
10%
10^5
10^6
10^7
10^8
10^9
SAMPLE AGE (YEARS)

Figure 4.3. Integrated fast neutron flux requirements to maximize ^{39}Ar production and minimize ^{40}Ar and ^{36}Ar interference effects (after Turner, 1971). Small vertical displacements may be necessary for application to the McMaster University reactor.

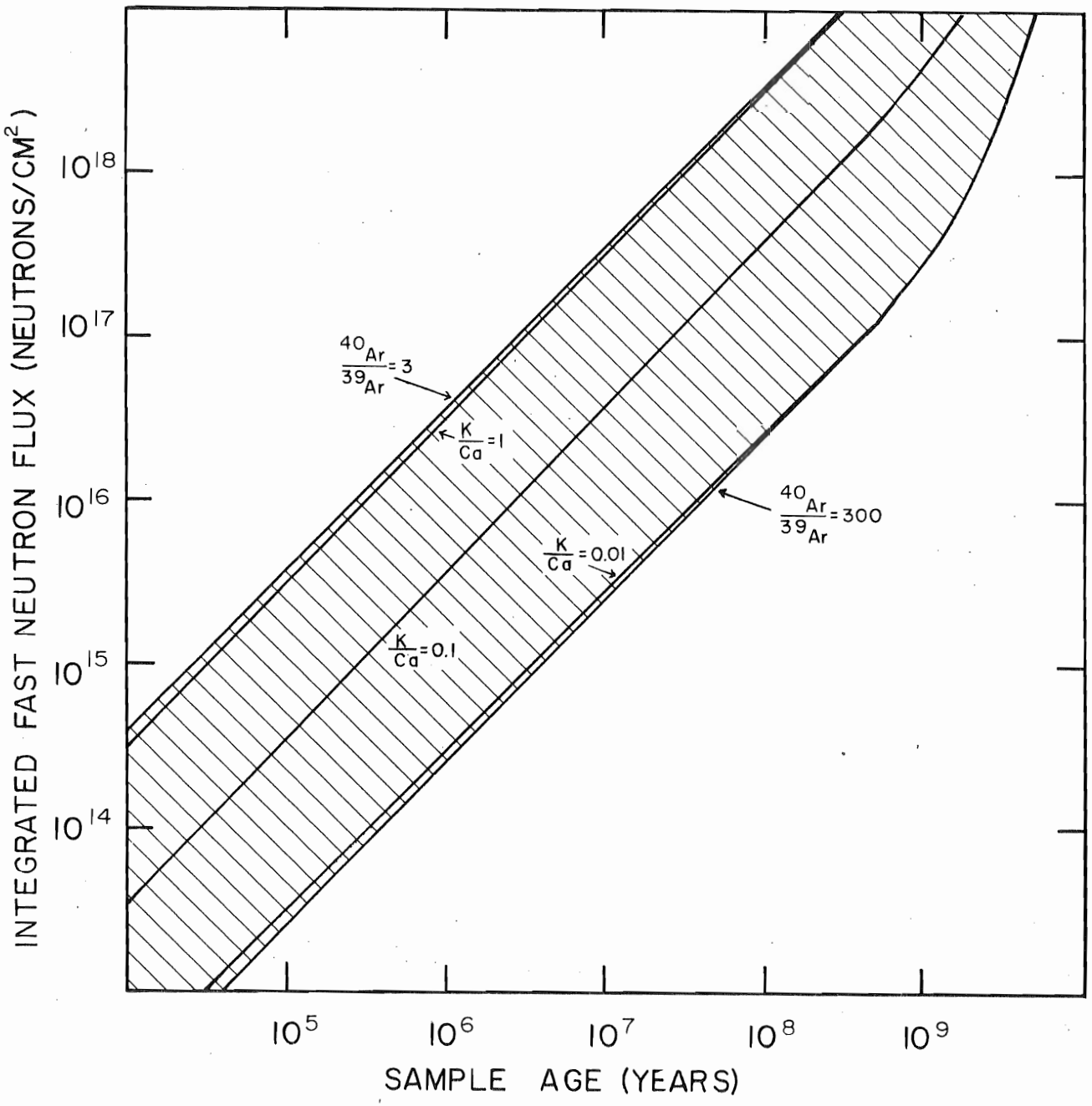
INTEGRATED FAST NEUTRON FLUX (NEUTRONS/CM^2)
10^{18}
10^{17}
10^{16}
10^{15}
10^{14}
$\frac{^{40}Ar}{^{39}Ar}=3$
$\frac{K}{Ca}=1$
$\frac{^{40}Ar}{^{39}Ar}=300$
$\frac{K}{Ca}=0.01$
$\frac{K}{Ca}=0.1$
10^5
10^6
10^7
10^8
10^9
SAMPLE AGE (YEARS)

In order to produce sufficient ^{39}Ar, say $^{40}Ar/^{39}Ar \leq 300$, the amount of integrated neutron flux must be greater than or equal to the curve $^{40}Ar/^{39}Ar = 300$ in Figure 4.3. Similarly, in order to minimize the interference from potassium derived ^{40}Ar and calcium derived ^{36}Ar, the amount of integrated neutron flux for a given K/Ca ratio, say 0.01 must be less than or equal to the curve K/Ca = 0.01 in Figure 4.3 The remaining parameter, age, then sets the area of optimum integrated fast neutron flux. Note that the flux is independent of the absolute potassium content.

For the present basalt samples, K/Ca $\approx$ .04 and they are about 60 my old (Paleocene). Hence, in order to obtain maximum ^{39}Ar production the optimum flux is approximately 1×10^{16} n cm^{-2}. More latitude exists for the trachytes as well as for biotite micas, which are rich in potassium and low in calcium. Thus, the above value will be good for all the samples and the standards.

The total flux density of the McMaster University reactor, where all the samples were irradiated, is $1.1 - 2.0 \times 10^{13}$ n cm^{-2} sec^{-1} of which approximately 5% is epithermal. Nominal flux density gradients are of the order of 1 - 2% (Berger and York, 1970).

Thirteen rock chip samples were wrapped in aluminum foil along with twenty-six standard samples and were arranged within a number of aluminum sample cans. Due to the size of the samples more than one can was necessary. The arrangements are shown in Figures 4.4 to 4.9. Sample sizes ranged from 40 mg for the biotites to 2 g. for the basalts. Time of irradiation varied from 12 to 48 hours subsequent to which

Figures 4.4 to 4.9. Sample arrangement in aluminum sample cans.

S	Standard
XX	Not in this Study
A, B	Halves of Same Sample

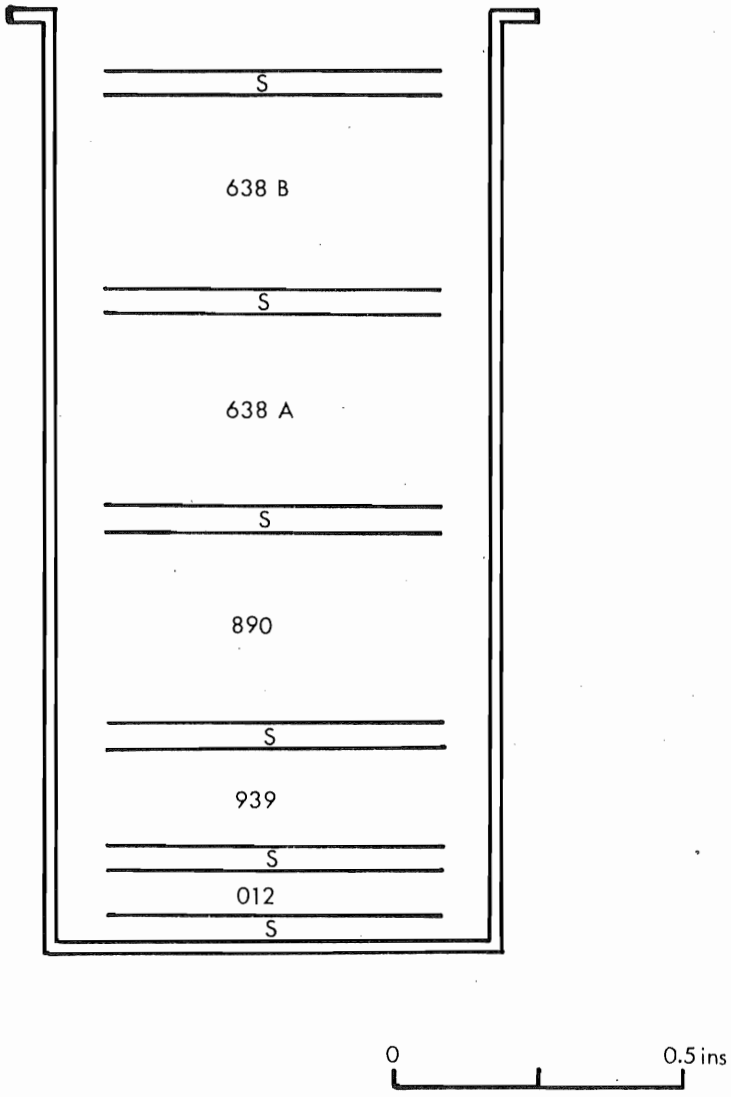

Figure 4.4. Can No. 1

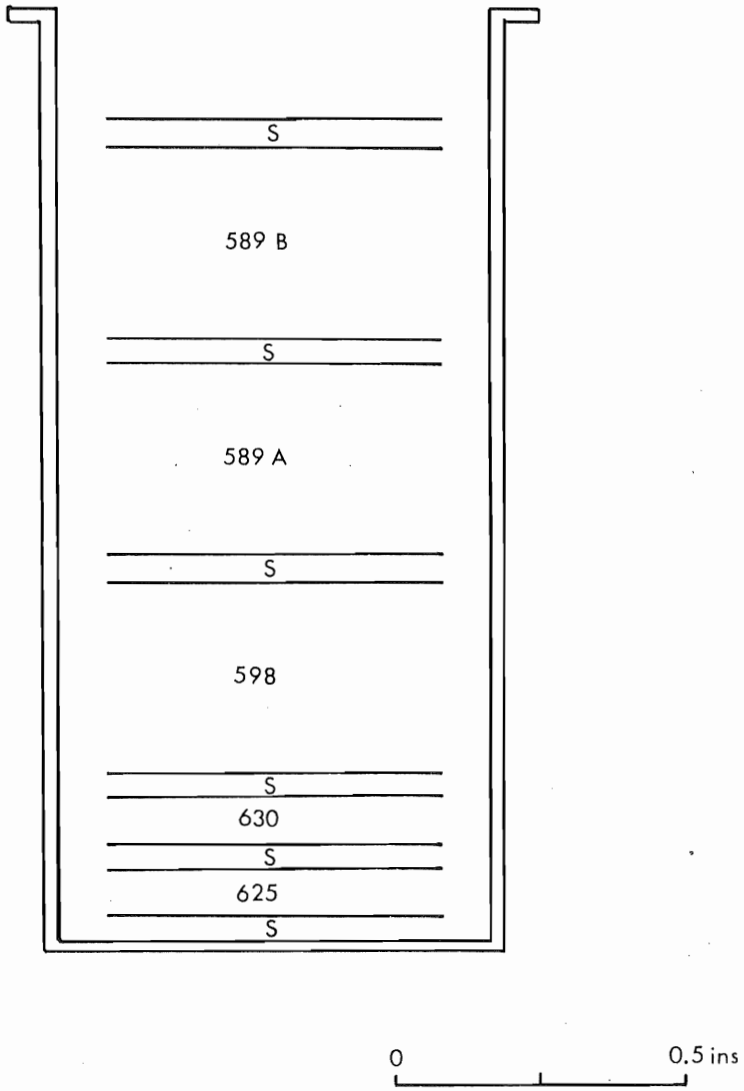

Figure 4.5. Can No. 2

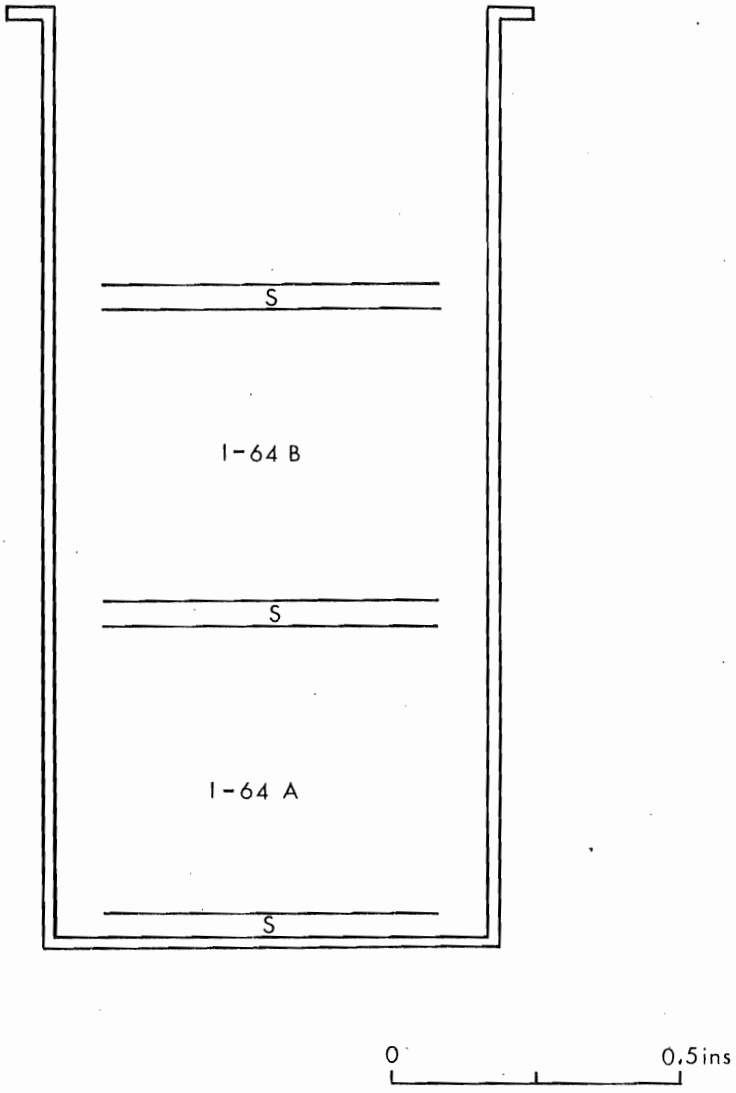

Figure 4.6. Can No. 3

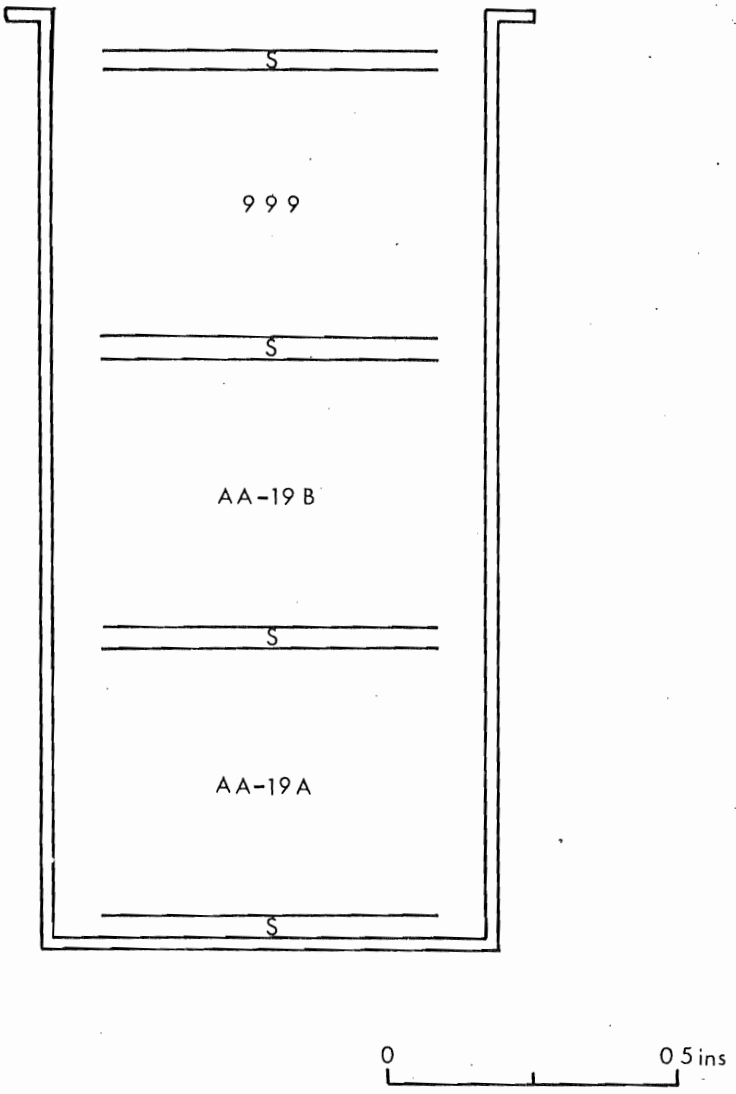

Figure 4.7. Can No. 4

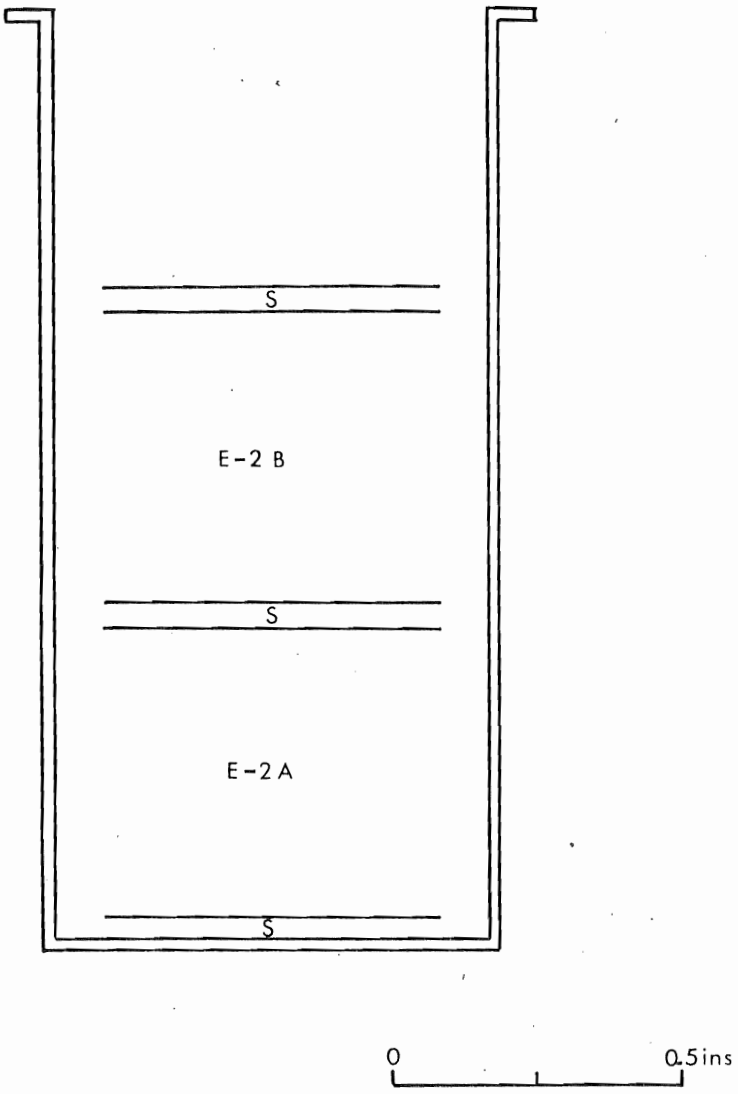

Figure 4.8. Can No. 5

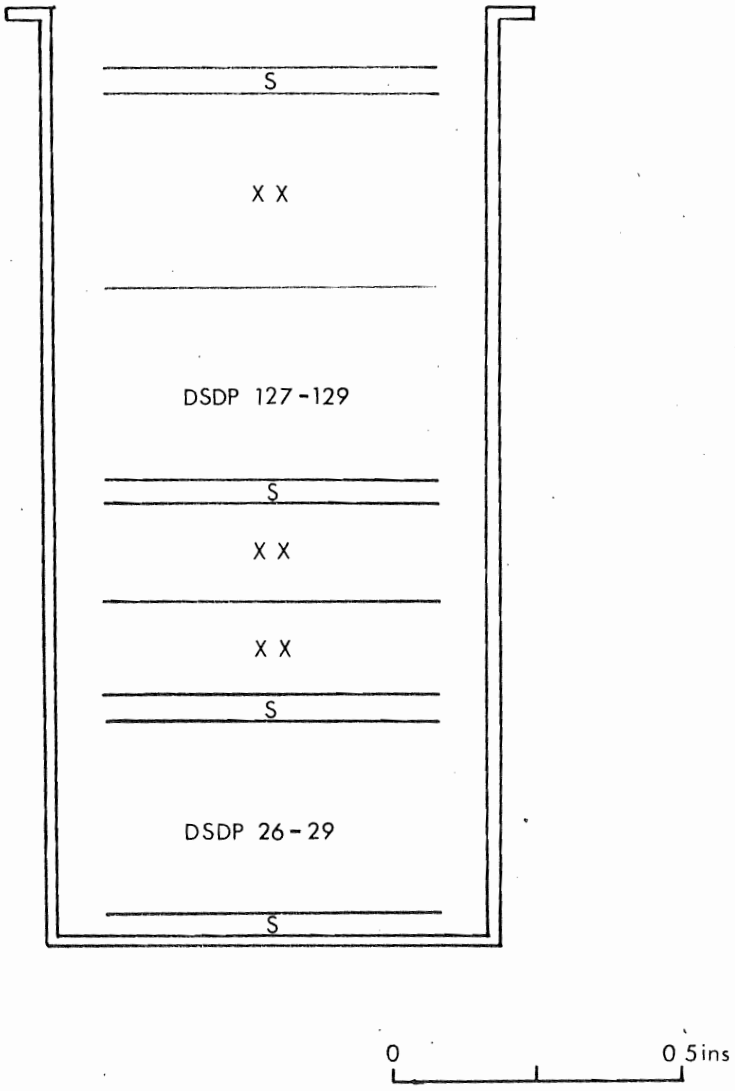

Figure 4.9. Can No. 6

samples were cooled for at least two weeks to allow time for short lived isotopes to decay.

Analysis

All the samples were outgassed in a step-wise manner; a procedure which involved at least five temperature steps. The gas evolved at each step was collected for analysis. The biotite standards were heated for one step only but were not totally outgassed. This was a safety procedure for in the case of sample loss the remaining gas would be availble for analysis. The samples were heated for one hour and cleaned in two steps of twenty minutes each. Mass spectrometrically produced peak heights corresponding to masses 40, 39, 37, 36 were measured in order to obtain the ratios $^{40}Ar/^{39}Ar$, $^{37}Ar/^{39}Ar$ and $^{36}Ar/^{39}Ar$. It is assumed that the respective peaks consist only of argon. The precision of measurement of these ratios was usually better than 1%. The uncertainties in mass spectrometer discrimination and in the isotopic fractionation produced by the leak value give rise to a probable error of ± 1%.

The absolute error in the $^{40}Ar^{*}/^{39}Ar^{NK}$ ratio can be calculated from the absolute errors in the measured isotopic ratios (denoted by superscript m) from:

$$\Delta F = \left(\left[\Delta \frac{^{40}Ar^{m}}{^{39}Ar^{m}}\right]^{2} - \left[295.5 \;\Delta \frac{^{36}Ar^{m}}{^{39}Ar^{m}}\right]^{2}\right) +$$

$$\left[a \frac{^{40}Ar^{m}}{^{39}Ar^{m}} - 295.5 \;a \frac{^{36}Ar^{m}}{^{39}Ar^{m}} + 295.5 \;b\right]\left[\Delta \frac{^{37}Ar^{m}}{^{39}Ar^{m}}\right]^{2}\Big)^{1/2}$$

where $F = \dfrac{^{40}Ar^{*}}{^{39}Ar^{NK}}$

This expression is derived in Appendix F1. The variance, σ_F^2 , may then be approximated by:

$$\sigma_F^2 = \frac{A^2\ \sigma_A^2 + 295.5^2\ B^2\ \sigma_B{}^2 + (aA - 295.5\ aB + 295.5\ b)^2 D^2 \sigma_D{}^2}{F^2}$$

where A, B and D refer to the isotopic ratios $\frac{^{40}Ar^m}{^{39}Ar^m}$, $\frac{^{36}Ar^m}{^{39}Ar^m}$ and $\frac{^{37}Ar^m}{^{39}Ar^m}$ respectively; and $\sigma_A{}^2$, $\sigma_B{}^2$, and $\sigma_D{}^2$ are their respective variances. The values for the isotopic interference correction factors were given earlier (see Table 3.2).

Chapter V: Experimental Results and Conclusions

Standards

The results obtained from the 26 biotite standards are shown in Table 5.1 Note that not all the standards have been run since the second parts of the large samples were not analyzed. J was calculated from equation (2.18) with $t_s = 370 \pm 4$ my. The variance of J in percent, σ_J^2, can be obtained by differentiating equation (2.15). The result (see Appendix F2) is:

$$\sigma_J^2 = \frac{(\lambda^2 t_s^2 e^{2\lambda t_s})}{(e^{\lambda t_s}-1)^2} \sigma t_s^2 + \sigma^2_F$$

σ_J^2 is primarily controlled by $\sigma_{t_s}^2$, the variance in the standard age. As can be seen in Table 5.1, σ_J seldom exceeds 1.5%.

Since insufficient quantities of ^{37}Ar were detected in all of the standard samples, corrections for interfering isotopes were small or non-existent. This is usually the case for minerals which have a high K/Ca ratio.

Horizontal flux gradients in the sample cans were assumed to be small. The vertical flux gradient was obtained by plotting the J value calculated from each standard sample against its position in the can. The observed variation in J over the length of the cans was in some cases as high as 14% (see Figures 5.1 to 5.6). The J-values for the unknown samples were interpolated from the respective figures and are good to within ± 2%.

TABLE 5.1

FLUX MONITOR RESULTS

Standard	$\frac{^{40}Ar}{^{39}Ar}$	$\frac{^{36}Ar}{^{39}Ar}$	$\frac{^{40}Ar^{*}}{^{39}Ar^{NK}}$	J	σ_J(%)
Can # 1, S1	80.97	0.0658	61.483	0.003527	1.26
S2	1302.02	4.2020	60.290	0.003597	40.29
S3	68.92	0.0291	60.280	0.003598	1.22
S4	89.06	0.0943	61.187	0.003544	1.28
S5	113.57	0.1714	62.899	0.003448	1.35
S6	93.08	0.0985	63.952	0.003391	1.31
Can # 2, S1	77.55	0.0472	63.581	0.003411	1.25
S2	77.41	0.0382	66.078	0.003282	1.23
S3	107.94	0.1334	68.479	0.003167	1.26
S4	101.05	0.1139	67.359	0.003220	1.25
S5	108.14	0.1323	69.032	0.003142	1.28
S6	120.32	0.1622	72.360	0.002997	1.27
Can # 3, S1			not analyzed		
S2	189.43	0.1197	154.04	0.001408	1.51
S3	171.32	0.0667	151.60	0.001431	1.34
Can # 4, S1			not analyzed		
S2	194.59	0.1026	164.26	0.001320	1.60
S3	203.69	0.1568	157.39	0.001378	1.65
S4	427.48	0.9273	153.44	0.001413	5.18
Can # 5, S1			not analyzed		
S2	206.71	0.0814	182.62	0.001188	1.39
S4	190.82	0.0349	180.49	0.001202	1.37
Can # 6, S1	156.99	0.0447	143.76	0.001509	1.27
S2	155.44	0.0819	131.21	0.001653	1.25
S3	156.10	0.0795	132.57	0.001636	1.22
S4	136.38	0.0327	126.68	0.001712	1.32

* this sample was partially lost in the purification procedure

Figures 5.1 to 5.6. Observed vertical variation in J over length of sample cans.

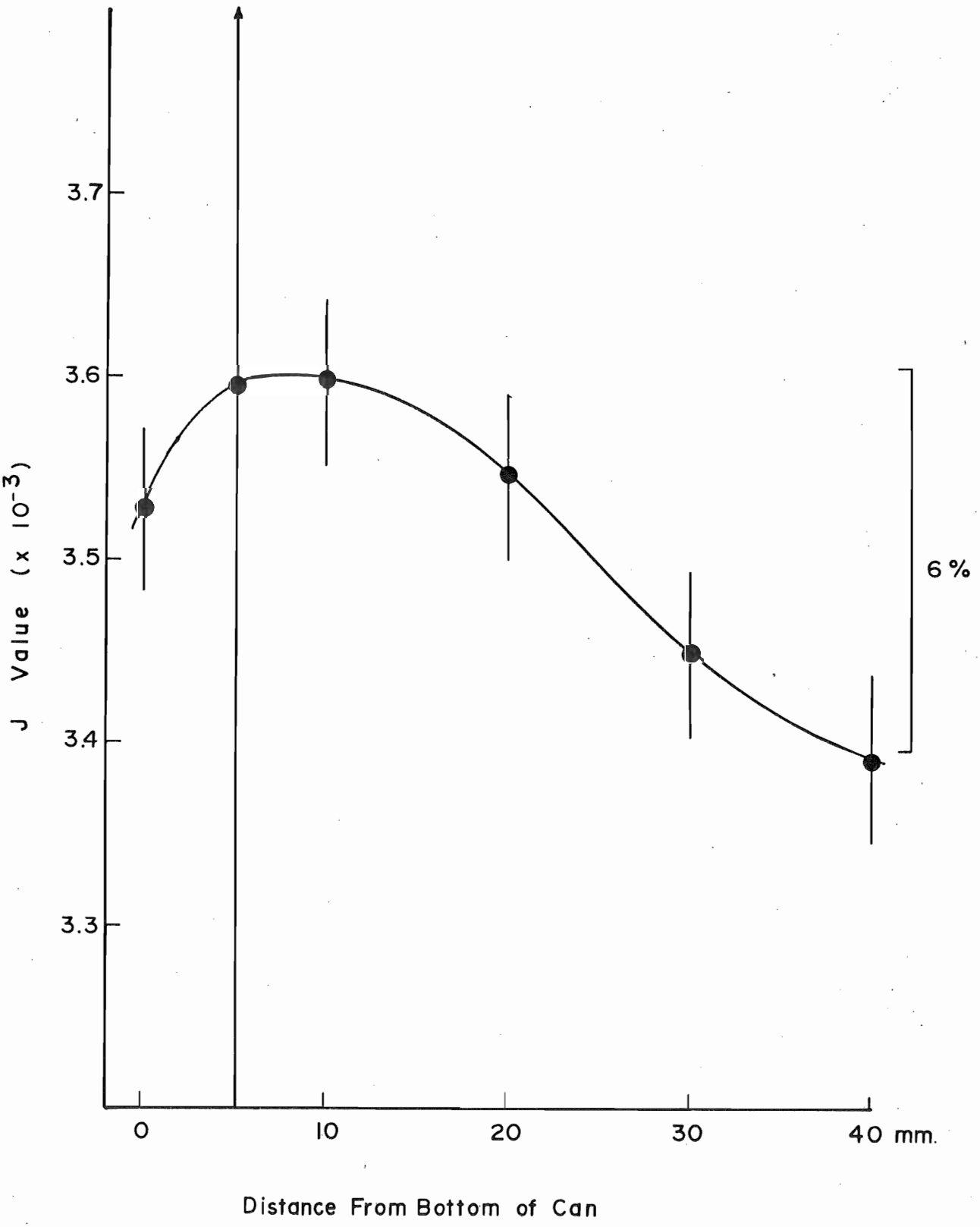

Figure 5.1. Can No. 1

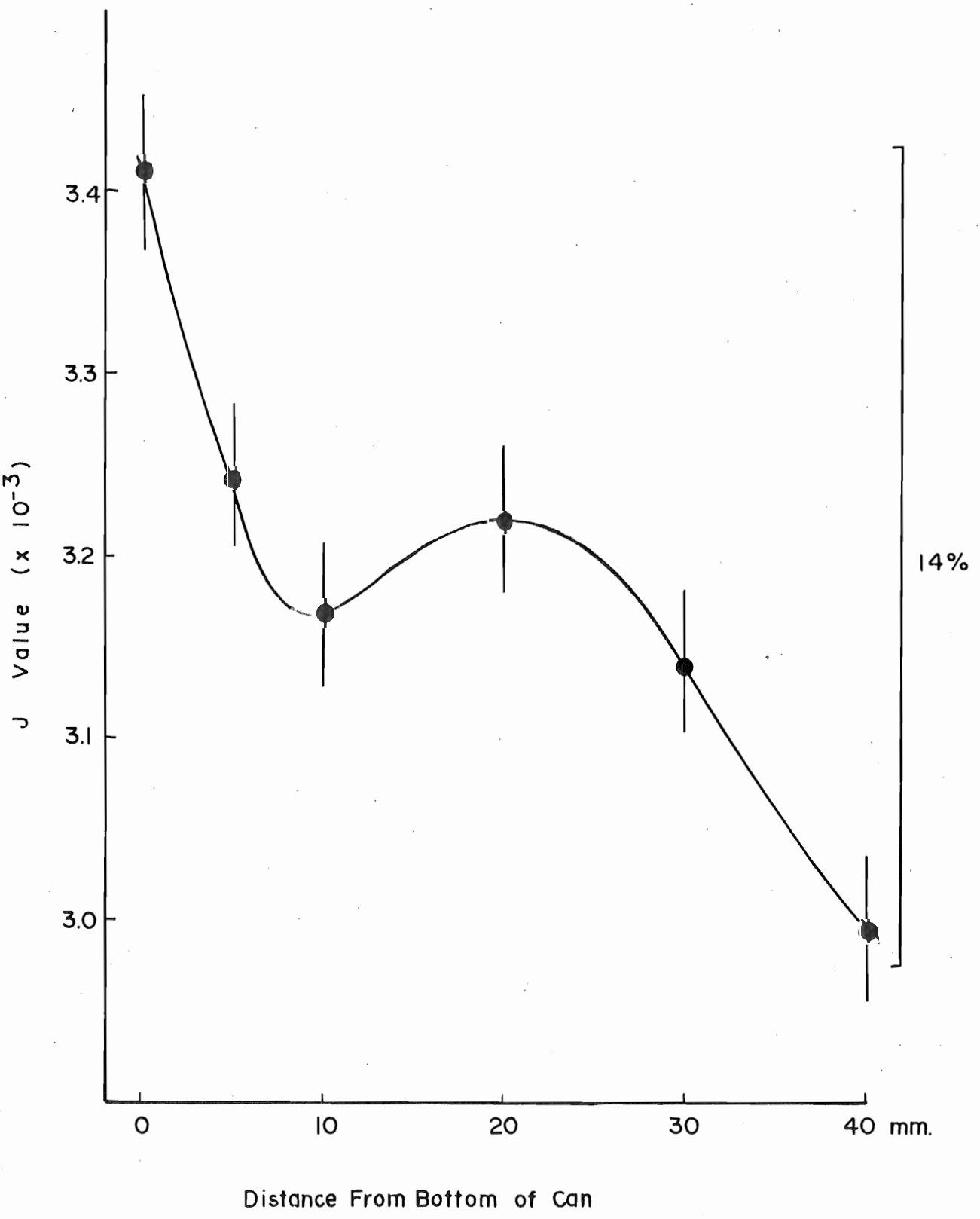

Figure 5.2. Can No. 2

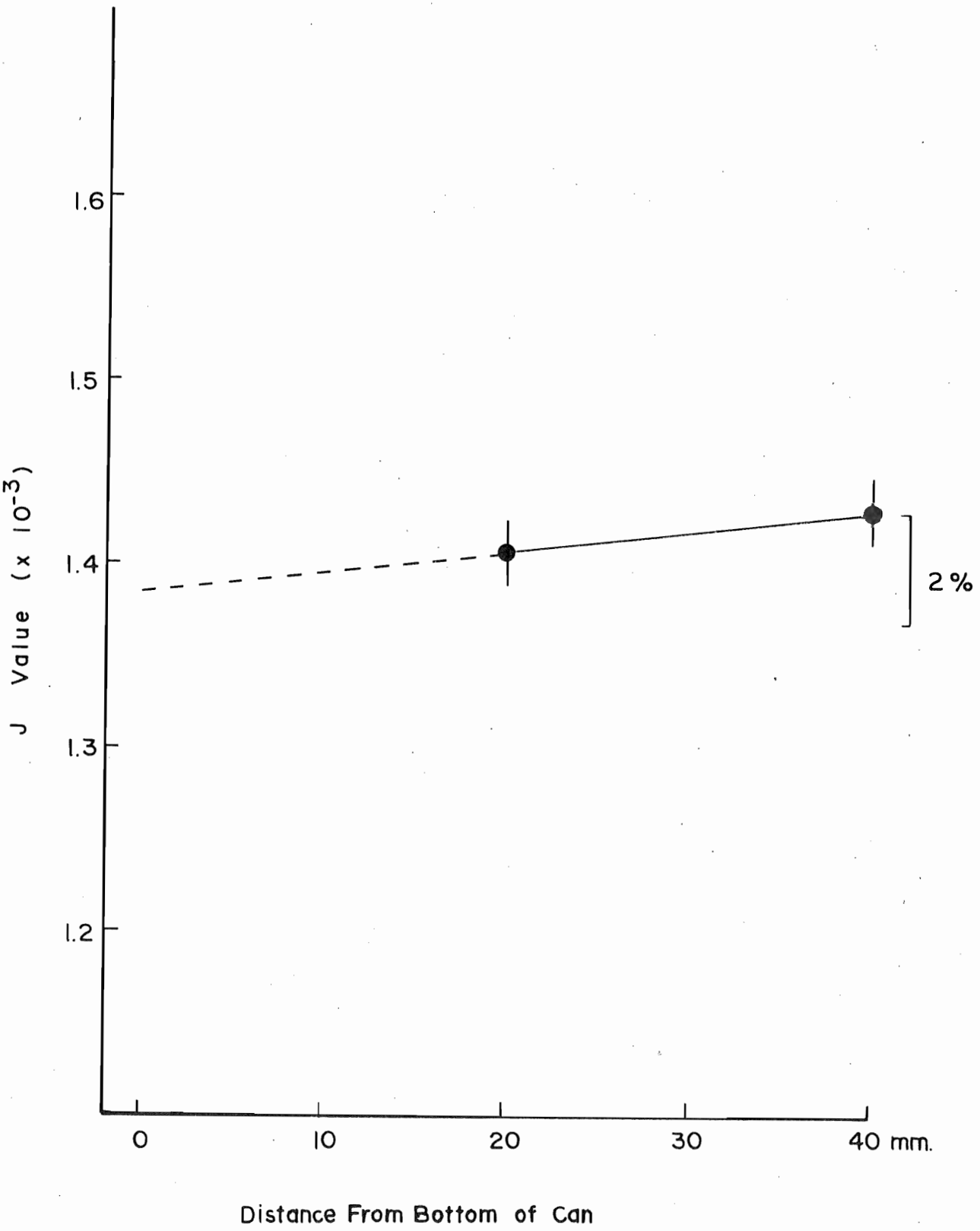

Figure 5.3. Can No.3

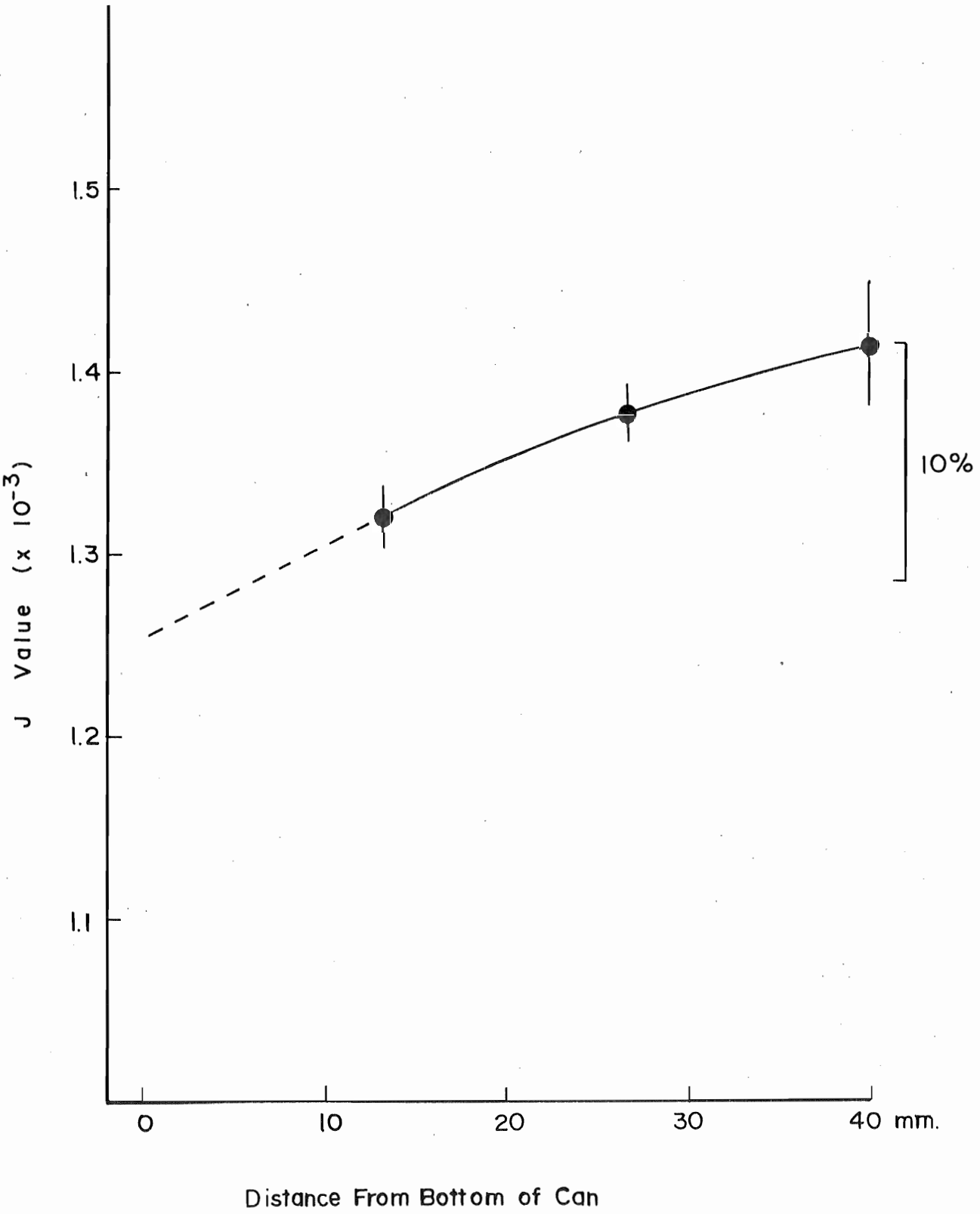

Figure 5.4. Can No. 4

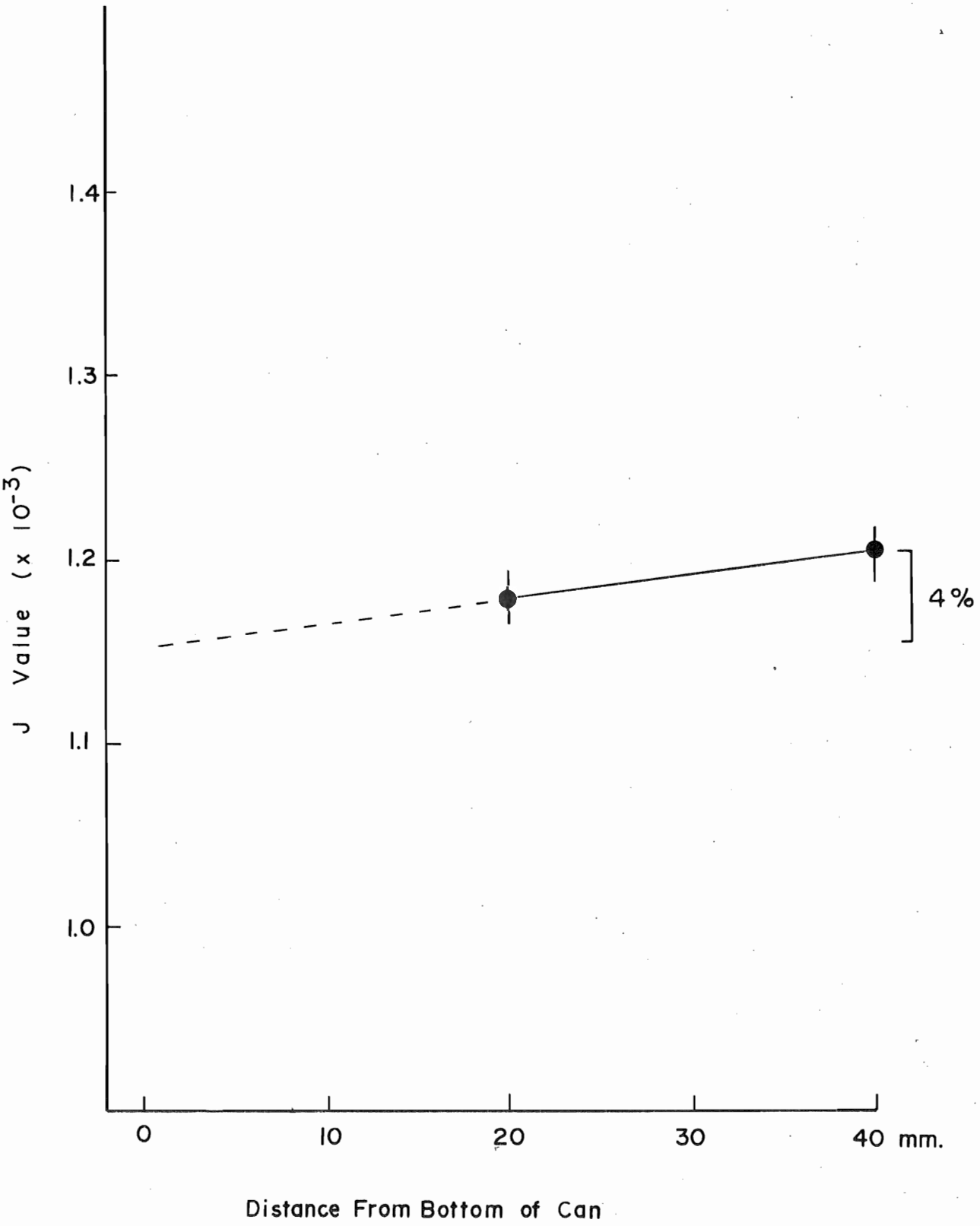

Figure 5.5 Can No.5

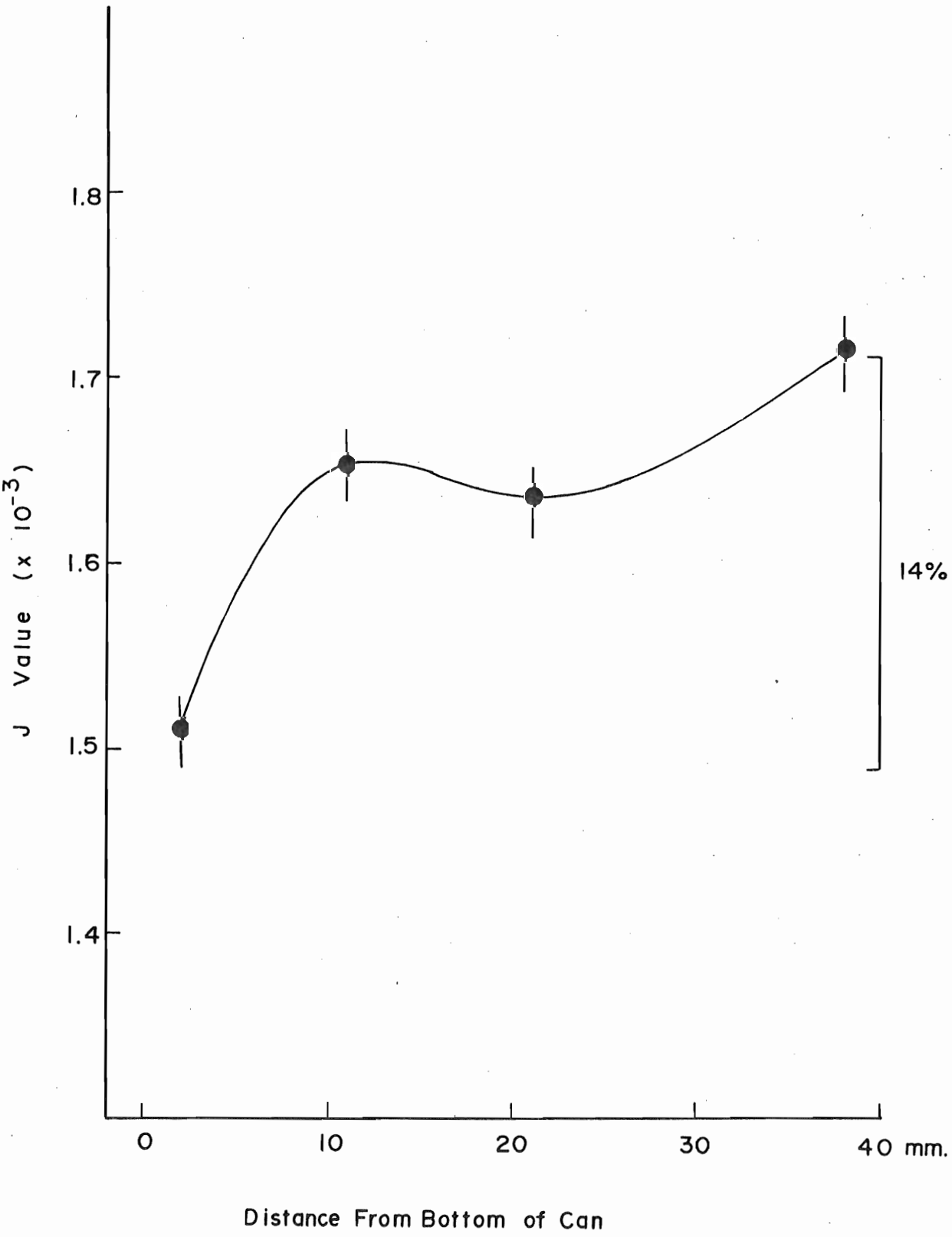

Figure 5.6. Can No. 6

The Unknown Samples

(a) General Observations: The apparent ages, t_u, were calculated using equation (2.20) and the variances in the apparent ages, σ_{t_u}, from the following expression

$$\sigma^2 t_u = \frac{J^2 F^2}{\lambda^2 t_u} \frac{(\sigma_F^2 + \sigma_J^2)}{(1 + FJ)^2} \qquad \text{(see Appendix F3)}$$

Apparent age ($\pm 2\sigma$) plotted against temperature for each heating step yields an age spectrum diagram for each of the samples (see Appendix C).

A cursory observation of the age spectra yields a few noteworthy features; the most apparent of these is the existence of negative ages. These probably result from the application of the standard atmospheric argon correction in cases where the true $^{40}Ar/^{36}Ar$ ratio is less than 295.5. Conversely, the extremely old apparent ages present in one sample are probably due to the fact that the true $^{40}Ar/^{36}Ar$ ratio is less than 295.5.

(b) Samples 625 and 630 (the youngest rocks from Svartenhuk Peninsula): From an observation of the release data a plateau age is not extremely well-defined in either sample; however, it is apparent that the ages are between 50 and 70 my (see Table 5.2 and Appendix C). The mean and total gas ages are shown in the summary table (Table 5.12). Isochron ages ($\pm 2\sigma$) are 57.9 ± 1.6 and 58.1 ± 3.8 my. respectively (see Table 5.3 and Appendix D). It should be noted that the large scatter for sample 625 is almost totally contributed by one point. A more careful examination of the release data suggests the existence of a double plateau, one at lower extraction temperatures and one at higher

TABLE 5.2 ANALYTICAL DATA FOR $^{40}Ar/^{39}Ar$ INCREMENTAL HEATING: SAMPLES 630 AND 625

Sample No.	Step(°C)	F	ΔF	Atmospheric Contamination	^{39}Ar released (% of total)	$^{37}Ar/^{39}Ar$	$t_u \pm 2\sigma$ (my)
630	300-500	9.98	0.80	85.4	1.9	0.00	59.4 ± 9.3
	500-590	10.08	0.21	47.7	25.2	0.06	60.0 ± 2.4
	590-690	9.66	0.04	26.3	42.4	0.05	57.6 ± 0.4
	690-760	9.56	0.05	36.4	17.7	0.05	57.0 ± 0.6
	760-830	8.92	0.14	65.1	3.7	0.16	53.2 ± 1.7
	830-950	9.39	0.23	67.9	5.4	0.30	56.0 ± 2.6
	950-1100	8.48	0.28	82.9	3.6	0.60	50.6 ± 2.4
	K% = 3.94	Ca% = 1.07		K/Ca = 3.68			
625	300-500	9.49	0.02	13.5	27.2	0.03	58.8 ± 0.2
	500-590	9.37	0.02	10.3	24.5	0.03	58.1 ± 0.3
	590-690	9.36	0.02	16.9	24.0	0.04	58.0 ± 0.3
	690-760	9.89	0.15	73.5	1.1	0.09	61.2 ± 1.8
	760-830	10.77	0.29	72.7	1.5	0.18	66.6 ± 2.5
	830-960	10.65	0.03	22.1	19.7	0.02	65.8 ± 0.3
	960-1100	9.30	0.25	83.7	2.0	0.30	57.7 ± 3.0
	K% = 4.68	Ca% = 0.71		K/Ca = 6.53			

TABLE 5.3 ANALYTICAL DATA FOR ISOCHRON CALCULATION: SAMPLES 630 AND 625

Sample No.	Step(°C)	$^{40}Ar/^{36}Ar$	$^{39}Ar/^{36}Ar$	$\Delta^{40}Ar/^{36}Ar$	$\Delta^{40}Ar/^{36}Ar$	$t_u \pm 2\sigma$ (my)
630	300-500	346.1	5.30	4.49	.059	59.5 ± 9.3
	500-590	619.9	33.48	8.86	.365	60.0 ± 2.4
	590-690	1125.2	89.32	8.21	.625	57.6 ± 0.4
	690-760	811.3	56.15	7.14	.483	57.0 ± 0.6
	760-830	454.2	18.51	3.86	.154	53.2 ± 1.7
	830-950	435.1	14.49	4.83	.158	56.0 ± 2.6
	950-1100	356.5	7.49	2.35	.043	50.6 ± 2.4
	Age = 57.9 ± 2.6 my		Intercept = 287. ± 3.5		SUMS = 26.4	
625	300-500	2182.1	199.0	15.93	1.433	58.8 ± 0.2
	500-590	2879.2	275.6	16.12	1.433	58.1 ± 0.3
	590-690	1747.3	155.1	9.44	.807	58.0 ± 0.3
	690-760	402.3	10.8	2.05	.051	61.2 ± 1.8
	760-830	406.6	10.3	3.94	.097	66.6 ± 2.5
	830-960	1339.2	98.0	5.89	.392	65.8 ± 0.3
	960-1100	353.0	6.18	1.73	.027	57.7 ± 3.0
625 + 630	Age = 58.1 ± 3.8 my		Intercept = 312.0 ± 23.7		SUMS = 2718.4	
	Age = 58.4 ± 3.2 my		Intercept = 302.0 ± 12.7		SUMS = 3123.1	

temperatures. The corresponding isochron ages are 66.4 my and 58.1 my for the high and low temperature data respectively. It is not likely that this sample has recorded a second thermal event postdating an initial cooling 66 my ago since the companion sample 625 apparently has not. Rather more likely, this high age is probably a perturbation effect due to the presence of initial argon with a $^{40}Ar/^{36}Ar$ ratio greater than 295.5. This will be discussed more fully later.

(c) Samples 589, 598, 999 (and 638) (basalts from Svartenhuk Peninsula): By observing the release data one can see that there is not the slightest suspicion of a plateau age in any sample (see Table 5.4, Appendix C). These "saddle" or "half-saddle" appearances (e.g. samples 589 and 598) seem to be characteristic of a rock sample with a $^{40}Ar/^{36}Ar$ initial ratio less than 295.5 (that of air; Nier, 1950). Sample 999 appears to have a random distribution.

The data for the isochrons are given in Table 5.5 and are graphically represented in Appendix D. Sample 589 (51.9 ± 20.0 my) has very poor accuracy and is not statistically different from the previous samples (at the 95% confidence limit). Sample 598 (59.8 ± 3.8 my) gives a more reliable age. Even though not statistically different from the previous samples (at the 95% confidence limit), stratigraphically this sample should be older than the others above. Finally, sample 999 (60.0 ± 32.2 my), although it should be the oldest, is not statistically different from the others either (at the 95% confidence limit). The uncertainties in the above ages result primarily from errors in the measurements of the isotopic ratios (a consequence of low potassium

TABLE 5.4 ANALYTICAL DATA FOR $^{40}Ar/^{39}Ar$ INCREMENTAL HEATING: SAMPLES 589, 598, 999 (AND 638).

Sample No.	Step(C°)	F	ΔF	Atmospheric Contamination	^{39}Ar Released (% of total)	$^{37}Ar/^{39}Ar$	$t_u \pm 2\sigma$ (my)
589	300-500	-39.17	144.5	102.5	4.1	5.19	-254.1 ± 1764.3
	500-590	-45.20	119.0	103.6	12.3	13.83	-295.3 ± 1683.3
	590-690	-20.45	9.93	103.3	7.7	5.70	-127.9 ± 128.6
	690-760	- 8.28	6.15	102.1	16.3	4.85	- 50.7 ± 76.4
	760-830	4.30	1.59	97.0	25.1	2.85	25.8 ± 18.9
	830-950	4.23	.72	96.0	32.1	3.72	25.4 ± 8.6
	950-1200	3.36	8.68	99.5	2.4	355.84	20.2 ± 102.9
	K% = .265	Ca% = 7.79		K/Ca = .034			
598	300-500	10.31	.43	58.7	9.8	1.66	60.0 ± 4.9
	500-590	10.09	.11	38.3	28.9	3.78	58.7 ± 1.3
	590-690	7.53	1.09	96.4	9.0	8.40	44.0 ± 12.6
	690-760	- 1.64	2.16	100.8	24.5	10.90	- 9.7 ± 25.7
	760-830	- 2.91	4.57	101.0	15.0	14.20	- 17.3 ± 54.5
	830-950	-14.29	14.38	103.1	4.1	29.53	- 86.4 ± 177.8
	950-1050	- 1.00		100.5	8.6	108.74	- 5.9 ± 40.6
	K% = .67	Ca% = 9.31		K/Ca = .072			

continued on following page

TABLE 5.4 (CONTINUED)

Sample No.	Step(°C)	F	ΔF	Atmospheric Contamination	^{39}Ar Released (% of total)	$^{37}Ar/^{39}Ar$	$t_u \pm 2\sigma$ (my)
999	300-500	38.22	12.26	96.0	5.7	37.42	98.0 ± 61.2
	500-590	34.66	7.01	93.3	9.8	35.39	89.1 ± 35.2
	590-690	41.90	6.36	92.3	9.7	41.05	107.1 ± 31.6
	690-760	33.36	7.79	93.6	5.8	42.56	85.8 ± 39.1
	760-830	49.72	8.33	92.4	11.9	49.73	126.5 ± 40.4
	830-950	29.60	2.39	91.0	23.4	68.97	76.3 ± 12.0
	950-1050	14.48	1.50	90.6	31.8	142.65	37.7 ± 7.7
	1050-1150	29.41	21.64	95.9	3.0	148.05	75.8 ± 109.2
	K% ≈ .3	Ca% ≈ 11	K/Ca ≈ .03				
638 A & B	300-500	4.96	77.87	99.5	--	0.0	32.0 ± 996.9
	500-590	.84	91.9	99.9	--	0.0	55.0 ±1192.8

TABLE 5.5 ANALYTICAL DATA FOR ISOCHRON CALCULATION: SAMPLES 589, 598, 999 (AND 638).

Sample No.	Step(°C)	$^{40}Ar/^{36}Ar$	$^{39}Ar/^{36}Ar$	$\Delta^{40}Ar/^{36}Ar$	$\Delta^{39}Ar/^{36}Ar$	$t_u \pm 2\sigma$ (my)
589	300-500	288.2	.186	26.43	.012	-253.1 ± 1764.4
	500-590	285.1	.229	26.71	.015	-295.3 ± 1683.3
	590-690	286.0	.465	4.55	.005	-127.9 ± 828.6
	690-760	289.4	.739	4.49	.008	- 50.7 ± 76.4
	760-820	304.6	2.121	3.41	.014	25.8 ± 18.9
	820-950	307.8	2.898	2.12	.015	25.4 ± 8.6
	950-1200	297.0	.447	3.89	.005	20.2 ± 102.9
	Age = 51.9 ± 20.0		Intercept = 283.3 ± 3.8		SUMS = 1.0	
598	300-500	502.3	20.14	13.91	.542	60.0 ± 4.9
	500-590	761.9	46.64	11.73	.704	58.7 ± 1.3
	590-690	306.2	1.46	1.62	.006	44.0 ± 12.6
	690-760	292.9	1.41	3.05	.011	- 9.7 ± 25.7
	760-830	292.4	.97	4.39	.010	- 17.3 ± 54.5
	830-950	286.3	.63	8.70	.013	- 86.4 ± 177.8
	950-1000	291.1	1.36	4.34	.015	- 5.9 ± 40.6

continued on following page

TABLE 5.5 (CONTINUED)

Sample No.	Step(°C)	$^{40}Ar/^{36}Ar$	$^{39}Ar/^{36}Ar$	$\Delta^{40}Ar/^{36}Ar$	$\Delta^{39}Ar/^{36}Ar$	$t_u \pm 2\sigma$ (my)	
999	300-500	307.9	.321	4.03	.003	98.0 ± 61.2	
	500-590	316.9	.610	4.40	.006	89.1 ± 35.2	
	590-690	320.1	.580	3.91	.005	107.1 ± 31.6	
	690-760	315.6	.603	4.92	.008	85.8 ± 39.1	
	760-830	323.0	.453	3.94	.004	126.5 ± 40.4	*
	830-950	324.9	.969	2.40	.005	76.3 ± 12.0	
	950-1050	328.0	2.072	2.36	.021	31.7 ± 7.7	*
	1050-1150	308.4	.413	9.15	.009	75.8 ± 109.7	
	Age = 60.0 32.2 my		Intercept = 302.3 4.6		SUMS = 1.7		
638 A & B	300-500	297.1	.313	24.48	.018	32.0 ± 996.9	
	500-590	295.1	.268	24.59	.016	5.5 ± 1192.8	

589 + 598 + 999 + 638A & B -- Age + 58.3 ± 4.6 Intercept = 289.7 ± 2.4 SUMS = 203.7

* not included for Isochron Calculation

contents and/or high atmospheric or initial argon contamination) rather than a noticeable scatter in the data itself.

(d) Samples AA-19B, I-64 A & B and E-2B (basalts from Baffin Island): While none of the samples gave precise ages, they do provide an approximate value for the age of the Baffin Island volcanics. Sample AA-19B gave an irregular release pattern although ages were in the 50 - 70 my bracket (Table 5.6, Appendix C). The isochron revealed an approximate elliptical pattern that was traced out by the successive heating steps (Table 5.7, Appendix D). An age of 57.5 ± 16.8 my is defined by the major axis of the "ellipse". The release pattern of sample I-64A showed an "inverse-saddle", the top of which defined an age in the 60 my range (Table 5.6, Appendix C). The elliptical pattern was more pronounced in this sample and an age could not be obtained. However, the combination of the high temperature data of sample I-64A with that of sample I-64B, yields a 'reasonable' age of 50.2 ± 13.4 my (Table 5.7, Appendix D). It would appear that the number of data points used in the construction of the isochron is a significant parameter. This will be discussed further later.

The remaining sample from Baffin Island, although not of much use in defining duration, commencement or termination of volcanism, shows an interesting feature: ages in excess of one billion years. The inverse-saddle structure immediately suggests a high $^{40}Ar/^{36}Ar$ initial ratio (Table 5.6, Appendix C), so too does the isochron diagram; however, the age given by the isochron is in excess of 700 my (Table 5.7, Appendix D). It should be noted that the last point (temperature step 950° - 1050°C) was not used in the calculation. It would appear that

TABLE 5.6 ANALYTICAL DATA FOR $^{40}Ar/^{39}Ar$ INCREMENTAL HEATING: SAMPLES AA-19B, I-64 A&B AND E-2B

Sample No.	Step(°C)	F	ΔF	Atmospheric Contamination	^{39}Ar Released (% of Total)	$^{37}Ar/^{39}Ar$	tu ± 2σ (my)
AA-19B	300-500	12.71	3.22	78.8	4.9	2.30	32.4 ± 16.1
	500-590	25.49	1.07	69.5	16.9	4.64	64.3 ± 5.3
	590-690	21.42	.80	47.6	15.2	8.50	54.2 ± 4.0
	690-760	28.54	.74	44.5	29.8	23.44	71.9 ± 3.6
	760-830	32.04	2.18	64.5	16.6	40.34	80.5 ± 10.7
	830-950	23.00	2.43	84.2	12.1	53.02	58.1 ± 12.1
	950-1050	24.83	3.10	81.7	4.6	321.254	62.7 ± 13.1
	K% = .108	Ca% = 10.21		K/Ca = .011			
I-64A	300-500	-11.15	7.81	101.9	13.5	22.40	-29.6 ± 41.8
	500-625	4.00	1.90	97.5	28.7	37.70	10.5 ± 10.0
	625-750	17.09	1.17	87.1	27.9	100.18	44.5 ± 6.0
	750-875	25.65	8.29	95.0	20.5	83.13	66.3 ± 42.2
	875-100	- 5.23	9.56	100.6	9.4	144.29	-13.8 ± 50.6

continued on following page

TABLE 5.6 (CONTINUED)

Sample No.	Step(°C)	F	ΔF	Atmospheric Contamination	^{39}Ar Released (% of Total)	$^{37}Ar/^{39}Ar$	$t_u \pm 2\sigma$ (my)
I-64B	450-690	13.19	4.76	71.6	16.4	53.72	34.7 ± 26.6
	690-760	11.61	1.78	74.4	40.4	76.85	30.6 ± 10.6
	760-830	28.39	14.42	79.0	10.9	91.48	73.9 ± 76.7
	830-950	25.5	14.06	89.8	13.4	87.76	66.7 ± 69.5
	950-1050	7.17	26.32	98.2	18.8	386.85	18.9 ± 92.3
	K% = .100	Ca% = 7.00		K/Ca = .014			
E-2B	300-500	396.43	32.5	38.7	2.0	4.96	727.5 ± 80.0
	500-590	589.54	27.06	24.5	2.8	8.62	1000.6 ± 56.0
	590-690	675.93	29.50	22.8	8.6	58.26	1111.1 ± 57.8
	690-760	591.69	17.76	10.7	7.8	14.75	1003.5 ± 36.1
	760-830	509.17	5.92	6.6	18.7	16.15	891.7 ± 12.5
	830-950	413.17	5.90	9.3	24.2	18.62	752.8 ± 15.1
	950-1050	151.67	3.06	20.9	36.0	26.45	312.3 ± 10.6
	K% = .108	Ca% = 6.43		K/Ca = .017			

TABLE 5.7 ANALYTICAL DATA FOR ISOCHRON CALCULATION: SAMPLES AA-19B, I-64 A & B AND E-2B.

Sample No.	Step (°C)	$^{40}Ar/^{36}Ar$	$^{39}Ar/^{36}Ar$	$\Delta^{40}Ar/^{36}Ar$	$\Delta^{39}Ar/^{36}Ar$	$t_u \pm 2\sigma$ (my)	
AA-19B	300-500	375.1	6.266	24.38	.372	32.4 ± 16.1	
	500-590	425.2	5.088	6.97	.073	64.3 ± 5.3	
	590-690	620.2	15.160	23.75	.569	54.2 ± 4.0	
	690-760	664.6	12.933	19.54	.371	71.9 ± 3.6	
	760-830	458.1	5.073	12.83	.096	8.5 ± 10.1	
	830-950	350.9	2.410	6.39	.034	58.1 ± 12.1	
	950-1050	361.5	2.658	9.29	.066	62.7 ± 13.1	
	Age = 57.5 ± 16.8		Intercept 306.2 ± 20.1		SUMS = 78.8		
I-64A	300-500	289.9	.500	3.85	.005	-29.6 ± 41.8	*
	500-625	303.2	1.929	3.73	.019	10.5 ± 10.0	*
	625-750	339.1	2.551	3.32	.023	44.5 ± 6.0	
	750-875	311.1	.608	5.20	.008	66.3 ± 42.2	
	875-1000	293.7	.354	3.38	.003	-13.8 ± 50.6	

continued on following page

TABLE 5.7 (CONTINUED)

Sample No.	Step(°C)	$^{40}Ar/^{36}Ar$	$^{39}Ar/^{36}Ar$	$\Delta^{40}Ar/^{36}Ar$	$\Delta^{39}Ar/^{36}Ar$	$t_u \pm 2\sigma$ (my)	
I-64B	450-690	412.8	8.840	54.24	1.155	34.7 ± 26.6	*
	690-760	397.4	8.730	18.64	.400	30.6 ± 10.6	*
	760-830	374.2	2.750	48.23	.313	73.9 ± 76.7	
	820-950	328.9	1.300	19.21	.059	66.7 ± 69.5	
	950-1050	300.9	.755	20.8	.031	18.9 ± 92.3	
	Age = 50.2 13.4		Intercept = 290.7 3.9		SUMS = 5.4		
E-2B	300-500	763.9	1.182	55.00	.062	727.5 ± 80.0	
	500-590	1207.4	1.547	59.28	.057	1000.6 ± 56.0	
	590-690	1310.8	1.484	63.93	.052	1111.1 ± 57.8	
	690-760	2760.7	4.166	126.44	.155	1003.5 ± 36.1	
	760-830	4468.7	8.196	96.97	.153	891.7 ± 12.5	
	830-950	3170.9	6.959	78.96	.148	752.8 ± 15.1	
	950-1050	1411.9	7.361	36.57	.153	312.3 ± 10.6	*
AA19B + I-64A & B	Age = 713.3 ± 186.4		Intercept = 615.3 ± 293.6		SUMS = 548.2		
	Age = 56.6 ± 12.8		Intercept = 284.7 ± 7.8		SUMS = 280.4		

this basalt incorporated radiogenic argon from the 1.7 by old country rock. The majority of this gas was released between 600° and 700°C with lesser amounts above and below these temperatures. The correlation of the first six points is perhaps fortuitous. If the heating had continued the final step might have given a better estimate for the maximum age if the "excess" argon did not occur in the higher temperature fraction.

(e) Samples D.S.D.P. 12-112-17-1-26-29 and 127-129 (core samples from site 112): The low potassium content and the high degree of weathering produce a release pattern with very large errors; this is especially noticeable in the case of the (stratigraphically) lower sample (ie. D.S.D.P. 12-112-17-1-127-129) (see Table 5.8, Appendix C). The low precision of the individual data points made it necessary to combine all the data for the purposes of computing the single isochron age of 58.7 ± 36.4 my. The large uncertainty is almost entirely due to the imprecision of the individual data (Table 5.9, Appendix D).

(f) Samples 890, 939, and 012 (lamprophyres from Ubekendt Ejland): The saddle and inverse-saddle structures are present in the release patterns (Table 5.10, Appendix C). As mentioned before these dykes were considered to have shortly post-dated the other volcanic activity, a conclusion not supported by the present isochron dates of 40.7 ± 12.2 my, 30.6 ± 6.4 my and 32.8 ± 6.8 my (Table 5.11, Appendix D).

To summarize the data that have been presented, a table has been compiled of all the ages (Table 5.12) including total gas and mean of the incremental ages (weighted and unweighted). One of the more interesting features is the fact that the total gas ages (equivalent to con-

TABLE 5.8 ANALYTICAL DATA FOR $^{40}Ar/^{36}Ar$ INCREMENTAL HEATING:

SAMPLES D.S.D.P. 12-112-17-1-26-29 AND 127-129

Sample No.	Step(°C)	F	ΔF	Atmospheric Contamination	^{39}Ar Release (% of Total)	$^{37}Ar/^{30}Ar$	$t_u \pm 2\sigma$ (my)
D.S.D.P. 12-17-1-26-29	300-500	78.79	7.35	82.0	13.6	5.65	221.8 ± 39.1
	500-625	23.85	3.68	92.7	33.6	20.17	70.4 ± 21.2
	625-750	12.99	2.64	95.0	26.4	68.51	39.9 ± 15.4
	750-875	14.73	5.12	96.2	11.7	132.94	46.8 ± 30.0
	875-1000	20.02	32.19	97.6	6.0	134.75	62.6 ±185.9
	1000-1125	-30.44	95.42	102.3	8.7	359.70	-95.3 ±585.1
D.S.D.P. 12-17-1-127-129	300-500	- 8.13	19.21	100.8	15.4	11.96	-25.5 ±121.8
	500-625	6.84	13.88	98.6	18.6	18.75	21.6 ± 85.8
	625-750	19.13	4.54	94.4	33.3	63.95	58.9 ± 27.5
	750-875	40.08	19.49	95.6	8.1	120.46	121.3 ±114.0
	825-1000	8.95	7.36	97.9	18.1	191.69	27.8 ± 45.2
	1000-1125	5.23	57.6	99.6	6.5	263.72	16.30±260.3

K% ≈ .2 Ca% ≈ 20 K/Ca ≈ .01

TABLE 5.9 Analystical Data for Isochron Calculation:
Samples D.S.D.P. 12-112-17-1-26-29 and 127-129

Sample No.	Step (°C)	$^{40}Ar/^{36}Ar$	$^{39}Ar/^{36}Ar$	$\Delta^{40}Ar/^{36}Ar$	$\Delta^{39}Ar/^{36}Ar$	$t_u \pm 2\sigma$ (my)
DSDP 12-112-17-1-26-29	300-500	360.6	.826	6.64	.011	221.8 ± 39.1 *
	500-625	318.7	.975	3.73	.008	70.4 ± 21.2
	625-750	311.2	1.209	3.24	.010	39.9 ± 15.4
	750-875	307.2	.796	4.09	.010	46.8 ± 30.0
	875-1000	302.8	.363	11.54	.011	62.5 ±185.9
	1000-1125	288.9	.217	18.52	.022	-95.3 ±585.1
DSDP 12-112-17-1-127-129	300-500	293.1	.298	5.69	.004	-25.5 ±121.8
	500-625	299.8	.624	8.75	.017	21.6 ± 85.8
	625-750	313.2	.923	4.35	.010	58.9 ± 27.5
	750-875	309.2	.341	6.62	.005	121.3 ±114.0
	875-1000	301.8	.704	5.04	.010	27.8 ± 45.0
	1000-1125	296.7	.233	12.64	.007	16.3 ±260.3

Age = 58.9 ± 36.4 Intercept 293.9 ± 5.0 SUMS = 9.9

* Not included in isochron calculation

TABLE 5.10 Analytical Data for $^{40}Ar/^{39}Ar$ Incremental Heating:

Samples 890, 939 and 012

Sample No.	Step(°C)	F	ΔF	Atmospheric Contamination	^{39}Ar Release (% of total)	$^{37}Ar/^{39}Ar$	tu ± 2σ (my)
890	300-500	7.14	.22	83.0	10.7	.99	47.6 ± 3.0
	500-590	5.60	.37	75.6	8.4	.93	37.4 ± 5.0
	590-690	5.09	.33	47.0	6.5	1.37	34.0 ± 4.4
	690-760	1.13	4.38	99.6	4.2	2.43	7.6 ± 58.8
	760-830	5.41	.17	86.4	26.6	2.68	36.2 ± 2.2
	830-950	6.70	.12	74.7	28.9	10.89	44.6 ± 1.5
	950-1200	7.09	.29	74.9	14.7	33.71	47.2 ± 3.9
	K% = .709	Ca% = 7.91		K/Ca = .101			
939	300-500	4.85	.65	87.7	1.5	.58	32.6 ± 8.6
	500-590	5.64	.15	73.0	5.3	.47	37.9 ± 2.0
	590-690	6.62	.63	49.1	2.5	.44	44.8 ± 8.3
	690-760	5.43	.28	89.4	14.1	.30	36.5 ± 3.8
	760-830	5.25	.08	75.7	45.3	.14	35.3 ± 1.1
	830-950	4.63	.09	68.6	12.3	.34	31.2 ± 1.2
	950-1100	4.74	.15	75.8	19.0	12.95	31.9 ± 2.0
	K% = 1.818	Ca% = 8.935		K/Ca = .203			
012	300-500	4.66	.20	88.9	15.0	.88	31.1 ± 2.6
	500-620	6.19	.21	81.0	19.9	1.87	41.2 ± 2.8
	620-720	6.40	.07	55.7	15.6	.36	42.6 ± 1.0
	720-800	6.64	.11	69.8	18.8	.68	44.2 ± 1.4
	800-880	5.78	.06	66.3	10.3	.86	38.5 ± 0.8
	880-960	4.936	.05	52.5	19.6	5.06	32.9 ± 0.6
	960-1120	5.25	5.46	90.8	0.8	243.02	32.4 ± 56.6
	K% = 2.474	Ca% = 10.22		K/Ca = .242			

TABLE 5:11 Analytical Data for Isochron Calculation: Samples 890, 939 and 012.

Sample No.	Step(°C)	$^{40}Ar/^{36}Ar$	$^{39}Ar/^{36}Ar$	$\Delta^{40}Ar/^{36}Ar$	$\Delta^{39}Ar/^{36}Ar$	tu ± 2σ (my)
890	300-500	356.0	8.47	2.17	.046	47.6 ± 3.0
	500-590	390.7	17.00	8.28	.355	37.4 ± 3.0
	590-690	629.3	65.61	45.18	4.698	34.0 ± 4.4
	690-766	296.7	1.03	4.51	.011	7.6 ±58.8
	766-830	341.9	8.57	1.50	.022	36.2 ± 2.2
	830-950	396.6	14.99	2.10	.069	44.6 ± 1.5
	950-1200	397.3	13.97	4.81	.148	47.2 ± 3.9
	Age = 40.7 ± 12.2		Intercept = 297.8 ± 10.0		SUMS = 103.6	
939	300-500	332.6	7.96	1.76	.041	32.6 ± 8.6
	500-620	365.0	11.22	2.77	.808	37.9 ± 2.0
	620-720	477.8	33.44	4.11	.281	44.8 ± 8.3
	720-800	423.4	19.26	2.92	.127	36.5 ± 3.8
	800-880	445.6	26.01	2.36	.130	35.3 ± 1.1
	880-960	563.3	54.02	4.06	.378	31.2 ± 1.2
	960-1120	326.1	0.54	3.82	.005	31.9 ± 2.0
	Age = 30.6 ± 6.4		Intercept = 304.4 ± 6.7		SUMS = 42.6	
012	300-500	336.9	8.54	6.30	.155	31.1 ± 2.6
	500-590	404.8	19.40	3.76	.167	41.2 ± 2.8
	590-690	602.1	46.00	58.10	4.421	42.6 ± 1.0
	690-760	330.1	6.43	1.98	.033	44.2 ± 1.4
	760-830	390.3	18.10	1.83	.072	38.5 ± 0.8
	830-950	430.3	29.20	3.31	.193	32.9 ± 0.6
	950-1100	390.8	20.00	3.56	.166	32.4 ±56.6
	Age = 32.8 ± 6.8		Intercept = 307.9 ± 11.3		SUMS = 230.2	
890+939+012	Age = 32.6 ± 4.4		Intercept = 306.8 ± 4.7		SUMS = 525.6	

TABLE 5.12 Summary of Isochron, Total Gas and Mean of Incremental Heating Ages.

Sample No.	Mean Ages (my) Weighted α^1/σ^2	Weighted $\alpha^{39}Ar$	Not Weighted	Isochron Age (my)	Isochron Intercept	Total Gas Age (my) $^{40}Ar/^{36}Ar$ = 295.5	Total Gas Age (my) = Intercept
630	57.2	57.6	56.3	57.9	287.3	51.4	52.8
625	59.9	59.9	60.9	58.1	312.0	62.9	61.7
630+625	-	-	-	58.4	302.0	- *	- *
589	12.3	-49.7	-93.7	51.9	283.3	-46.1	49.0
598	58.4	17.8	6.2	59.8	287.5	18.5	42.8
999	55.1	74.1	87.9	60.0	302.3	78.2	54.7
589+598+999	-	-	-	58.3	289.7	-	-
AA-19B	65.9	65.4	60.6	57.5	306.2	68.0	63.3
I-64A	34.4	23.8	15.6	50.2	290.7	-	-
I-64B	32.4	38.7	45.0			-	-
E-2B	628.6	677.9	828.5	713.3	615.3	681.2	559.5
AA-19B+I-64A&B	-	-	-	56.6	284.7	-	-
DSDP 26-29	63.7	65.3	57.7	58.9	293.9	-	-
DSDP 127-129	48.7	35.6	36.7			-	-
890	42.4	39.0	36.4	40.7	297.8	44.8	44.8
939	34.0	34.7	35.7	30.6	304.4	37.9	34.6
012	37.0	38.5	37.6	32.8	307.9	44.2	38.5
890+939+012	-	-	-	32.6	306.8	-	-

* Total gas ages were not computed for pooled data

ventional K-Ar dates) bear, in some cases, no resemblance to the isochron ages. The latter are probably closer to the real ages as indicated by the small range of isochron values (50.2 - 60.0 my, basalts only) as compared to the larger range of total gas values (78.2 - minus 46.1 my, basalts only).

Conclusions on Data

SUMS, the weighted sum of the residuals and presented in the previous tables of isochron data, is an indication of the scatter of the points on the isochron, and in the ideal case of an infinite number of points, repeated an infinite number of times

$$\left(\frac{SUMS}{n-2} \right)^{1/2} < 1$$

where n is the number of points. However, in practice a value $\lesssim$ 2.5 indicates an isochron without geological error. As the previously presented data indicates, very few samples exhibit this criteria.

In order to explain why there is excess scatter, it is necessary to first consider the ideal case in which there is no air contamination although initial argon is present. The computed isochron will in this case be defined by the $^{40}Ar/^{36}Ar$ initial ratio (the intercept) and the age of the sample (the slope). No scatter should occur in excess of experimental error. The introduction of atmospheric argon ($^{40}Ar/^{36}Ar$ = 295.5), whether it be from the system blank or from the sample (see Chapter III), will have the effect of perturbing the points on the isochron towards the $^{40}Ar/^{36}Ar$ axis along a line joining the individual

points and $^{40}Ar/^{36}Ar = 295.5$. The best example of this is the one point for sample 625 already mentioned, but in a reverse sense. For this heating step the "atmospheric" contamination drops sharply so the relative amount of initial argon is increased and so the point moves away from $^{40}Ar/^{36}Ar = 295.5$. The question is: what does this do to the isochron?

Studies on the system blank when a sample is present indicate that it varies with furnace temperature, being higher at low and high temperatures, and that the magnitude depends primarily of the system pressure. This continuous variation in the system blank would result in the low and high temperature points being perturbed more than the middle temperature ones. A normal distribution of air contamination would result in an anomalously young or anomalously old isochron age (depending on whether the $^{40}Ar/^{36}Ar$ initial ratio is lower or higher than that of air). A skew distribution of air contamination would result in a elliptical pattern of points on an isochron (see samples AA-19B, I-64A or B). The long axis of the ellipse is not necessarily the correct age but may be a minimum or maximum estimate of the age (depending on whether the initial ratio is higher or lower than that of air). Irregular atmospheric contamination would produce a random scatter of points which would result in a very large uncertainty and a large SUMS.

In this regard, a synthetic study was performed in this laboratory. A set of data points was obtained by assigning random present-day $^{39}Ar/^{36}Ar$ values (as would be measured in the laboratory now) and random effective initial $^{40}Ar/^{36}Ar$ values selected between certain arbitrary

limits ('effective' implies the result of variable mixing of initial argon and atmospheric argon). The data points are assumed to have the same age (arbitrarily picked) and from these random values corresponding present-day $^{40}Ar/^{36}Ar$ may be calculated. Isochrons calculated for such a synthetic array of (present-day) points was found to give a false age for less than fifteen points but was found to converge on the correct value when fifteen or more points were used.

Discussion

It is apparent from the ages presented above that some can be classified as good while others are not so good. It would be useful to be able to predict the geochronological value of a particular sample.

In almost all cases the samples were selected on the basis of potassium content. Since the sample size was limited by the furnace capacity, samples with $K < 0.1\%$ could not be adequately analyzed. Other samples were selected on the basis of availability. One would expect that the higher potassium content in a sample would produce a better controlled age, but this is not necessarily so. Sample 589 is a good example. Petrographic examination showed that the sample is a least partially altered (see Appendix E). Microprobe analysis shows that the potassium has a higher concentration in this alteration (zeolite) than in the plagioclase itself. Alteration of this sample at a later date would have the effect of adding potassium and removing radiogenic argon which would result in the observed lowering of the expected age.

Additional microprobe analysis showed that better ages could be obtained from samples that have a potassium-bearing phase as opposed to

those that have the potassium randomly distributed throughout the sample. This was observed in the case of samples which contain plagioclase phenocrysts; the finer grained plagioclase crystals were found to contain a higher level of potassium. Similar results were obtained on certain samples from Bermuda (P. Rice, 1975 personal communication). Rice found that, in addition, the phenocrysts themselves gave anomalously high ages, a result attributed to the presence of significant amounts of excess argon. In the case of Bermuda, however, it was found that (within detectable limits) the alteration was contemporaneous with the formation of the basalts. If two potassium-bearing phases are present in significant quantities in the same sample, it is possible that they may interfere. The samples from Ubekendt Ejland contain feldspar and in some cases biotite as well. The amount of initial argon as well as the release of argon on heating differs between any two minerals and so one mineral may dominate over only a portion of the heating spectrum; this would contribute to irregular argon release patterns.

Funkhouser et al. (1968), in a study of deep-sea rocks, showed that glass content can be a measure of the presence of excess argon. Samples with greater than 70% glass always gave anomalously high ages, because the rapidly chilled basalts are incompletely outgassed of radiogenic Ar. This is perhaps seen in sample 999 which contains as much as 50% glass and is most probably the case in sample E-2B which contains 80% glass.

As previously mentioned, the ages for Svartenhuk Peninsula, Baffin Island and the mid-Labrador Sea ridge are indistinguishable. This is not to imply that volcanism was occurring in all areas at exactly the

same time. From other evidence it is more probable that volcanism ceased at the mid-Labrador Sea ridge, commenced in Baffin Island and Svartenhuk Peninsula and then continued in western Greenland only (see below: "Evolution of the Labrador Sea"); however, it is not possible to resolve these differences in the dates alone. The late igneous activity on Ubekendt Ejland can be considered a separate event and does not imply a continuation of activity for 25 my. Other basaltic provinces, such as the Hawiian chain (MacDonald, 1949) and Bermuda (Reynolds and Aumento, 1974), have also produced later silica-undersaturated magmas millions or tens of millions of years after the main activity.

Volcanism first occured in the Davis Strait volcanic province about 60-61 my ago and lasted only a few millions of years. A comparison of the above dates with those from Baffin Island, East Greenland, the Faraes and Britain, previously mentioned in Chapter I, would indicate that all areas underwent volcanism at the same time.

Farrar's (1966) data from Baffin Island are comparable to the data from Baffin Island in this study. The spread in the former may now be attributed to variation in the effective $^{40}Ar/^{36}Ar$ initial ratio (values range from 306 to 290 in the present study). For similar reasons, Beckinsale et al's suggested 15 my time span for the igneous activity of East Greenland may be entirely fictitious, and so too the 49 my to 62 my apparent spread in ages for the Faroes.

As previously mentioned, there is a large spread in existing conventional K-Ar age data for the British igneous province, namely 26 my to 86 my, although the extreme values can usually be omitted on the basis

of geological evidence or poor analytical procedures. Even so, it would be convenient to ascribe a major part of the scatter to variable $^{40}Ar/^{36}Ar$ initial ratio. Mellor and Mussett (1975) have calculated a number of conventional K-Ar isochron ages from data originally presented by Evans et al. (1973) and Purdy et al. (1972). Ages originally ranging from 39.7 my to 68.3 my were reduced to values between 55.1 my and 62.0 my. $^{40}Ar/^{36}Ar$ initial ratios range from a low of 212 to a high of 309.

Because of the perturbation of conventional K-Ar ages in cases where initial argon is present, it is not possible to assign precise values for the times of beginning, termination or duration of volcanism, even when the precision of measurement of the apparent ages approaches 0.5%. Evans et al. (1973) noted that variable initial $^{40}Ar/^{36}Ar$ ratios were probably present and so discarded obviously erroneous data. However, their reliance on the remaining data, based solely on the fact that it did not obviously conflict with independent geological evidence, is not justifiable. Hence, their suggestion that volcanism started 66 my ago and lasted 6 my is probably incorrect.

It is possible to consider the Davis Strait volcanic province and the Brito-Arctic province to be related, at least in time. The petrological differences have already been mentioned in Chapter I. In both areas, volcanism first occurred probably not before about 62 my ago and lasted only a few millions of years. This conclusion is supported by this work and by the work of Mellor and Musset (1975). There is some indication that some intrusive igneous activity occurred in Britain around 52 my ago (Evans et al., 1973). The conventional K-Ar age deter-

minations of Beckinsale et al. (1974) on the igneous intrusive from West Greenland would seem to indicate that the later intrusive activity is not a local feature. The apparent conflict with the much older Rb-Sr age determination from the same West Greenland intrusive can be resolved when one considers that K-Ar ages are susceptible to slow cooling rates as was proposed by Beckinsale et al.. It should be noted however, that the control on the Rb-Sr age is not good. Slow cooling might also account for the apparent igneous activity 52 my ago in Britain since most age determinations are by the K-Ar method.

Evolution of the Labrador Sea

The occurrence of oceanic crust in the Labrador Sea and Baffin Bay (Drake et al., 1963; C. Keen et al., 1972; Keen and Barrett, 1972) and magnetic lineations in the Labrador Sea (Mayhew, 1969; Le Pichon et al., 1971; Van der Linden and Srivastava, 1975; Vogt and Avery, 1974) indicate that the Labrador Sea and Baffin Bay formed by sea-floor spreading. A first attempt to reconstruct the Labrador Sea by geometrical means (i.e. by utilizing the major fracture zones in the northern Atlantic) was made by Le Pichon et al. (1971). C. Keen et al. (1972), on the basis of studies in Baffin Bay, modified the previous work.

Major opening of the Labrador Sea - Baffin Bay area commenced about 80 my ago about a pole located at 80°N 90°W (Le Pichon et al., 1971). C. Keen et al. (1972) modified this position slightly to account for folding and faulting in the northern Arctic Islands in Early Tertiary time (Thorsteinsson and Tozer, 1970). A second phase of opening commenced about 60 my ago about a different pole of rotation. This resulted in a north-south motion in the Labrador Sea and translation along Nares

Strait and Baffin Bay. This second phase lasted until about 47 my ago and possibly occurred in conjunction with spreading about the Alpha ridge in the Arctic Ocean, 40 to 60 my ago (Vogt and Ostenso, 1970). A hypothetical removal of this second phase of opening would place the Baffin Island basalts beside those of West Greenland. The age of these basalts then accords well with the beginning of the second phase. In line with this view, it has been reported that Baffin Island type volcanics have been found in West Greenland (D. B. Clarke, 1975 personal communication).

The geometry is not as simple as it seems though. Many geologists have argued that there cannot be substantial horizontal movement along the Nares Strait; others have said 150 to 200 km is possible. For the geometry stated above, about 150 km displacement is required. Also, the Labrador Sea cannot be completely closed without substantial overlap of continents in Baffin Bay. There is, however, a general insufficiency of good data and, in addition, poorly understood deformation in the Arctic Islands which might indicate that opening is more complex than originally thought. A final possibility is that some portion of the Labrador Sea opened during an earlier phase, perhaps in conjunction with the early Atlantic. This may account for the coast-parallel dyke swarm of southwest Greenland (Watt, 1969) with ages between 100 and 200 my (Hansen and Larsen, 1974; Bridgewater, 1970), and the Cretaceous-Jurassic lamprophyres of Labrador (King and McMillan, 1975).

Hyndman (1973) has postulated that the mantle plume now under Iceland is the same one that was under Davis Strait 60-80 my ago. How-

ever, in the light of new age data presented herein and a subsequent reassessment of published ages, the difference in the ages of the Davis Strait volcanics and those of the British-East Greenland area is so small, if indeed there is a definite difference, that it seems unlikely that one plume could travel fast enough with respect to the Greenland plate to produce these two volcanic areas. (Postulated plate speeds of < 1 cm/yr would require ≈ 50 my for the hot spot to travel from Davis Strait to Iceland). However, it also seems unlikely that slow-moving plume now localized under Iceland, could account for the known volcanics, since these areas are separated by 1000 km and no similar occurence has ever been reported. The second phase of opening in the Labrador Sea requires a transform fault in the Davis Strait area. The C.S.S. Hudson cruise in 1974 located structures which resemble transform faults. This may account for the localization of the Davis Strait volcanics since they seem to lie along the trace of this fault.

In summary, opening of the Labrador Sea appeared to have started in a minor way when the Atlantic started to open, perhaps in the Jurassic. Van der Linden (1975) postulated this but stated that the spreading certre, which terminated in the early Cretaceous, was the mid-Labrador Sea ridge. The age determination from D.S.D.P. 112 reported in this thesis, although not precise, does not support this view. Instead it is proposed that Jurassic spreading occurred about a spreading centre that, as yet, has not been located and is perhaps now masked by later activity. Major spreading, the so-called first phase, started around 80 my ago. This involved Baffin Bay and the Labrador Sea with the spreading centre situated on the mid-Labrador Sea ridge. This phase

ended with the commencement of the second phase. The second phase utilized a different pole and spreading centre, the latter being the Ran Ridge, an east-west structure south of Greenland (Vogt and Avery, 1974). Spreading from this centre resulted in north-south movement in the Labrador Sea and movement along Nares Strait. The structure of the mid-Labrador Sea ridge now has the two ridge crests (characteristic of mid-Atlantic type ridges) diverging towards the north (unpubl. data, Atlantic Geoscience Centre). This may be a result of north-south shearing and extension along the original mid-Labrador Sea ridge.

Work by a variety of agencies is being undertaken in the Davis Strait area, Nares Strait area and Baffin Bay. Until the nature of these areas and the existence of magnetic lineations in Baffin Bay have been determined, a more detailed picture of the evolution of the Labrador Sea and Baffin Bay will have to wait.

Bibliography

Aldrich, L. T. and Wetherill, G. W. (1958). Geochronology by radioactive decay, Ann. Rev. Nucl. Sci., 8, 257.

Armstrong, R. L. (1973). Proposal for simultaneous adoption of new U, Th, Rb and K decay constants for calculation of radiometric dates (Unpub. Man.).

Athavale, R. N. and Sharma, P. V. (1975). Paleomagnetic results on early Tertiary lava flows from West Greenland and their bearing on the evolution history of the Baffin Bay - Labrador Sea region, Can. J. Earth Sci., 12, 1.

Backenstoss, G. and Goebel, K. (1955). Die Zahl der r-Quanten des Kaliums, Z. Naturforsch, 10a, 920.

Beckinsale, R. D., Brooks, C. K. and Rex, D. C. (1970). Ages for the Tertiary of East Greenland, Bull. geol. Soc. Denmark, 20, 27.

Beckinsale, R. D. and Gale, N. H. (1969). A reappraisal of the decay constants and branching ratio of ^{40}K, Earth Planet. Sci. Letters, 6, 289.

Beckinsale, R. D., Thompson, R. N. and Durham, J. J. (1974). Petrogenetic significance of initial $^{87}Sr/^{86}Sr$ ratios in the North Atlantic Tertiary igneous province in the light of Rb-Sr, K-Ar and ^{18}O-abundance studies of the Sarqâta qáqâ intrusive complex Ubekendt Djland, West Greenland, JL. Petr., 15, 525.

Berger, G. W. and York, D. (1970). Precision of the $^{40}Ar/^{39}Ar$ dating technique, Earth Planet. Sci. Letters, 9, 29.

Brandt, S. D. and Voronovsky, S. N. (1967). Dehydration and diffusion of radiogenic argon in micas, Internat. Geol. Rev., 9, 1504.

Brereton, N. R. (1970). Corrections for interfering isotopes in the $^{40}Ar/^{39}Ar$ Dating Method, Earth Planet. Sci. Letters, 8, 427.

Bridgewater, D. (1970). A compilation of K/Ar age determinations on rocks from Greenland carried out in 1969, In: Rapport Grønlands Geol. Unders., 28, 47.

Brinkman, G. A., Aten, A. H. W. and Veenbour, J. Th. (1965). Natural radioactivity of K-40, Rb-87 and Lu-176, Physica, 31, 1305.

Brooks, C. K. (1973). Tertiary of Greenland - a volcanic and plutonic record of continental break-up, Mem. Amer. Ass. Petrol. Geol., 19, 150.

Brooks, C., Hart, S. R. and Wendt, I. (1972). Realistic use of two-error regression treatments as applied to Rubidium-Strontium data, Rev. Geophys. Space Phys., 10, 551.

Brooks, C., Wendt, I. and Harre, W. (1968). A two-error regression treatment and its application to Rb-Sr and initial Sr^{87}/Sr^{86} ratios of younger Variscan granitic rocks from the Schwarzwald massif, Southwest Germany, J. Geophys. Res., 73, 6071.

Burch, P. R. J. (1953). Specific Y-activity, the branching ratio and half-life of potassium-40, Nature, 172, 361.

Casey, R. (1964). The Cretaceous period. In: Part IV of The Phanerozoic Time-scale - a supplement, Quart. J. geol. Soc. Lond., 120S, 191.

Cherdyntsev, V. V. and Shitov, Y. V. (1967). Excess argon-36 in volcanic and post-volcanic gases, Geochem. Int., 4, 507 (Geokhimiya, 5, 618).

Clarke, D. B. (1967). Tertiary basalts from Baffin Island and west Greenland, Proc. Geol. Soc. Lond., 1637, 50.

Clarke, D. B. (1968a). The basalts of Svartenhuk Peninsula, progress report, In: Rapport Grønlands Geol. Unders., 53, 4.

Clarke, D. B. (1968b). Tertiary basalts of the Baffin Bay area, Ph.D. thesis, University of Edinburgh.

Clarke, D. B. (1970). Tertiary basalts of Baffin Bay: possible primary magma from the mantle, Contr. Min. and Petrol., 25, 203.

Clarke, D. B. (1973). New mapping in the western part of Ubekendt Ejland. In: Rapport Grønlands Geol. Unders., 53, 5.

Clarke, D. B. (1975). Tertiary basalts dredged from Baffin Bay, Can. J. Earth. Sci., 12, 1396.

Clarke, D. B. and Upton, B. G. J. (1971). Tertiary basalts of Baffin Island: Field relations and tectonic setting, Can. J. Earth Sci., 8, 248.

Dalrymple, G. B. (1969). $^{40}Ar/^{36}Ar$ analyses of historic lave flows, Earth Planet. Sci. Letters, 6, 47.

Dalrymple, G. B. and Lanphere, M. A. (1969). Potassium-Argon-Dating, Freeman and Co., San Francisco.

Deming, W. E. (1943). Statistical Adjustment of Data, John Wiley, New York.

de Ruyter, A. W., Aten, A. H. W., Van Dulman, A., Krol-Koning, Mrs. C., and Zuidema, Miss E. (1966). Specific gamma emission of natural potassium and lanthanum, Physica, 32, 991.

Drake, C. L., Campbell, N. J., Sander, G. and Nafe, J. E. (1963). A mid-Labrador Sea Ridge, Nature, 200, 1085.

Egelkraut, K. and Leutz, H. (1960). Hallowertzeit des K^{40}, Phys. Verhandl., 11, 67.

Engelkemeir, D. W., Flynn, K. F. and Glendenin, L. E. (1959). Positron emission in the decay of K^{40}, Phys. Rev., 126, 1818.

Endt, P. M. and Van der Leun, C. (1967). Energy levels of Z = 11-21 nuclei (IV). Nuclear Phys. A., A105, 1.

Evans, A. L., Fitch, F. J. and Miller, J. A. (1973). Potassium-argon age determinations on some British Tertiary igneous rocks, JL. geol. Soc. Lond., 129, 419.

Evernden, J. F. and Curtis, G. H. (1965). The potassium-argon dating of late Cenozoic rocks in East Africa and Italy, Current Anthropology, 6, 343.

Evernden, J. F., Curtis, G. H., Kistler, R. W. and Obradovich, J. (1960). Argon diffusion in glauconite, microcline, sanadine, leucite and phlogopite, Am. J. Sci., 258, 583.

Evernden, J. F. and Evernden, R. K. S. (1970). The Cenozoic Time Scale. In: Radiometric Dating and Paleontologic Zonation. Special Paper of the Geological Society of America, No. 124. Boulder, Colorado, 71.

Farrar, E. (1966). The extraction and ultra-high vacuum mass spectrometry of argon from rocks, Ph.D. Thesis. University of Toronto.

Fuller, R. E. (1931). The aqueous chilling of basaltic lava on the Columbia River Plateau. Amer. J. Sci., 21, 281.

Funnell, B. M. (1964). The Tertiary Period. In: Past IV of The Phanerozoic Time-Scale - a supplement, Quart J. geol Soc. Lond., 120S, 179.

Giesecke, C. L. (1823). On the mineralogy of Disko Island. Trans. R. Soc. Edinb., 9, 263.

Giesecke, K. L. (1910). Karl Ludwig Gieseckes mineralogisches Reisejournal über Grönland, 1806-1813, Meddr Grønland, 35, 1.

Glendenin, L. E. (1961). Present status of the decay constants, Ann. N. Y. Acad. Sci., 91, 166.

Good, M. L. (1951). Beta ray spectrum of K^{40}, Phys. Rev., 83, 1054.

Grant, A. C. (1975). Structural modes of the western margin of the Labrador Sea. In: Offshore Geology of Eastern Canada. Geol. Surv. Can., Paper 74-30, 2, 217.

Grasty, R. L. and Mitchell, J. G. (1966). Single sample potassium-argon ages using the Omegatron. Earth Planet. Sci. Letters, 1, 121.

Hansen, K. and Larsen, O. (1974). K/Ar age determinations on Mesozoic lamprophyre dykes near Ravns Storø, Fiskenæsset region, southern west Greenland, Rapport Grønlands geol. Unders., 66, 9.

Hood, P. and Bower, M. E. (1973). Low-level aeromagnetic surveys of continental shelves bordering Baffin Bay and the Labrador Sea, In: Earth Science Symposium on Offshore Eastern Canada, Geol. Surv. Can., Paper 71-23, 573.

Houtermans, F. G., Haxel, O. and Heintze, J. (1950). Die Halbwertszeit des K^{40}, Z. Physik, 128, 651.

Hyndman, R. D. (1973). Evolution of the Labrador Sea, Can. J. Earth Sci., 10, 637.

Hyndman, R. D. (1975). Marginal basins of the Labrador Sea and the Davis Strait hot spot, Can. J. Earth Sci., 12, 1041.

Hyndman, R. D., Clarke, D. B., Hume, H., Johnson, J., Keen, M. J., Park, I. and Pye, G. (1973). Geophysical and geologikal studies in Baffin Bay and the Labrador Sea, In: Earth Science Symposium on Offshore Eastern Canada, Geol. Surv. Can., Paper 71-23, 621.

Jessen, P., Borman, M., Dreyer, F. and Neuert, H. (1966). Experimental excitation functions for (n, p), (n, t), (n, α), (n, 2n) (n, np) and (n, nα) reactions Nuctear Data, A1, 103.

Jones, J. G. (1966). Intraglacial volcanoes of southwest Iceland and their significance in the interpretation of the form of the marine basaltic volcanoes, Nature, 212, 586.

Kanasewich, E. R., Ellis, R. M., Chapman, C. H., and Gutowski, P. R. (1973). Seismic array evidence of a core boundary source for the Hawaiian volcanic chain, J. Geophys. Res., 78, 1361.

Keeling, D. L. and Naughton, J. J. (1974). K-Ar dating: Addition of atmospheric argon on rock surfaces from crushing, Geophys. Res. Letters, 1, 43.

Keen, C. E. and Barrett, D. L. (1972). Seismic refraction studies in Baffin Bay: an example of a developing ocean basin, Royal Astron. Soc. Geophys. Jour., 30, 253.

Keen, C. E., Barnett, D. L., Manchester, K. S. and Ross, D. I. (1972). Geophysical studies in Baffin Bay and some tectonic implications, Can. J. Earth Sci., 9, 239.

Keen, M. J. and Clarke, D. B. (1974). Tertiary basalts of Baffin Bay: geochemical evidence for a fossil hot-spot, In: Kristjansson (ed.), Geodynamics of Iceland and the North Atlantic Area, D. Reidel Publ. Co., Dordrecht-Hollond, 127-137.

Keen, M. J., Johnson, J. and Park, I. (1972). Geophysical and geological studies in eastern and northern Baffin Bay and Lancaster Sound, Can. J. Earth. Sci., 9, 689.

Kelly, W. H., Beard, G. B. and Peters, R. A., (1959). The beta decay of K^{40}, Nucl. Phys. 11, 492.

King, A. F. and McMillan, N. J. (1975). A mid-Mesozoic breccia from the coast of Labrador. Can. J. Earth. Sci. 12, 44.

Kono, S. (1955). Scintillation spectrometer studies on the beta-activity of K^{40}, J. Phys. Soc. (Japan), 10, 495.

Kublick, E. E. (1972). Potassium-argon dating of slates from the Meguma group, Nova Scotia. M.Sc. thesis, Dalhousie University.

Laughton, A. S., et al. (1972). Initial Reports of the Deep Sea Drilling Project, vol. 12, pp. 1181-1189. U. S. Government Printing Office Washington, D. C.

Le Pichon, X., Hyndman, R. D. and Pautot, G. (1971). Geophysical study of the opening of the Labrador Sea, J. Geophys. Res., 76, 4724.

Leutz, H., Schulz, G. and Wenninger, H. (1965). The decay of potassium -40, Z. Physik., 187, 151.

Mayhew, M. A. (1969). Marine geophysical measurements in the Labrador Sea: relations to Precambrian geology and seafloor spreading. Ph.D. thesis, Columbia University.

McDougall, I. (1966). Precision methods of potassium-argon isotopic age determinations on young rocks, In: Methods and Techniques in Geophysics, vol II, S. K. Runcorn, Ed., Interscience, London, 279.

McNair, A., Glover, R. N. and Wilson, W. H. (1955). The decay of potassium-40, Phil. Mag., 1, 199.

McIntyre, G. A., Brooks, C., Compston, W. and Turek, A. (1966). The statistical assessment of Rb-Sr isochrons, J. Geophys. Res., 71, 5459.

Mellor, P. W. and Mussett, A. E. (1975). Evidence for initial ^{36}Ar in volcanic rocks, and some implications. Earth Planet. Sci. Letters, 26, 312.

Merrihue, C. M. (1965). Trace-element determinations and potassium-argon dating by mass spectroscopy of neutron irradiated samples, Trans. Am. Geophys. Union (Abs.), 46, 125.

Merrihue, C. M. and Turner, G. (1966). Potassium-argon dating by activation with fast neutrons. J. Geophys. Res., 71, 2852.

Mitchell, J. G. (1968a). Potassium-argon dating of neutron-irradiated minerals, Ph.D. thesis, University of Cambridge.

Mitchell, J. G. (1968b). The argon-40/argon-39 method for potassium-argon age determinations, Geochim. Cosmochim. Acta., 32, 781.

Moorbath, S., Sigurdsson, H. and Goodwin, R. (1968). K-Ar ages from the oldest exposed rocks in Iceland. Earth Planet. Sci. Letters, 4, 197.

Morgan, W. J. (1972). Deep mantle convection plumes and plate motions, Am. Assoc. Petroleum Geologists Bull., 56, 203.

Munck, S. and Noe-Nygaard, A. (1957). Age determinations of the various stages of the Tertiary volcanism in the West Greenland basalt province, Rep. 20th int. geol. congr. Mexico (1), 1, 247.

Murthy, V. R. and Compston W. (1965). Rb-Sr Ages of chondrules and carbonaceous chondrites, J. Geophys. Res., 70, 5297.

Mussett, A. E. and Dalrymple, G. B. (1968). An investigation of the source of air Ar contamination in K-Ar dating, Earth Planet. Sci. Letters, 4, 422.

Nier, A. O. (1950). A redetermination of the relative abundances of the isotopes of carbon, nitrogen, oxygen, argon and potassium, Phys. Rev., 77, 789.

Noe-Nygaard, A. (1974). Cenozoic to recent volcanism in and around the North Atlantic basin, In: Nairn, A. E. M. and Stehli, F. G. (Eds), The ocean basins and margins, 2, 391.

O'Hara, M. J. (1973). Non-primary magmas and dubious mantle plume beneath Iceland, Nature, 243, 507.

O'Nions, R. K. and Clarke, D. B. (1972). Comparative trace element geochemistry of Tertiary basalts from Baffin Bay, Earth Planet. Sci. Letters, 15, 436.

Park, I., Clarke, D. B., Johnson, J. and Keen, M. J. (1971). Seaward extension of the West Greenland Tertiary volcanic province, Earth Planet. Sci. Letters, 10, 235.

Pulvertaft, T. C. R. and Clarke, D. B. (1966). New mapping on Svartenhuk Peninsula, In: Rapport Gronlands Geol. Unders., 11, 15.

Purdy, J. W., Mussett, A. E., Charlton, S. R., Eckford, M. J. and English, H. N. (1972). The British Tertiary Igneous Province: potassium-argon ages of the Antrim Basalts, Geophys. J. R. Astr. Soc., 27, 327.

Rast, N. (1971). Isotope dating in the U.S.S.R. - an essay review, In: Part I of The Phonerozoic Time-scale - a supplement, Special Publication of the Geological Society No. 5, London, 39.

Rink, H. (1853). Udsigt over Nordgrönlands Geognosi, isœr med Hensyn til Bjergmassernes mineralogiske Sammensœtning, K. danske Vidensk. Selsk. Skr. (5), 3, 71.

Rosenkrantz, A. and Pulvertaft, T. C. R. (1969) Cretaceous-Tertiary stratigraphy and tectonics in northern West Greenland, Mem. Amer. Ass. Petrol. Geol., 12, 883.

Ross, D. I. and Henderson, G. (1973). New geophysical data on the continental shelf of central and northern west Greenland, Can. Jour. Earth Sci., 10, 485.

Rutherford, E. (1900). A radioactive substance emitted from Thorium compounds, Phil. Mag. 5th Series, 49, 1.

Saha, N. K. and Gupta, J. B. (1960). The γ/β branching ratio in the decay scheme of K^{40}, Proc. Natl. Inst. Sci. India, 26A, 486.

Sawyer, G. A. and Wiedenbeck, M. L. (1949). Gamma-ray of K^{40}, Phys. Rev., 76, 1535.

Schilling, J. G. (1973). Iceland mantle plume: geochemical study of Reykjanes Ridge, Nature, 242, 565.

Smith, A. G. (1964). Potassium-argon decay constants and age tables, In: The Phanerozoic Time-scale - a supplement, Quart J. Geol. Soc. London, 120S, 129.

Stukas, V. (1971). The argon-40/argon-39 dating technique: an overall outlook, B.Sc. thesis, University of Toronto.

Sutherland, P. C. (1853). On the geological and glacial phenomena on the coast of Davis Strait and Baffin Bay, Quart J. Geol. Soc. London, 9, 296.

Suttle, A. D. and Libby, W. F. (1955). Absolute assay of beta radioactivity in thick solids (application to naturally radioactive potassium), Anal. Chem., 27, 921.

Tarling, D. H. and Gale, N. H. (1868). Isotopic dating and paleomagnetic polarity in the Faroe Islands, Nature, Lond., 218, 1043.

Thorsteinsson, R. and Tozer, E. T. (1970). Geology of the Arctic Archipelago, In: Geology and economic minerals of Canada, 5th ed. Can. Geol. Survey Econ. Geol. Rept., 1, 548.

Tilley, D. R., and Madansky, L. (1959). Search for positron emission in K^{40}, Phys. Rev., 116, 413.

Turner, G. (1970). Argon 40-argon 39 dating of lunar rock samples, Geochim. Cosmochim. Acta, Lunar Science Conf. Supplement, 2, 1665.

Turner, G. (1971). Argon 40-argon 39 dating: the optimization of irradiation parameters, Earth Planet. Sci. Letters, 10, 227.

Turner, G., Miller, J. A. and Grasty, R. L. (1966). The thermal history of the Bruderheim meteorite, Earth Planet. Sci. Letters, 1, 155.

Van der Linden, W. J. M. (1975). Mesozoic and Cainozoic opening of the Labrador Sea, the North Atlantic and the Bay of Biscay. Nature, 253, 320.

Van der Linden, W. J. M. and Srivastava, S. P. (1975). The crustal structure of the continental margin off central Labrador, In: Offshore Geology of Eastern Canada, Geol. Surv. Can., Paper 74-30, 2, 233.

Vogt, P. R. and Avery, O. E. (1974). Detailed magnetic surveys in the Northeast Atlantic and Labrador Sea, J. Geophys. Res., 79, 363.

Vogt, P. R. and Ostenso, N. A. (1970). Magnetic and gravity profiles across the Alpha Cordillera and their relationto Arctic sea-floor spreading. J. Geophys. Res., 75, 4925.

Wanless, R. K., Stevens, R.D. Lachance, G. R. and Rimsaite, J. Y. H. (1966). Age determinations and geological studies, K-Ar isotope ages, Report 6 Geol. Surv. Can., Paper 65-17.

Watt, W. S. (1969). The coast-parallel dike swarm of southwest Greenland in relation to the opening of the Labrador Sea, Can. J. Earth Sci., 6, 1320.

Weast, R. C. (1970). Handbook of chemistry and physics. The Chemical Rubber Company.

Weast, R. C. and Selby, S. M. (1966). Handbook of chemistry and physics. The Chemical Rubber Company.

Wetherill, G. W. (1957). Radioactivity of potassium and geologic time, Science, 126, 545.

Wetherill, G. W., Wasserburg, G. J., Aldrich, L. T., Tilton, G. R. and Hayden, R.J. (1956). Decay constants of K^{40} as determined by radiogenic argon content of potassium minerals, Phys. Rev. 103, 987.

Williamson, J. H. (1968). Least-squares fitting of a straight line, Can. J. Phys., 46, 1845.

Wilson, J. T. and Clarke, D. B. (1965). Geological expedition to Capes Dyer and Searle, Baffin Island, Canada, Nature, 205, 349.

York, D. (1966). Least-squares fitting of a straight line, Can. J. Phys., 46, 1845.

York, D. (1969). Least-squares fitting of a straight line with correlated errors, Earth Planet. Sci. Letters, 5, 320.

Zartman, R. E., Wasseburg, G. J. and Reynolds, J. M. (1961). Helium, argon and carbon in some natural gases, J. Geophys. Res., 66, 277.

Addendum

Funkhouser, J. G., Fisher, D. E., and Bonatti, E. (1968). Excess argon in deep-sea rocks, Earth Planet. Sci. Letters, 5, 95.

MacDonald, G. A. (1949). Hawaiin petrographic province. Geol. Soc. Am. Bull., 60, 1541.

Reynolds, P. H. and Aumento, F. (1974). Deep Drill 1972. Potassium-argon dating of the Bermuda drill core, Can. J. Earth Sci., 11, 1269.

Appendix A. Interfering Isotopes

After a sample which contains potassium and calcium has been irradiated, the measured volumes of the argon isotopes ^{36}Ar, ^{37}Ar, ^{38}Ar, ^{39}Ar and ^{40}Ar can be written:

$$^{36}Ar = {}^{36}Ar^{Atm} + {}^{36}Ar^{NCa} - {}^{36}Ar^{RR}$$

$$^{37}Ar = {}^{37}Ar^{NCa}$$

$$^{38}Ar = {}^{38}Ar^{Atm} + {}^{38}Ar^{NK} + {}^{38}Ar^{NCa} - {}^{38}Ar^{RR}$$

$$^{39}Ar = {}^{39}Ar^{NK} + {}^{39}Ar^{NCa}$$

$$^{40}Ar = {}^{40}Ar^{Atm} + {}^{40}Ar^{*} + {}^{40}Ar^{NK} + {}^{40}Ar^{NCa} - {}^{40}Ar^{RR}$$

where the superscrips Atm, NCa, NK, RR and * denote the components of the measured volumes: Atm = atmospheric, NCa = neutron induced from calcium, NK = neutron induced from potassium, RR = removed by neutron reaction and * = radiogenic.

Now consider a sample of a pure calcium compound containing no potassium and of zero age, then after irradiation:

$$^{36}Ar' = {}^{36}Ar^{Atm'} + {}^{36}Ar^{NCa'} - {}^{36}Ar^{RR'}$$

$$^{37}Ar' = {}^{37}Ar^{NCa'}$$

$$^{38}Ar' = {}^{38}Ar^{Atm'} + {}^{38}Ar^{NCa'} - {}^{38}Ar^{RR'}$$

$$^{39}Ar' = {}^{39}Ar^{NCa'}$$

$$^{40}Ar' = {}^{40}Ar^{Atm'} + {}^{40}Ar^{NCa'} - {}^{40}Ar^{RR'}$$

and similarly for a pure potassium compound of zero age, containing no calcium:

$$^{36}Ar'' = {}^{36}Ar^{Atm''} - {}^{36}Ar^{RR''}$$

$$^{37}Ar'' = 0$$

$$^{38}Ar'' = {}^{38}Ar^{Atm''} + {}^{38}Ar^{NK''} - {}^{38}Ar^{RR''}$$

and

$$\frac{^{40}Ar^{NK}}{^{37}Ar^{NCa}} = \left[\frac{^{39}Ar}{^{37}Ar} - \frac{^{39}Ar'}{^{37}Ar'}\right]\left[\frac{^{40}Ar''}{^{39}Ar''} - \frac{^{36}Ar''}{^{39}Ar''}\,x + \left(\frac{^{40}Ar^{RR''}}{^{39}Ar^{NK''}} - \frac{^{36}Ar^{RR''}}{^{39}Ar^{NK''}}\,x\right)\right] \qquad (A.3)$$

where x is the atmospheric argon ratio. Substituting equation (A.3) into equation (A.2) and then dividing by equation (A.1) we get

$$\frac{^{40}Ar^{*}}{^{39}Ar^{NK}} = \left[1/\left(\frac{^{39}Ar}{^{37}Ar} - \frac{^{39}Ar'}{^{37}Ar'}\right)\right]\left[\left(\frac{^{40}Ar}{^{37}Ar} - \frac{^{40}Ar'}{^{37}Ar'}\right) - \left(\frac{^{36}Ar}{^{37}Ar} - \frac{^{36}Ar'}{^{37}Ar'}\right)x + \left(\frac{^{40}Ar^{RR}}{^{37}Ar^{NCa}} - \frac{^{36}Ar^{RR}}{^{37}Ar^{NCa}}\,x\right) - \left(\frac{^{40}Ar^{RR'}}{^{37}Ar^{NCa'}} - \frac{^{36}Ar^{RR'}}{^{37}Ar^{NCa'}}\,x\right) \qquad (A.4)$$

The terms $^{40}Ar^{RR'}$ and $^{36}Ar^{RR'}$ represent the total loss of original ^{40}Ar and ^{36}Ar during irradiation. In other words they are a function of the total neutron reaction cross sections for these isotopes. If the cross sections are equivalent in value then as the neutron flux is the same, the total number of ^{40}Ar lost is proportional to the total number of ^{36}Ar lost. The proportionality constant is the ratio of atoms originally present, that is x since

$$^{40}Ar^{Atm} = {}^{36}Ar^{Atm}\ x$$

then

$$^{40}Ar^{RR'} = {}^{36}Ar^{RR'}\ x$$

$$^{40}Ar^{RR''} = {}^{36}Ar^{RR''}\ x$$

$$^{40}Ar^{RR} = {}^{36}Ar^{RR}\ x$$

$$^{39}Ar'' = {}^{39}Ar^{NK''}$$

$$^{40}Ar'' = {}^{40}Ar^{Atm''} + {}^{40}Ar^{NK''} - {}^{40}Ar^{RR''}$$

It can be shown experimentally that the ratios of the argon isotopes produced from the same element in two or more compounds irradiated in different positions in a reactor and for different lengths of time (i.e. different neutron flux) will be constant.

Thank is:

$$\frac{{}^{39}Ar^{NCa}}{{}^{37}Ar^{NCa}} = \frac{{}^{39}Ar^{NCa'}}{{}^{37}Ar^{NCa'}}$$

or

$$\frac{{}^{39}Ar^{NK}}{{}^{40}Ar^{NK}} = \frac{{}^{39}Ar^{NK''}}{{}^{40}Ar^{NK''}}$$

Utilizing the previous equations and this arguement it can be shown that:

$$\frac{{}^{39}Ar^{NK}}{{}^{37}Ar^{NCa}} = \frac{{}^{39}Ar}{{}^{37}Ar} - \frac{{}^{39}Ar'}{{}^{37}Ar'} \qquad (A.1)$$

$$\frac{{}^{40}Ar^{*}}{{}^{37}Ar^{NCa}} = \frac{{}^{40}Ar}{{}^{37}Ar} - \frac{{}^{40}Ar'}{{}^{37}Ar'} - \left[\frac{{}^{36}Ar}{{}^{37}Ar} - \frac{{}^{36}Ar'}{{}^{37}Ar'}\right] x +$$

$$\left[\frac{{}^{40}Ar^{RR}}{{}^{37}Ar^{NCa}} - \frac{{}^{36}Ar^{RR}}{{}^{37}Ar^{NCa}} x\right] - \frac{{}^{40}Ar^{RR'}}{{}^{37}Ar^{NCa'}} - \frac{{}^{36}Ar^{RR'}}{{}^{37}Ar^{NCa'}}\Big] x$$

$$- \frac{{}^{40}Ar^{NK}}{{}^{37}Ar^{NCa}} \qquad (A.2)$$

In general the RR terms are small and can be ignored. All the RR terms now reduce to zero and by rearranging the terms, equation (A.4) becomes

$$\frac{^{40}Ar^*}{^{39}Ar^{NK}} = [1/(\frac{^{39}Ar}{^{37}Ar} - \frac{^{39}Ar'}{^{37}Ar'})] \; [\frac{^{40}Ar - {}^{36}Ar\ x}{^{37}Ar} - \frac{^{40}Ar' - {}^{36}Ar'\ x}{^{37}Ar'}$$

$$- [\frac{^{40}Ar'' - {}^{36}Ar''\ x}{^{39}Ar''} \qquad (A.5)$$

Of all the argon isotopes considered ^{39}Ar and ^{37}Ar are the only unstable ones. ^{39}Ar has a half-life of 269 years. Unless there is a long delay between analysis of the sample and irradiation (more than one year), the effects of ^{39}Ar decay are negligible.

^{37}Ar is different, with a half-life of 35.1 days; hence, any time delay between irradiation and analysis will have a noticeable effect on the volume of gas measured. In addition, if the sample is irradiated for more than a few hours, the ^{37}Ar atoms produced at the beginning will be decaying while new atoms are being formed. If the duration of time that the sample is irradiated is Δt and the time from removal of sample from reactor to analysis is t, then the corrected volume of ^{37}Ar is

$$^{37}Ar^C = {}^{37}Ar \; e^{\lambda t} \Delta t \; (1 - e^{-\lambda \Delta t})^{-1}$$

where ^{37}Ar is the measured volume of ^{37}Ar and λ is the decay constant for ^{37}Ar. Now if we define

$$a = \frac{^{39}Ar'}{^{37}Ar'} = \frac{^{39}Ar^{NCa}}{^{37}Ar^{NCa}}$$

$$b = \frac{^{36}Ar' - {}^{40}Ar'/x}{^{37}Ar'} = \frac{^{36}Ar^{NCa}}{^{37}Ar^{NCa}}$$

and $$c = \frac{^{40}Ar'' - {}^{36}Ar''x}{^{39}Ar''} = \frac{^{40}Ar^{NK}}{^{39}Ar^{NK}}$$

It is possible to show that a, b and c are approximately constant by the same arguements that preceded equation A.1. Thus equation (A.5) becomes

$$\frac{^{40}Ar^*}{^{39}Ar^{NK}} = \frac{\frac{^{40}Ar}{^{39}Ar} - \frac{^{36}Ar}{^{39}Ar}x + \frac{^{37}Ar}{^{39}Ar}fe^{\lambda t}(bx + ac) - c}{1 - \frac{^{37}Ar}{^{39}Ar}afe^{\lambda t}}$$

where $f = \lambda\Delta t\ (1 - e^{-\lambda\Delta t})^{-1}$.

Appendix B. The Isochron

In order to obtain the best line in a least squares sense set of points ($X_i \pm \Delta X_i$, $Y_i + \Delta Y_i$) a number of methods have been developed. McIntyre et al. (1966) and York (1966) independently developed their methods first and were followed by a model developed by Wendt (Brooks et al., 1968). York (1969) presented a modification in his second model and so did Wendt (Brooks et al., 1972). It is the York (1969) model which will be discussed in more detail than the others, since it is the method used for this study. A summary and comparison of all methods is found in Brooks et al. (1972).

A study by Deming (1943) proposed that the "best" straight line is given by minimizing

$$S = \sum_i \{w(X_i)\ (x_i - X_i)^2 + w(Y_i)\ (y_i - Y_i)^2\} \qquad (B.1)$$

where X_i, Y_i are the observations, x_i, y_i are the adjusted values of these observations and $w(X_i)$, $w(Y_i)$ are the weights of the respective observations. The adjusted points x_i, y_i lie on a straight and satisfy the expression

$$y_i = ax_i + b \qquad i = 1, \ldots, n \qquad (B.2)$$

Deming simplified the equation by expanding the straight line function in a Taylor Series about assumed values of slope intercept and adjusted points. As opposed to following this approach, the one outlined by Williamson (1968) will be followed, since the Deming method does cause

significant errors in some instances by neglecting the higher order terms.

Inserting equation (B.2) into equation (B.1) yields

$$S = \sum_i \{(x_i - X_i)^2 \, w(X_i) + (a + bx_i - Y_i)^2 \, w(Y_i)\}$$

Setting

$$\frac{\partial S}{\partial x_i} = 0$$

in order to minimize S, yields:

$$x_i = W_i \left[\frac{X_i}{w(Y_i)} + \frac{b}{w(X_i)} (Y_i - a) \right]$$

where

$$W_i = \frac{w(X_i) \, w(Y_i)}{b^2 \, w(Y_i) + w(X_i)}$$

This has a simple geometrical interpretation in terms of the equivalent weight in the y coordinate caused by the weight in the x-coordinate. The sum of squares then becomes

$$S = \sum_i W_i \, (a + b \, X_i - Y_i)^2$$

(This is where McIntyre (1966) starts for his solution) Setting

$$\frac{\partial s}{\partial a} = 0$$

gives $a + b \, \overline{X} = \overline{Y}$ (B.3)

and

$$S = \Sigma_i \, W_i \, (bX_i' - Y_i')^2$$

where

$$\overline{X} = \frac{\Sigma_i \, W_i \, X_i}{\Sigma_i \, W_i}$$

$$\overline{Y} = \frac{\Sigma_i \, W_i \, Y_i}{\Sigma_i \, W_i}$$

$$X_i' = X_i - \overline{X}$$

and $$Y_i' = Y_i - \overline{Y}$$

Finally setting

$$\frac{\partial s}{\partial b} = 0$$

yields

$$\Sigma_i \left\{2W_i \, X_i' \, (bX_i - Y_i) - \frac{2W_i^2 \, b(bX_i' - Y_i')^2}{W(X_i)}\right\} = 0 \qquad \text{(B.4)}$$

Because the slope, b, occurs in the denominator of W_i, this equation may be written as a polynomial of any degree whatsoever in b. York (1966) chose to consider as a cubic equation:

$$b^3 \, \Sigma_i \, \frac{W_i^2 \, X_i'^2}{w(X_i)} - 2b^2 \, \Sigma \frac{W_i^2 \, X_i'^2 \, Y_i'^2}{w(X_i)}$$

$$-b \left\{ \sum_i W_i X_i'^2 - \sum_i \frac{W_i^2 Y_i'^2}{w(X_i)} \right\} + \Sigma_i W_i U_i V_i = 0 \qquad (B.5)$$

which he called the "Least-Squares Cubic". The solution is obtained by inserting an approximate value for b into one of the roots of this equation. Any desired degree of accuracy may be obtained by iteration, inserting the solution for b back in W_i and repeating. The intercept is obtained from equation (B.3).

Williamson (1968) noted that it is obviously simpler to write equation (B.4) in a linear form. Expanding equation (B.4) into its individual terms:

$$\Sigma_i W_i X_i'^2 b - \Sigma_i W_i X_i' Y_i' - \Sigma_i \frac{W_i^2 b^3 X_i'^2}{w(X_i)}$$

$$+ \Sigma_i \frac{2W_i^2 b^2 X_i' Y_i'}{w(X_i)} - \Sigma_i \frac{W_i^2 b Y_i'^2}{w(X_i)} = 0$$

by inserting

$$b^2 = \frac{w(X_i)}{W_i} - \frac{w(X_i)}{w(X_i)}$$

into the third term of the previous equation, as well as half of the fourth term, we get:

$$\Sigma_i W_i X_i'^2 b - \Sigma_i W_i X_i' Y_i' - (\Sigma W_i X_i'^2 b + \Sigma \frac{W_i^2 b X_i^2}{w(Y_i)})$$

$$+ \Sigma \frac{W_i^2 b^2 X_i' Y_i'}{w(X_i)} + \Sigma W_i X_i' Y_i' - \Sigma \frac{W_i^2 Y_i' Y_i'}{w(Y_i)} - \Sigma \frac{W_i^2 b Y_i'^2}{w(X_i)} = 0$$

By cancelling and collecting terms this reduces to:

$$b = \frac{\Sigma_i W_i^2 X_i' \left(\frac{X_i'}{w(Y_i)} + \frac{b Y_i'}{w(X_i)} \right)}{\Sigma_i W_i^2 Y_i' \left(\frac{X_i'}{w(Y_i)} + \frac{b Y_i'}{w(X_i)} \right)}$$

The solution is determined by the same method as the "least-squares cubic".

However, as in our particular case, it is often necessary to obtain the best straight line when the X and Y errors are correlated. That is, an error in X results in a similar error in Y. This may be obtained by minimizing the expression (York, 1969)

$$S = \Sigma_i \{w(X_i) (x_i - X_i)^2 - 2r_i w(X_i) w(Y_i) \cdot (x_i - X_i) (y_i - Y_i) + w(Y_i) (y_i - Y_i)^2\} \frac{1}{(1 - r_i^2)} \qquad (B.6)$$

where the r_i are the correlations between the X and Y errors and X_i, Y_i, x_i, y_i and $w(X_i)$, $w(Y_i)$ are as before. Substituting equation (B.2) into equation (B.6) and minimizing with respect to x_i yields:

$$S = \Sigma_i Z_i (a + b X_i - Y_i)^2$$

where

$$Z_i = \frac{w(X_i) w(Y_i)}{b^2 w(Y_i) + w(X_i) - 2br_i w(X_i) w(Y_i)}$$

Solving in the same manner as in the uncorrelated errors analysis, one finds the generalized version of the least-quares cubic which may be solved for b to yield the best slope using the root of the equation:

$$b^3 \Sigma_i \frac{Z_i^2 X_i'^2}{w(X_i)} - b^2 \frac{2\Sigma_i Z_i^2 X_i' Y_i'}{w(X_i)} + \frac{\Sigma_i Z_i^2 r_i X_i'^2}{\alpha_i}$$

$$- b \Sigma_i Z_i X_i^2 - \frac{2\Sigma_i Z_i^2 r_i X_i' Y_i'}{\alpha_i} - \frac{\Sigma_i Z_i^2 Y_i'^2}{w(X_i)}$$

$$+ \Sigma_i Z_i X_i' Y_i' - \frac{\Sigma_i Z_i^2 r_i Y_i'^2}{\alpha_i} = 0 \qquad \text{(B.7)}$$

this may be reduced algebraically to a least-squares quadratic

$$b^2 \Sigma_i Z_i^2 \frac{X_i' Y_i'}{w(X_i)} - \frac{r_i X_i'^2}{\alpha_i} + b \Sigma_i Z_i^2 \frac{X_i'^2}{w(Y_i)} - \frac{Y_i'^2}{w(X_i)}$$

$$- \Sigma_i Z_i^2 \frac{X_i' Y_i'}{w(X_i)} - \frac{r_i Y_i'^2}{\alpha_i} = 0 \qquad \text{(B.8)}$$

where X_i', Y_i' are as before

$$\alpha_i = w(X_i)\ w(Y_i)$$

$$\bar{X} = \frac{\Sigma_i Z_i X_i}{\Sigma Z_i}$$

and $$\bar{Y} = \frac{\Sigma_i Z_i Y_i}{\Sigma Z_i}$$

The similarity between equation (B.7) the correlated least-squares cubic, and equation (B.5) the uncorrelated least-squares cubic should be noted and that the latter may be obtained from equation (B.7) by setting $r_i = 0$. It should be noted that the best straight line goes through the point $(\bar{X}, \bar{Y})$ as indicated by equation (B.3). The slope of the best straight line may now be found as a root of equation (B.8), i.e.

$$b = - \Sigma_i Z_i^2 \left[\frac{X_i'^2}{w(Y_i)} - \frac{Y_i'^2}{w(X_i)}\right] + \Sigma_i Z_i^2 \left[\frac{X_i'^2}{w(Y_i)} - \frac{Y_i'^2}{w(X_i)}\right]^2$$

$$+ 4 \Sigma_i Z_i^2 \left[\frac{X_i Y_i}{w(X_i)} - \frac{r_i X_i'^2}{\alpha_i}\right] \Sigma_i Z_i^2 \left[\frac{X_i' Y_i'}{w(Y_i)} - \frac{r_i Y_i'^2}{\alpha_i}\right]$$

$$2 \Sigma_i Z_i^2 \left[\frac{X_i' Y_i'}{w(X_i)} - \frac{r_i Y_i'^2}{\alpha_i}\right]^{-1} \qquad \text{(B.9)}$$

X_i', Y_i' and Z_i contain the parameter b so a solution is obtained by inserting an approximate value for b into these terms and calculating a new b. The process is repeated by inserting the new b into the left side of equation (B.9), until the desired accuracy is obtained.

The correlated least squares cubic may be solved by a method analagous to that outlines earlier (Williamson, 1968). In this case the best slope is found from the equation:

$$b = \frac{\Sigma_i Z_i^2 Y_i' \left[\frac{X_i'}{w(Y_i)} + \frac{b Y_i'}{w(X_i)} - \frac{r_i Y_1'}{\alpha_i}\right]}{\Sigma_i Z_i^2 X_i' \left[\frac{X_i'}{w(Y_i)} + \frac{b Y_i'}{w(X_i)} - \frac{r_i X_i'}{\alpha_i}\right]} \qquad \text{(B.10)}$$

Again by iteration the value of the slope is found to the desired accuracy. The best intercept is found from equation (B.3) which yields

$$a = \overline{Y} - b\overline{X} \qquad \text{(B.11)}$$

The variance in the estimate of the slope (σ_b^2) and intercept (σ_a^2) are found by the partial differentiation of equations (B.8) and (B.11) respectively, that is

$$\sigma_b^2 = \Sigma_i \left[\frac{\partial \phi}{\partial X_i} \right]^2 \frac{1}{w(X_i)} + \left[\frac{\partial \phi}{\partial Y_i} \right]^2 \frac{1}{w(Y_i)} + \frac{2r_i}{w(X_i)\, w(Y_i)}$$

$$\left[\frac{\partial \phi}{\partial X_i} \quad \frac{\partial \phi}{\partial Y_i} \quad \frac{\partial \phi}{\partial b} \right]^2$$

where ϕ represents the left hand side of equation (B.8).

$$\frac{\partial \phi}{\partial X_i} = \sum_j Z_j^2 \, \delta_{ij} - \frac{Z_i}{\Sigma_i Z_i} \left[\frac{b^2 Y_j'}{w(X_j)} - \frac{2 b^2 r_j X_j'}{\alpha_j} + \frac{2bX_j'}{w(Y_j)} - \frac{Y_j'}{w(Y_j)} \right]$$

$$\frac{\partial \phi}{\partial Y_i} = \Sigma_j Z_j^2 \, \delta_{ij} - \frac{Z_i}{\Sigma_i Z_i} \left[\frac{b^2 X_j'}{w(X_j)} - \frac{2 b Y_i'}{w(X_j)} - \frac{X_j'}{w(Y_j)} + \frac{2 r_j Y_j'}{\alpha_j} \right]$$

$$\frac{\partial \phi}{\partial b} = \Sigma_i Z_i^2 X_i^2 \left[\frac{1}{w(Y_i)} - \frac{2br_i}{\alpha_i} + \frac{Y_i'}{w(X_i)} \right] (2b X_i' - Y_i')$$

$$+ b^2 \frac{\partial A}{\partial b} + b \frac{\partial B}{\partial b} + \frac{\partial C}{\partial b}$$

where $A = \Sigma_i Z_i^2 \left[\frac{X_i' Y_i'}{w(X_i)} - \frac{r_i X_i'^2}{\alpha_i} \right]$

$$B = \Sigma_i \, Z_i^2 \left(\frac{X_i'^2}{w(Y_i)} - \frac{Y_i'^2}{w(X_i)} \right)$$

$$C = \Sigma_i \, Z_i^2 \left(\frac{X_i' \, Y_i'}{w(X_i)} - \frac{r_i \, Y_i'^2}{\alpha_i} \right)$$

and δ_{ij} is the Kronecka delta.

Similarly

$$\sigma_a^2 = \Sigma_i \left(\frac{\partial a}{\partial X_i} \right)^2 \frac{1}{w(X_i)} + \left(\frac{\partial a}{\partial Y_i} \right)^2 \frac{1}{w(Y_i)} + \frac{2 r_i}{w(Y_i) \, w(X_i)} \frac{\partial a}{\partial X_i} \frac{\partial a}{\partial Y_i}$$

where

$$\frac{\partial a}{\partial X_i} = - \frac{b Z_i}{\Sigma_i Z_i} + \frac{2}{\Sigma_i Z_i} \frac{Z_i^2}{\alpha_i^2} [C_i - b w(Y_i)][Y_i' - b X_i'] - \bar{X} - \frac{\partial \phi / \partial X_i}{\partial \phi / \partial b}$$

and

$$\frac{\partial a}{\partial Y_i} = \frac{Z_i}{\Sigma_i Z_i} + \frac{2}{\Sigma_i Z_i} \Sigma_i \frac{Z_i}{} [C_i - b w(Y_i)] [Y_i' - b X_i'][Y_i' - b X_i'] - \bar{X}$$

$$\frac{\partial \phi / \partial Y_i}{\partial \phi / \partial b}$$

where $C_i = r_i \alpha_i$.

Reasonable approximate values for these quantities are given by the expressions (York, 1969):

$$\sigma_b^2 = 1 / \Sigma_i \, Z_i \, U_i^2$$

$$\sigma_a^2 = \sigma_b^2 \, \Sigma(Z_i \, x_i^2) / \Sigma_i \, Z_i$$

These are the expressions used in this study.

Appendix C. Stepwise Degassing Release Curves for Unknown Samples.

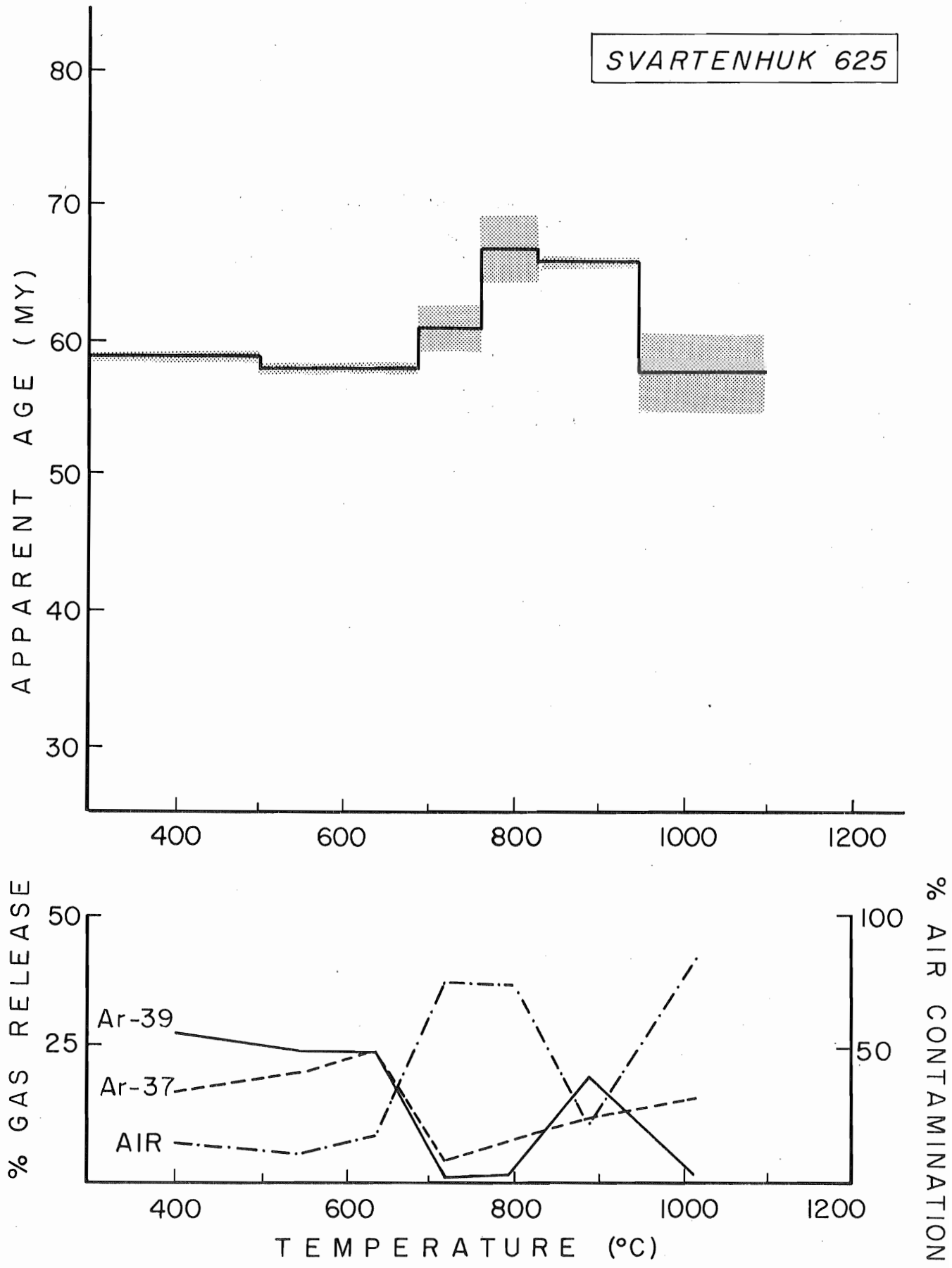
SVARTENHUK 625
APPARENT AGE (MY)
80
70
60
50
40
30
400
600
800
1000
1200
% GAS RELEASE
50
25
Ar-39
Ar-37
AIR
100
50
% AIR CONTAMINATION
400
600
800
1000
1200
TEMPERATURE (°C)

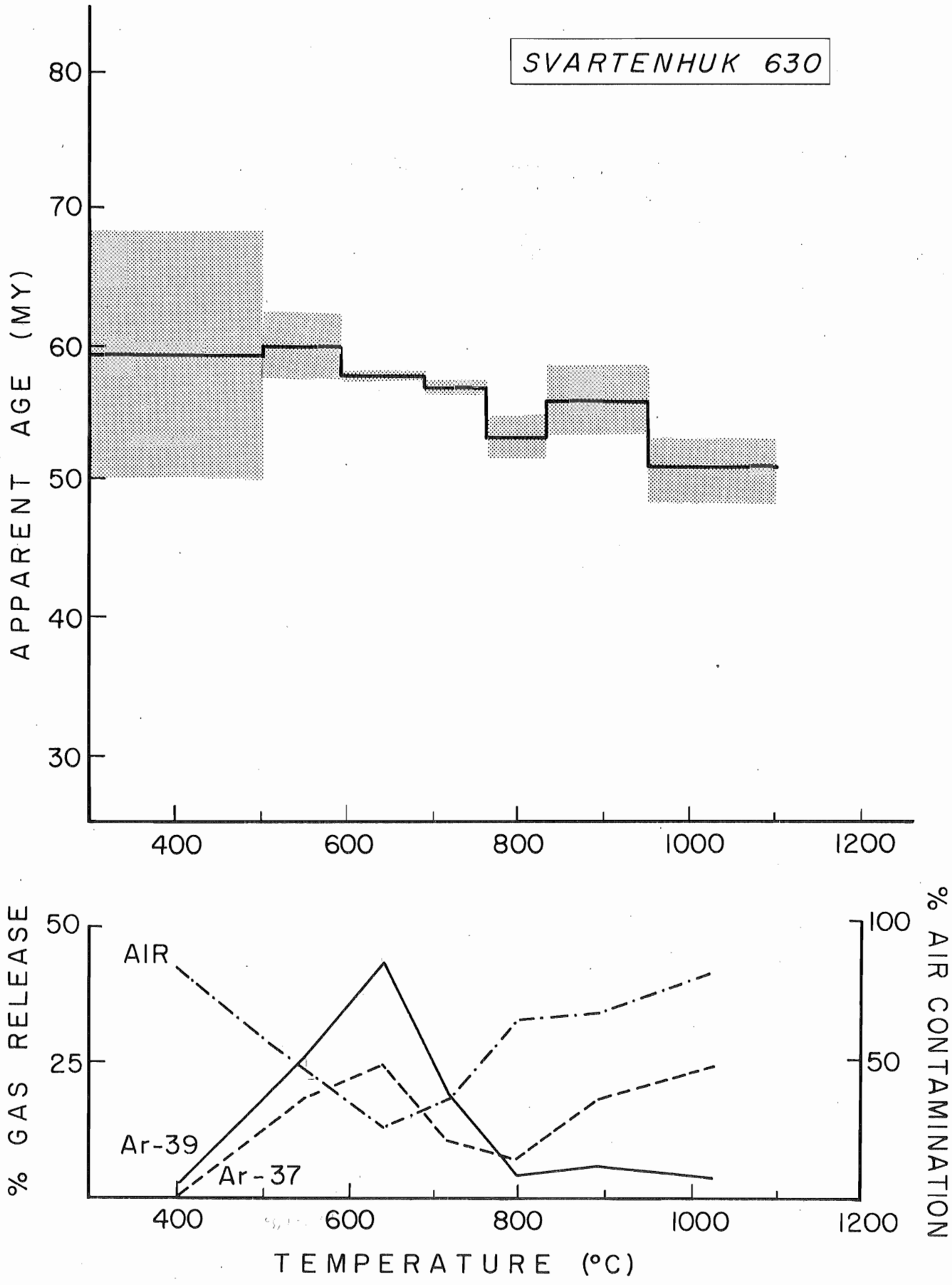
SVARTENHUK 630
APPARENT AGE (MY)
80
70
60
50
40
30
400
600
800
1000
1200
% GAS RELEASE
50
25
AIR
Ar-39
Ar-37
% AIR CONTAMINATION
100
50
TEMPERATURE (°C)

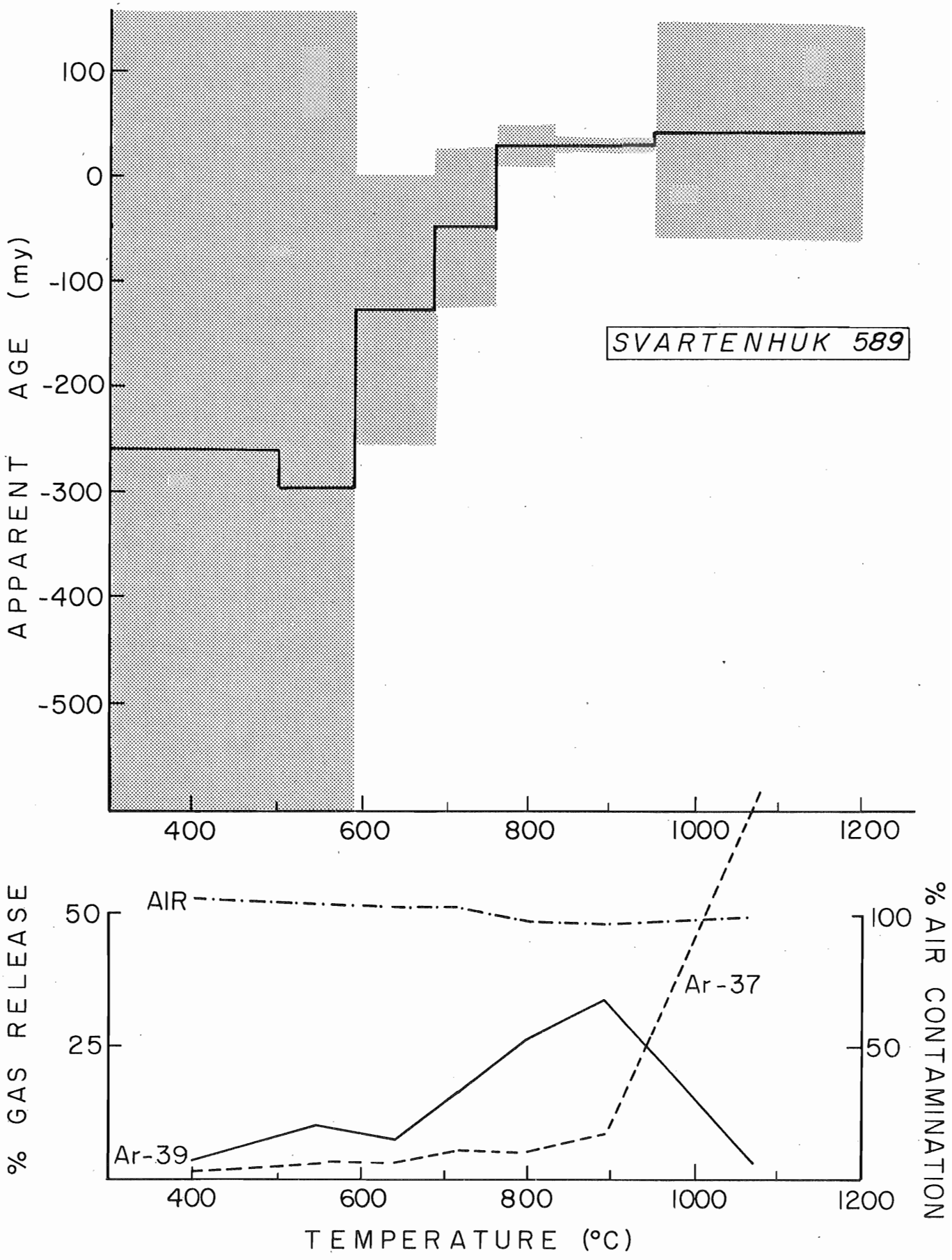
SVARTENHUK 589
APPARENT AGE (my)
100
0
-100
-200
-300
-400
-500
400
600
800
1000
1200
% GAS RELEASE
50
25
AIR
Ar-37
Ar-39
100
50
% AIR CONTAMINATION
400
600
800
1000
1200
TEMPERATURE (°C)

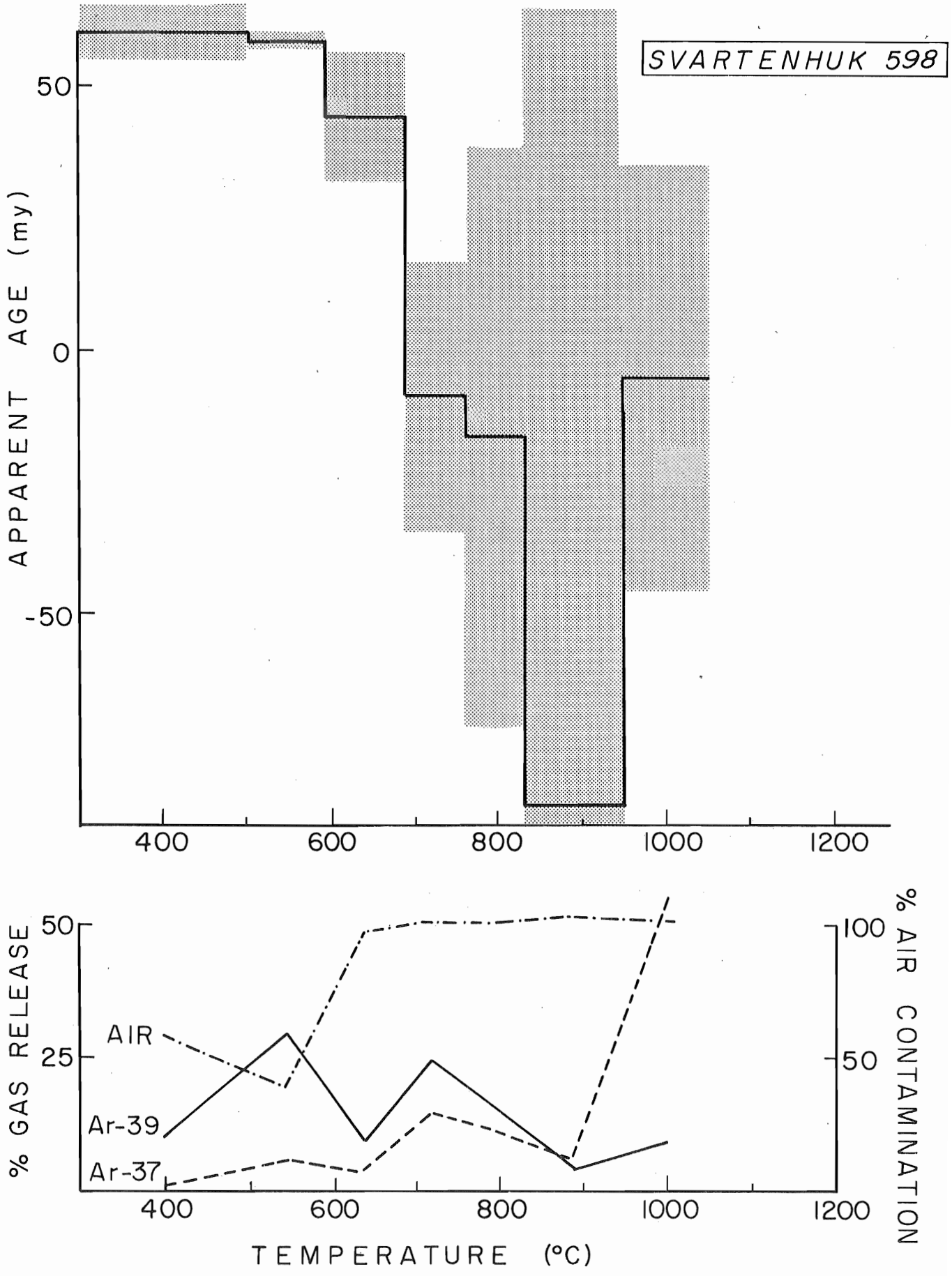
SVARTENHUK 598
APPARENT AGE (my)
50
0
-50
400
600
800
1000
1200
% GAS RELEASE
50
25
AIR
Ar-39
Ar-37
% AIR CONTAMINATION
100
50
TEMPERATURE (°C)

SVARTENHUK 999

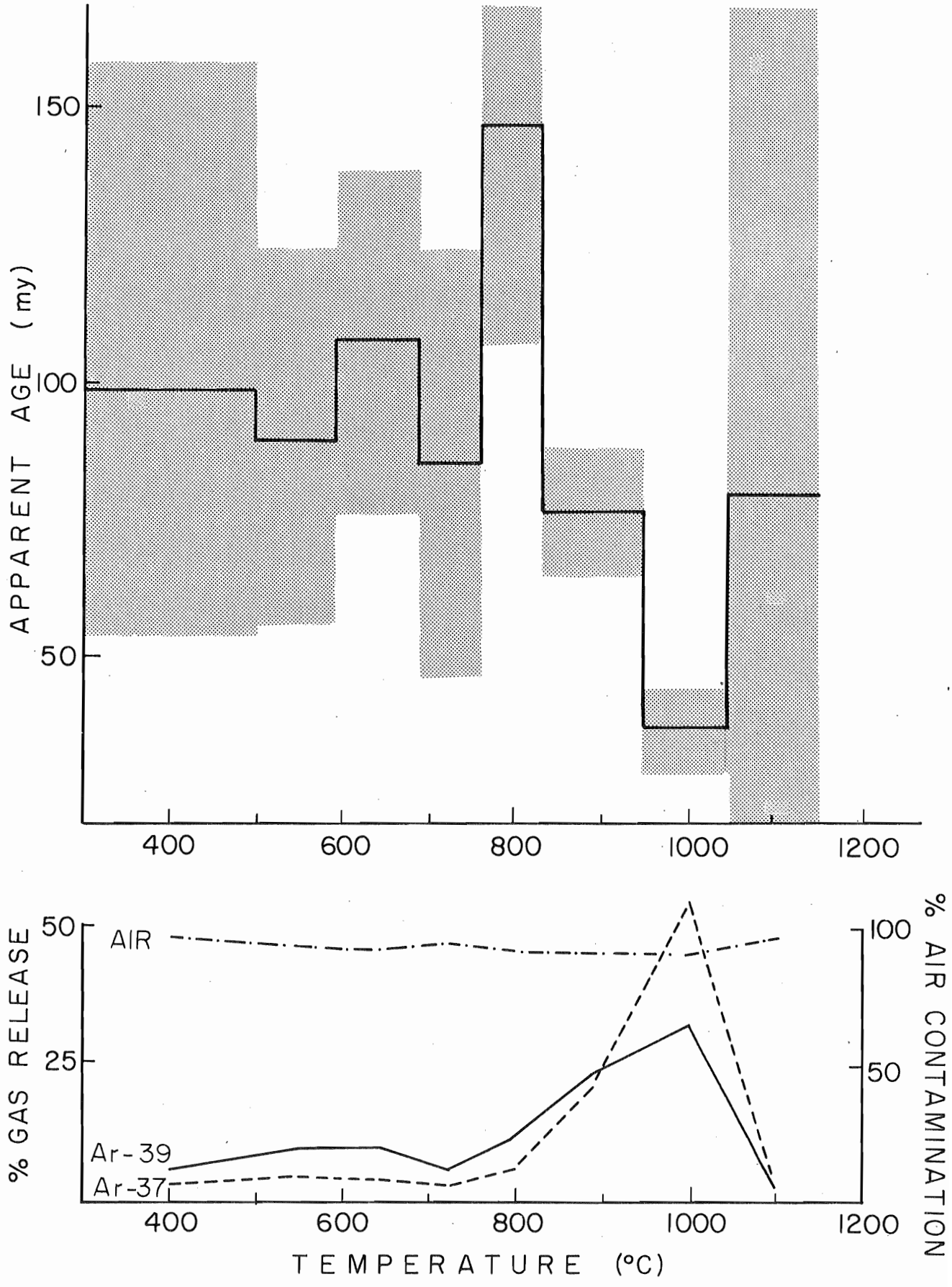

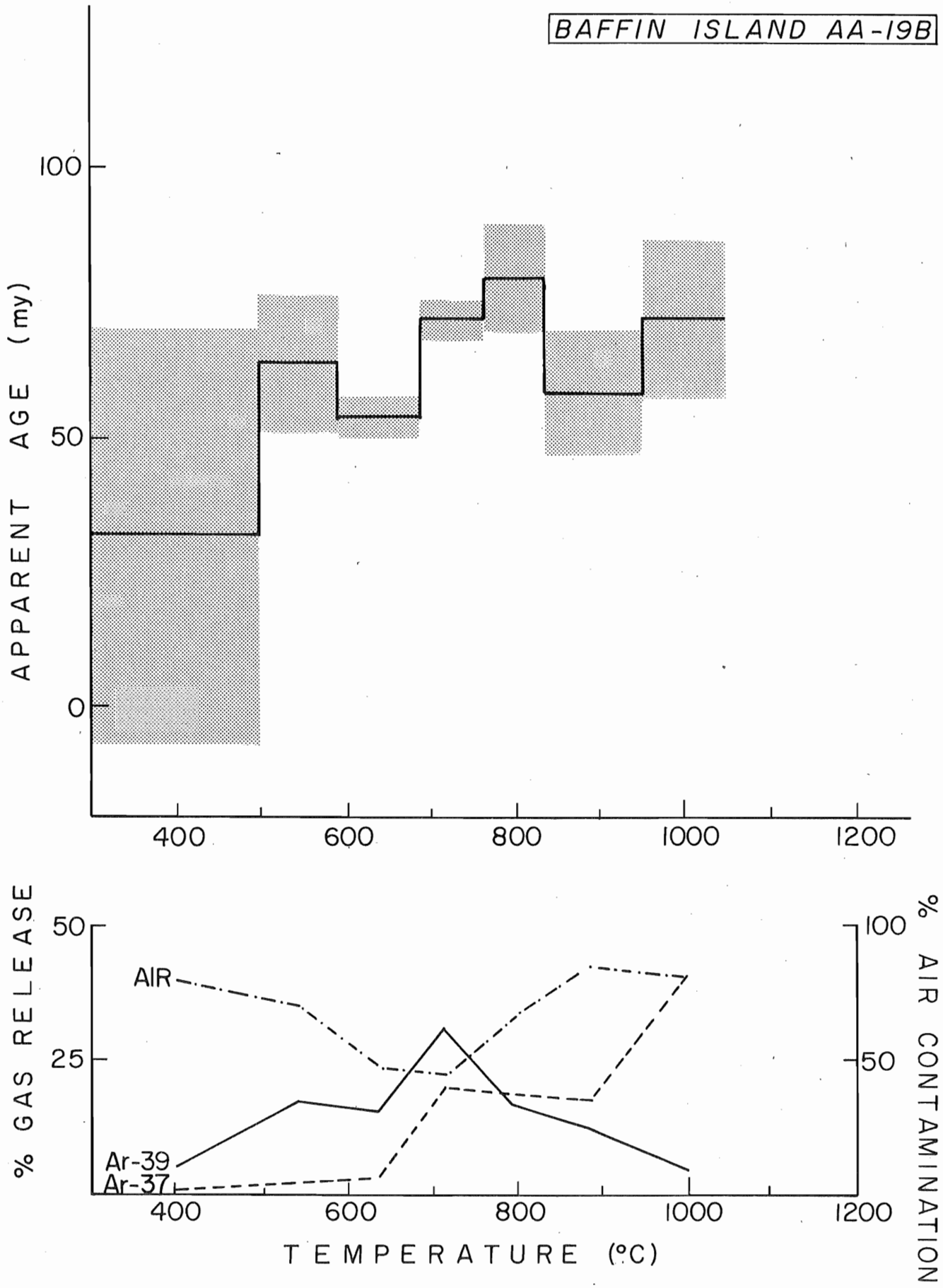
BAFFIN ISLAND AA-19B
APPARENT AGE (my)
100
50
0
400
600
800
1000
1200
% GAS RELEASE
50
25
AIR
Ar-39
Ar-37
% AIR CONTAMINATION
100
50
TEMPERATURE (°C)

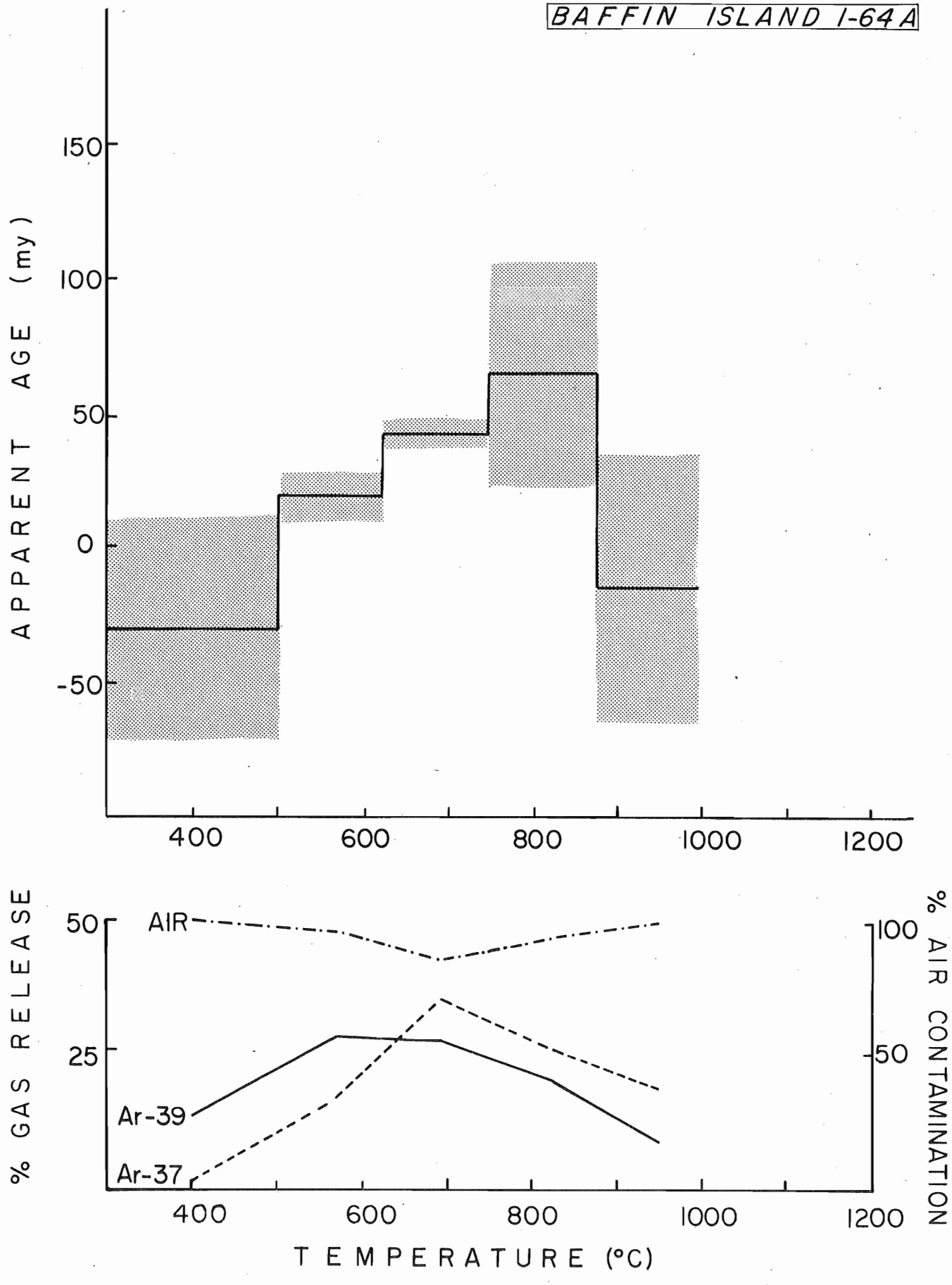
BAFFIN ISLAND I-64A
APPARENT AGE (my)
150
100
50
0
-50
400
600
800
1000
1200
% GAS RELEASE
50
25
AIR
Ar-39
Ar-37
100
50
% AIR CONTAMINATION
400
600
800
1000
1200
TEMPERATURE (°C)

BAFFIN ISLAND I-64 B

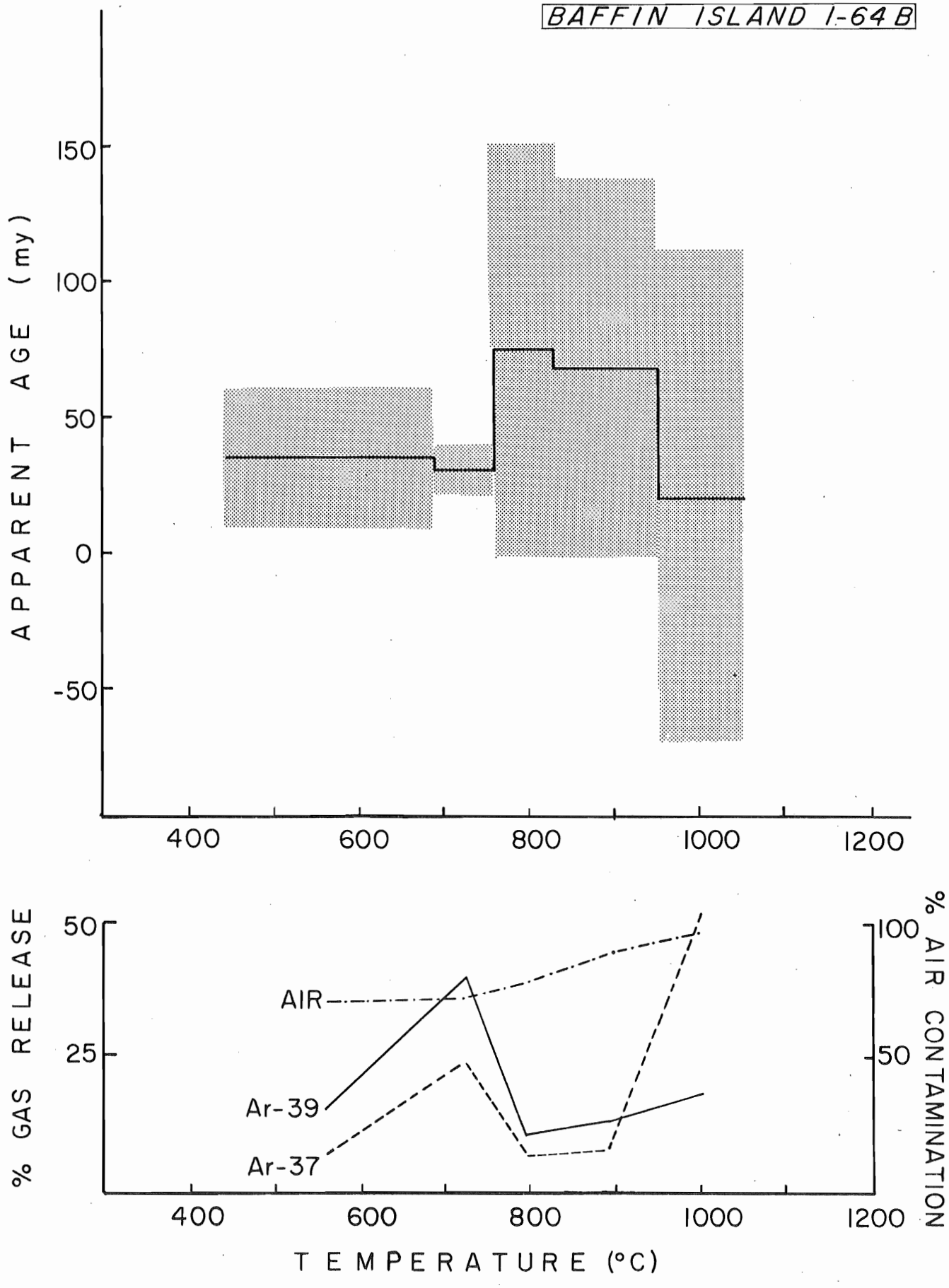

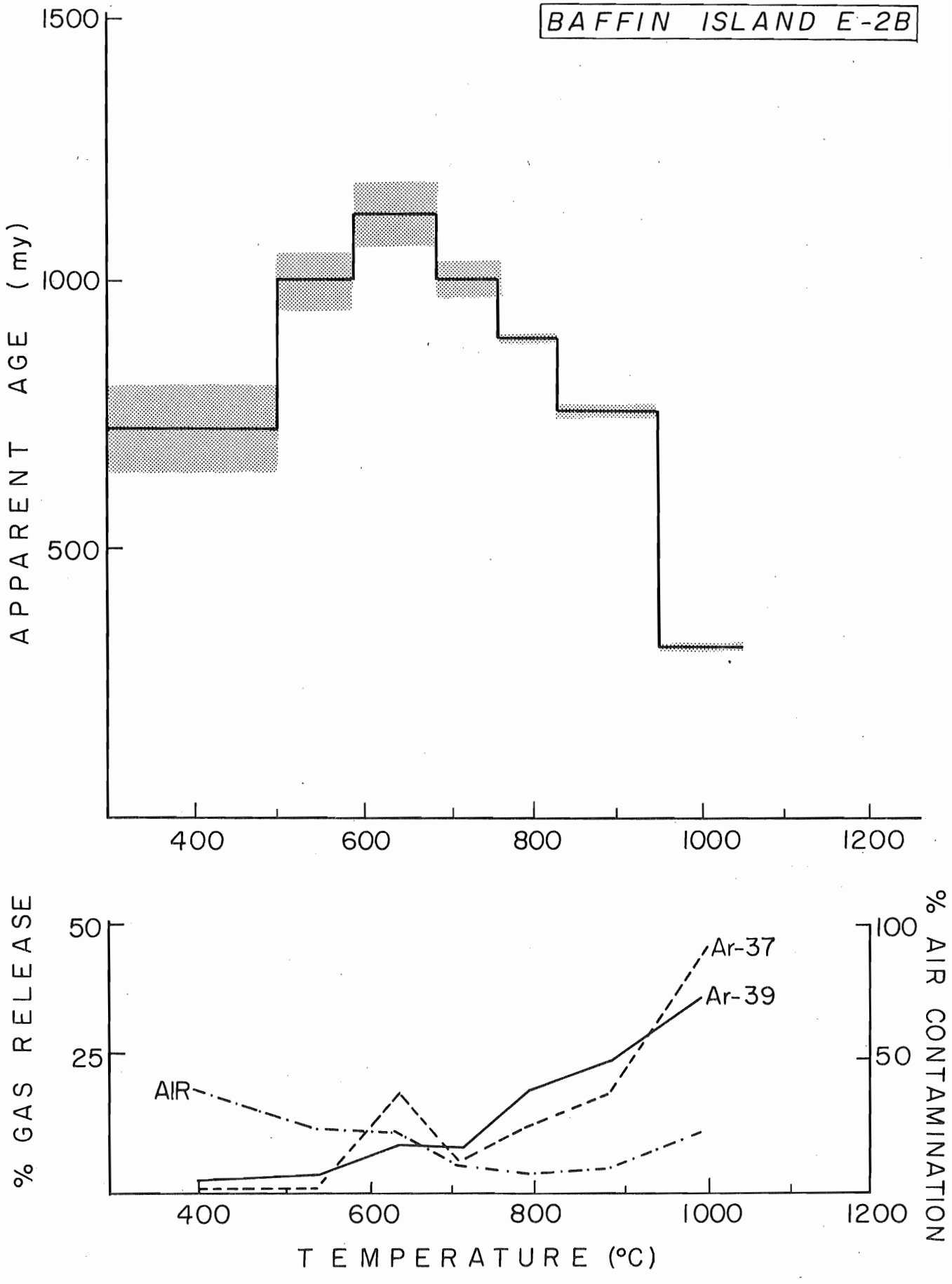
BAFFIN ISLAND E-2B
APPARENT AGE (my)
1500
1000
500
400
600
800
1000
1200
% GAS RELEASE
50
25
% AIR CONTAMINATION
100
50
Ar-37
Ar-39
AIR
400
600
800
1000
1200
TEMPERATURE (°C)

D.S.D.P. 12-112-17-1-26-29

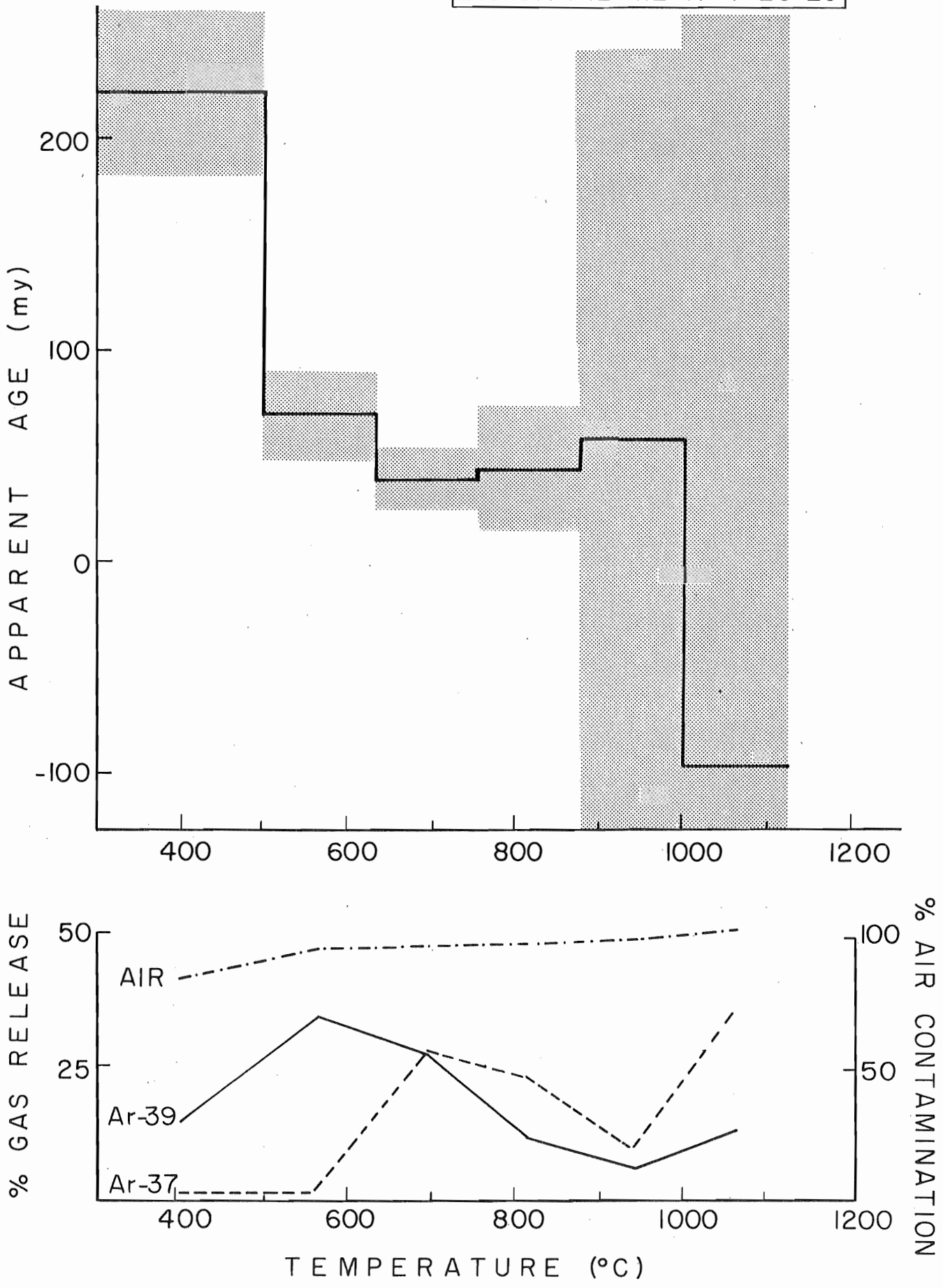

D.S.D.P. 12-112-17-1-127-129

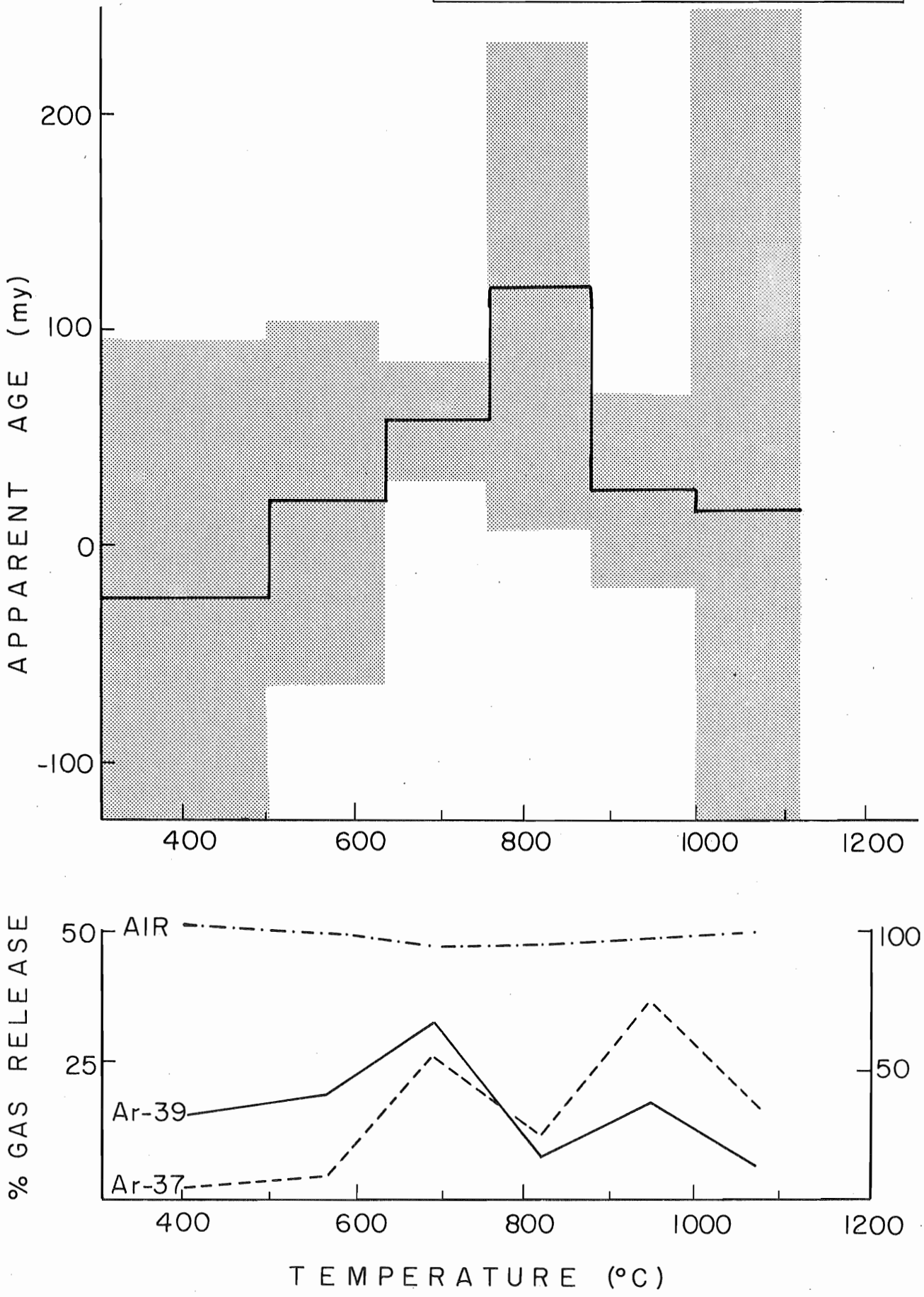

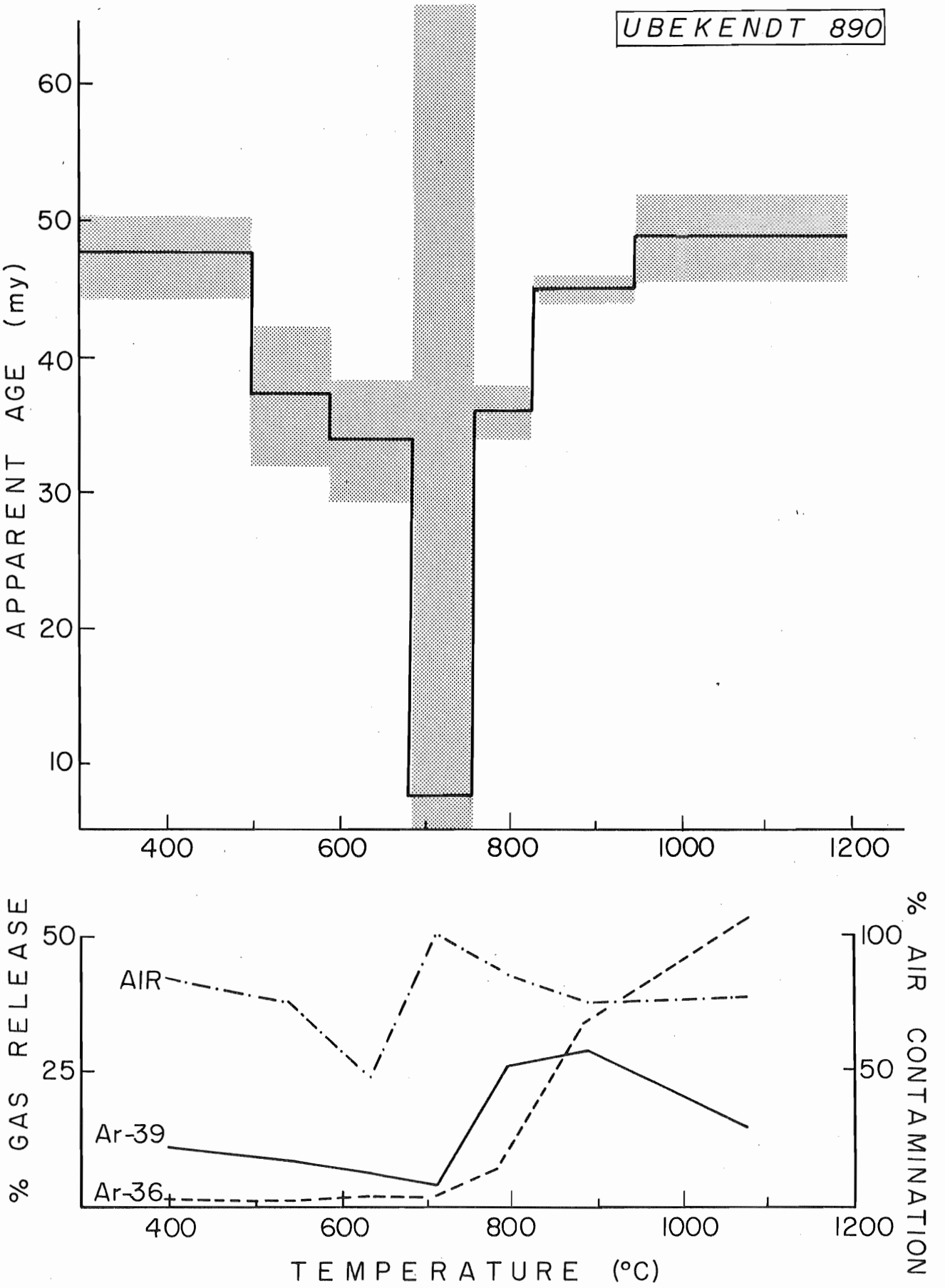
UBEKENDT 890
APPARENT AGE (my)
60
50
40
30
20
10
400
600
800
1000
1200
% GAS RELEASE
50
25
AIR
Ar-39
Ar-36
% AIR CONTAMINATION
100
50
TEMPERATURE (°C)

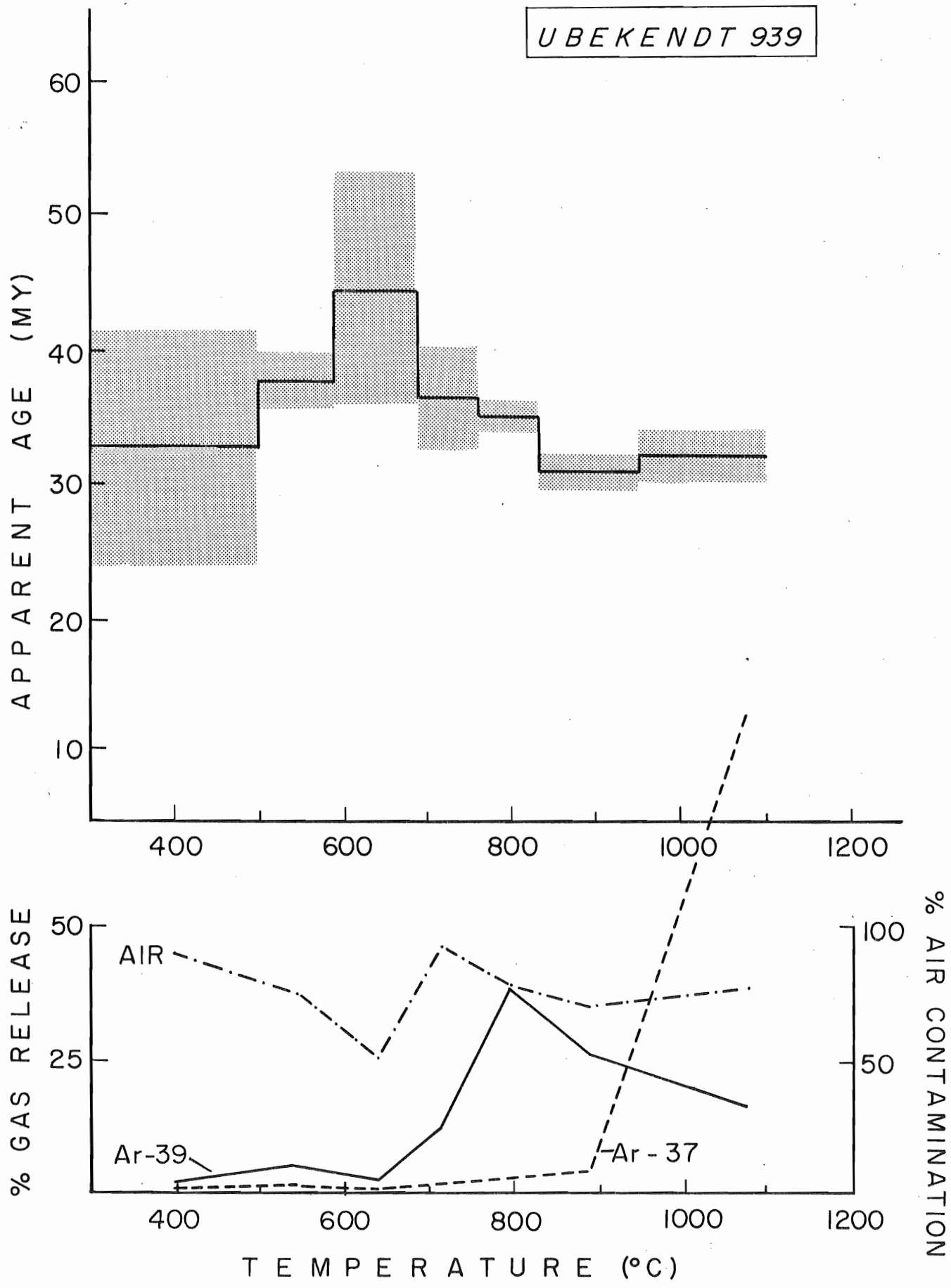
UBEKENDT 939
APPARENT AGE (MY)
60
50
40
30
20
10
400
600
800
1000
1200
% GAS RELEASE
50
25
AIR
Ar-39
Ar-37
100
50
% AIR CONTAMINATION
400
600
800
1000
1200
TEMPERATURE (°C)

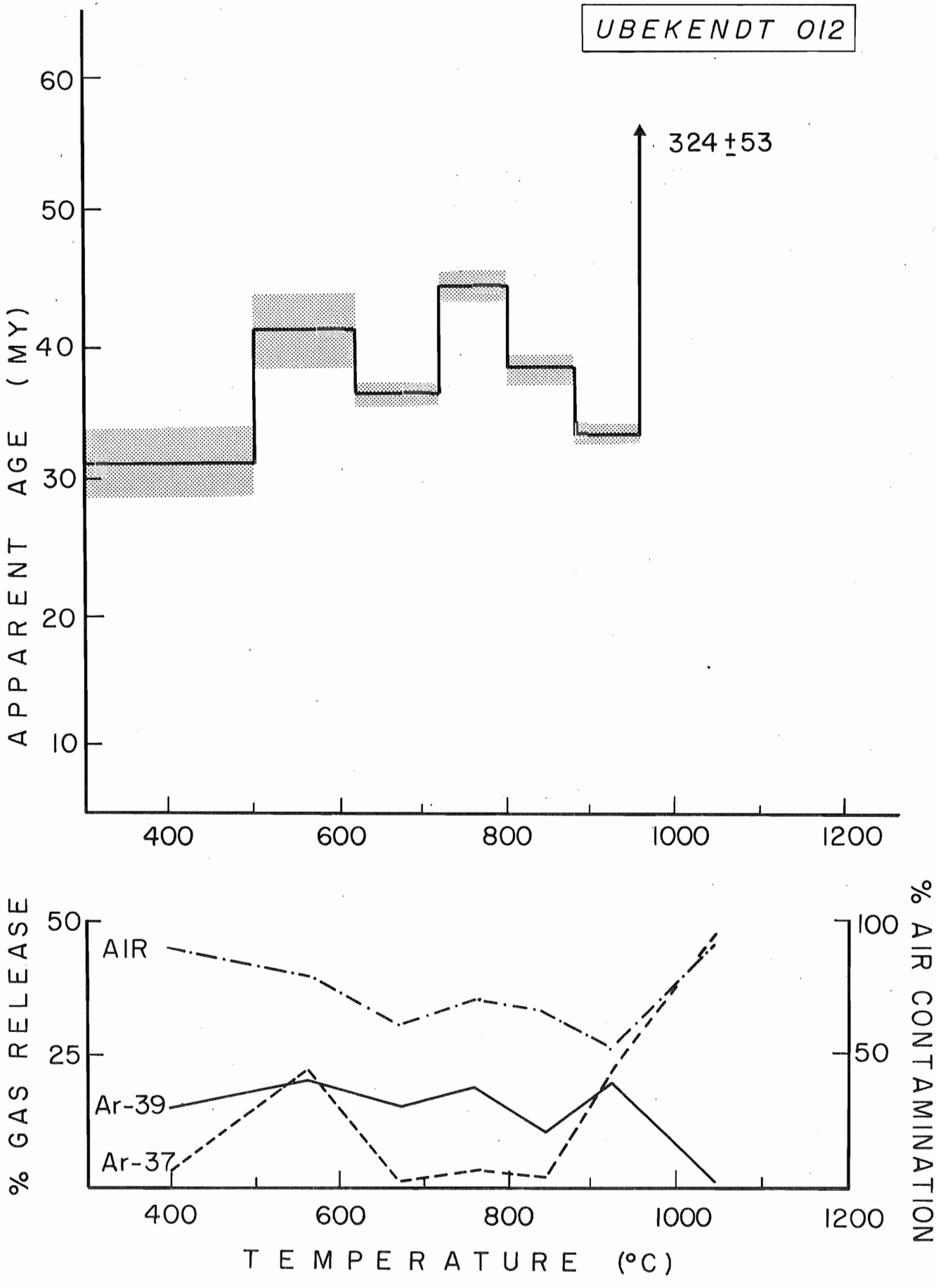
UBEKENDT 012
324 ± 53
APPARENT AGE (MY)
60
50
40
30
20
10
400
600
800
1000
1200
% GAS RELEASE
% AIR CONTAMINATION
AIR
Ar-39
Ar-37
50
25
100
50
TEMPERATURE (°C)

Appendix D. Isochron Diagrams for Unknown Samples.

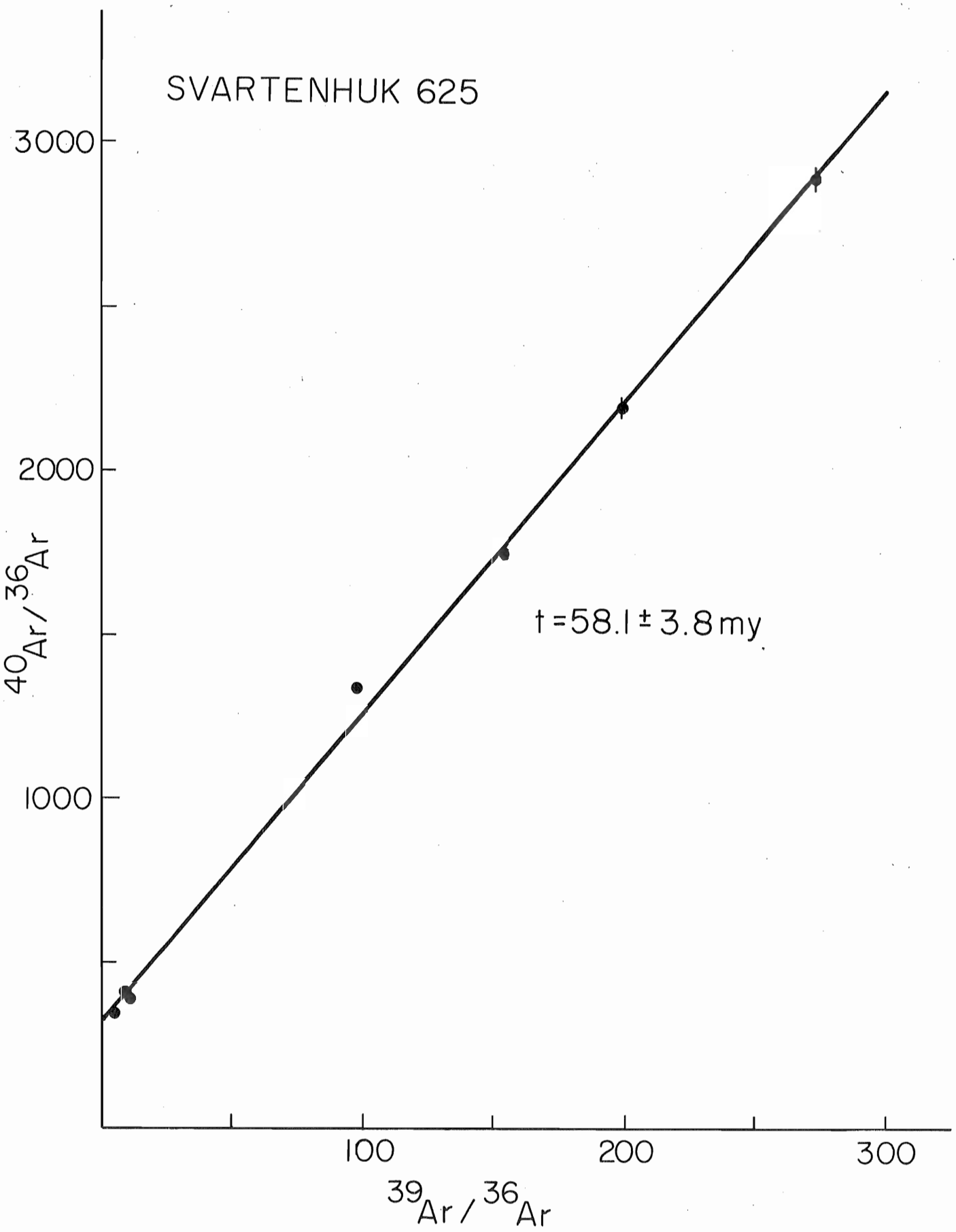
SVARTENHUK 625
3000
2000
1000
$^{40}Ar/^{36}Ar$
t = 58.1 ± 3.8 my
100
200
300
$^{39}Ar/^{36}Ar$

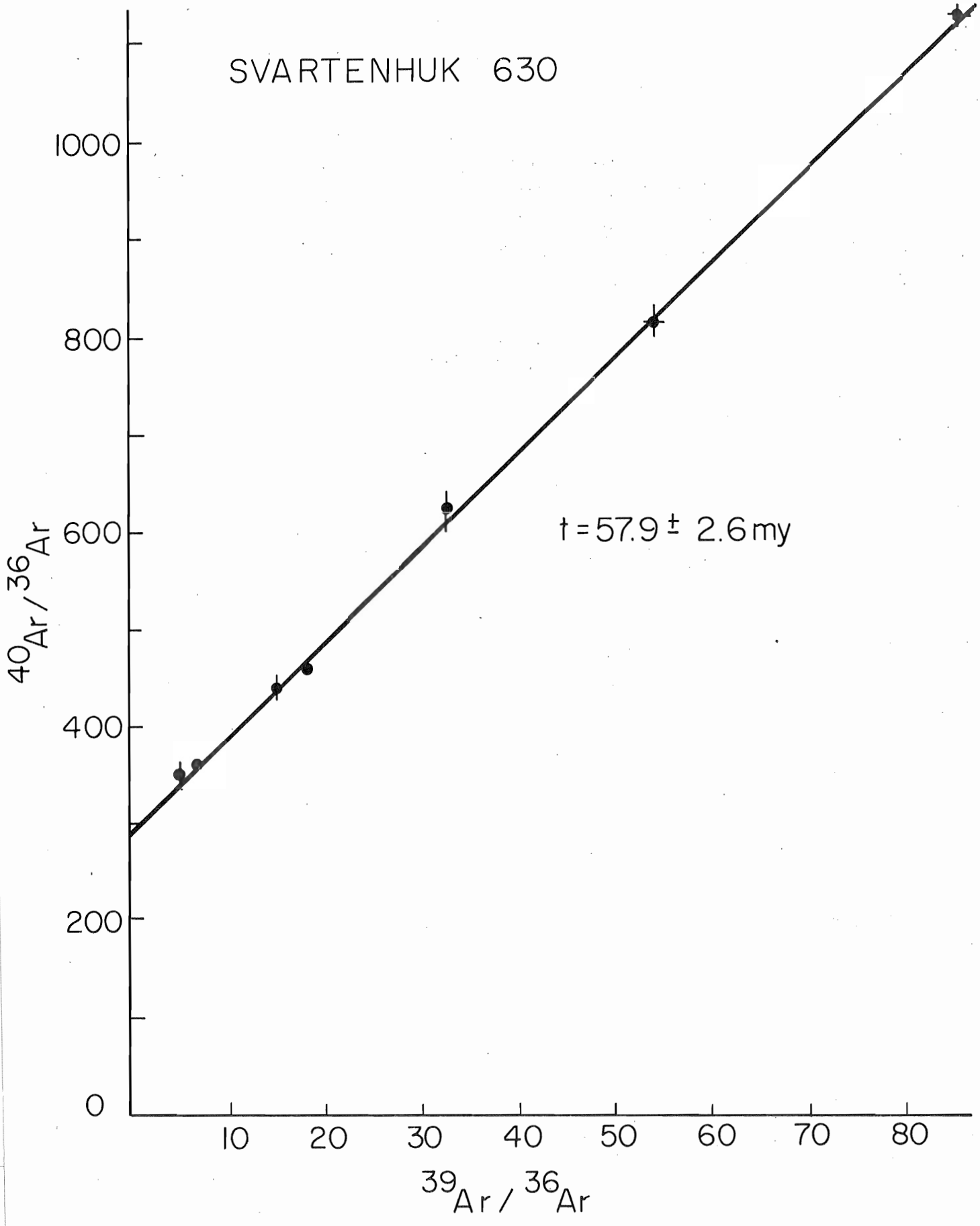
SVARTENHUK 630
t = 57.9 ± 2.6 my
$^{40}Ar/^{36}Ar$
$^{39}Ar/^{36}Ar$
0
200
400
600
800
1000
10
20
30
40
50
60
70
80

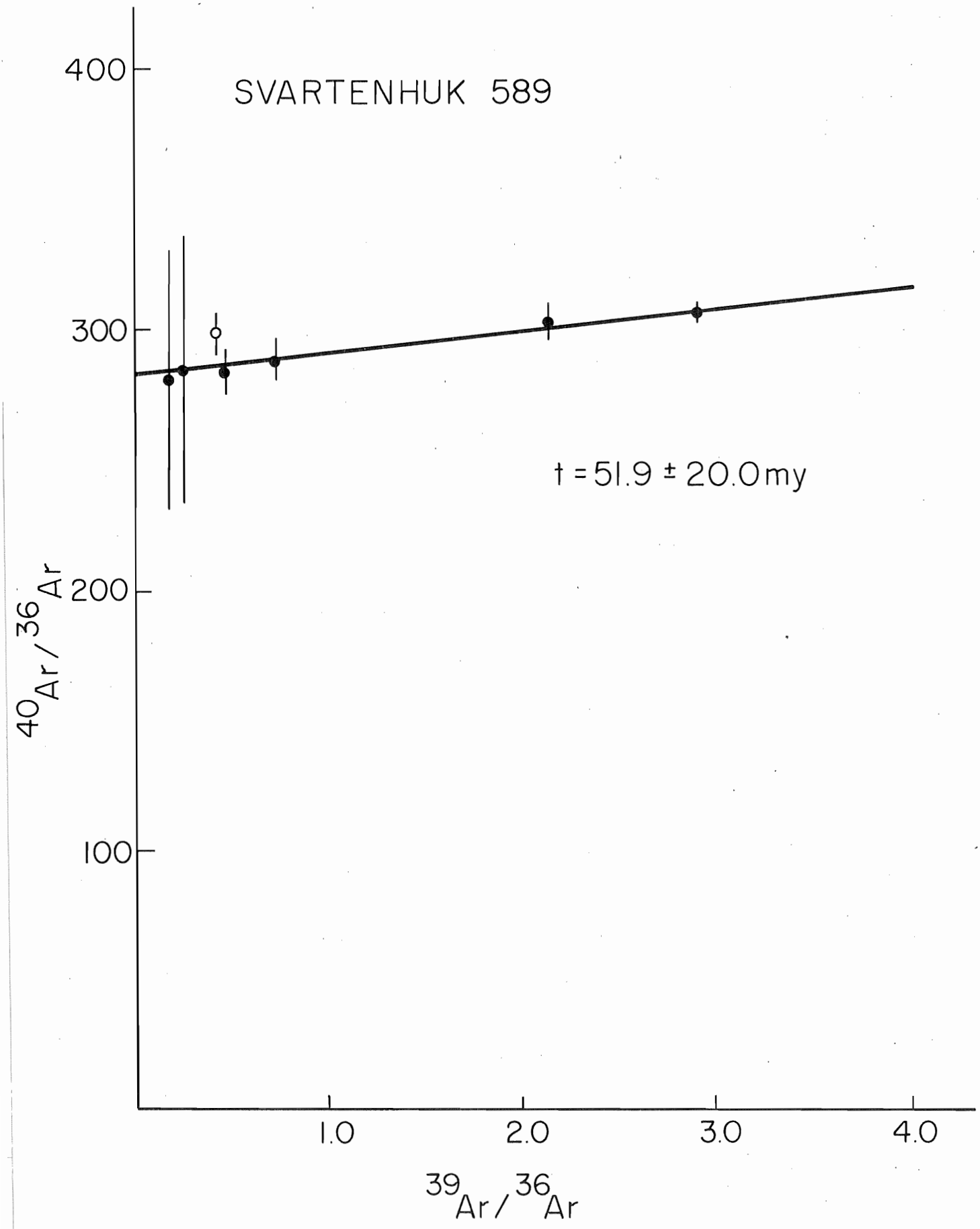
SVARTENHUK 589
t = 51.9 ± 20.0 my
400
300
200
100
$^{40}Ar/^{36}Ar$
1.0
2.0
3.0
4.0
$^{39}Ar/^{36}Ar$

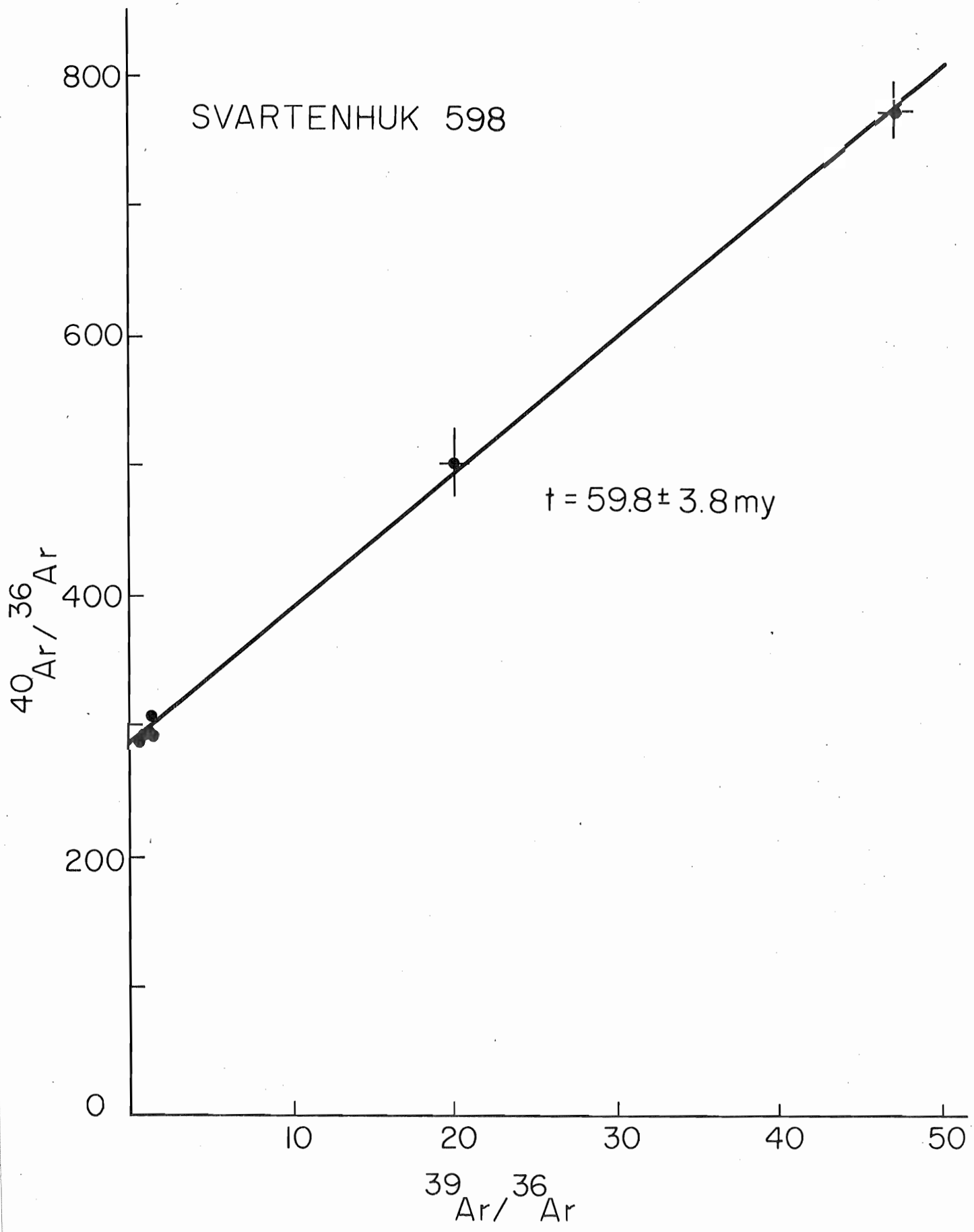
SVARTENHUK 598
t = 59.8 ± 3.8 my
800
600
400
200
0
10
20
30
40
50
40Ar/36Ar
39Ar/36Ar

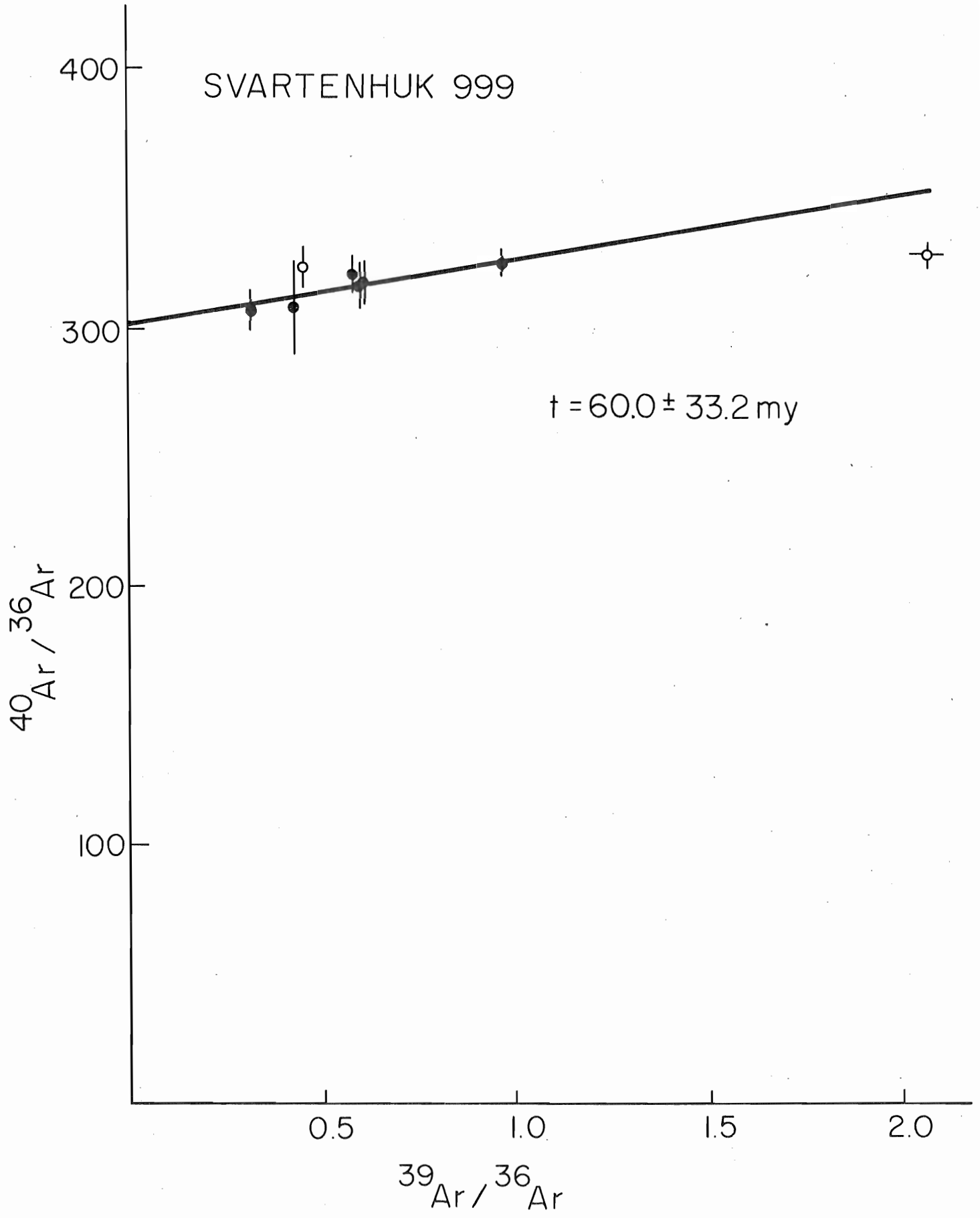
SVARTENHUK 999
t = 60.0 ± 33.2 my
400
300
200
100
0.5
1.0
1.5
2.0
40Ar / 36Ar
39Ar / 36Ar

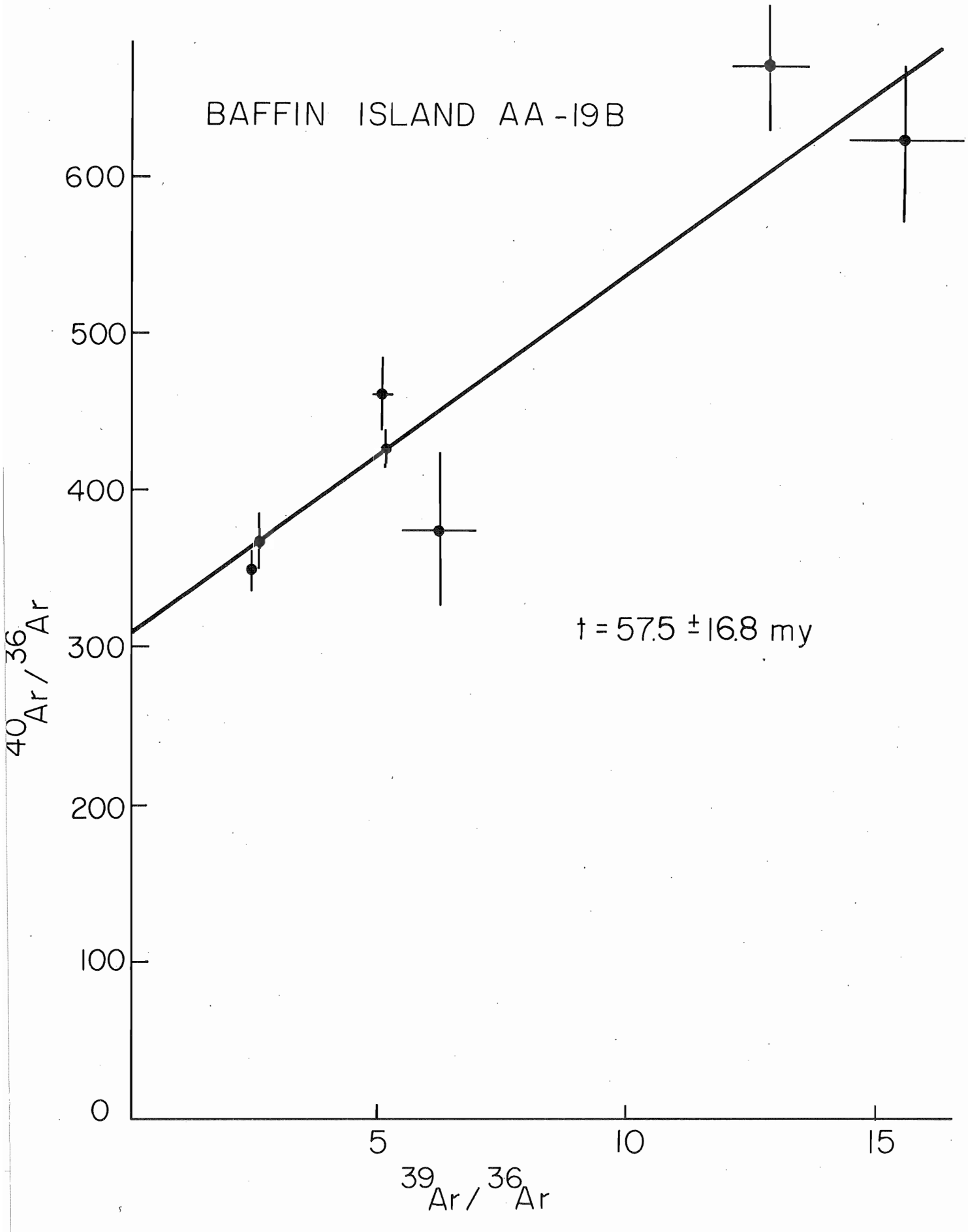
BAFFIN ISLAND AA-19B
600
500
400
300
200
100
0
5
10
15
$^{40}Ar/^{36}Ar$
$^{39}Ar/^{36}Ar$
t = 57.5 ± 16.8 my

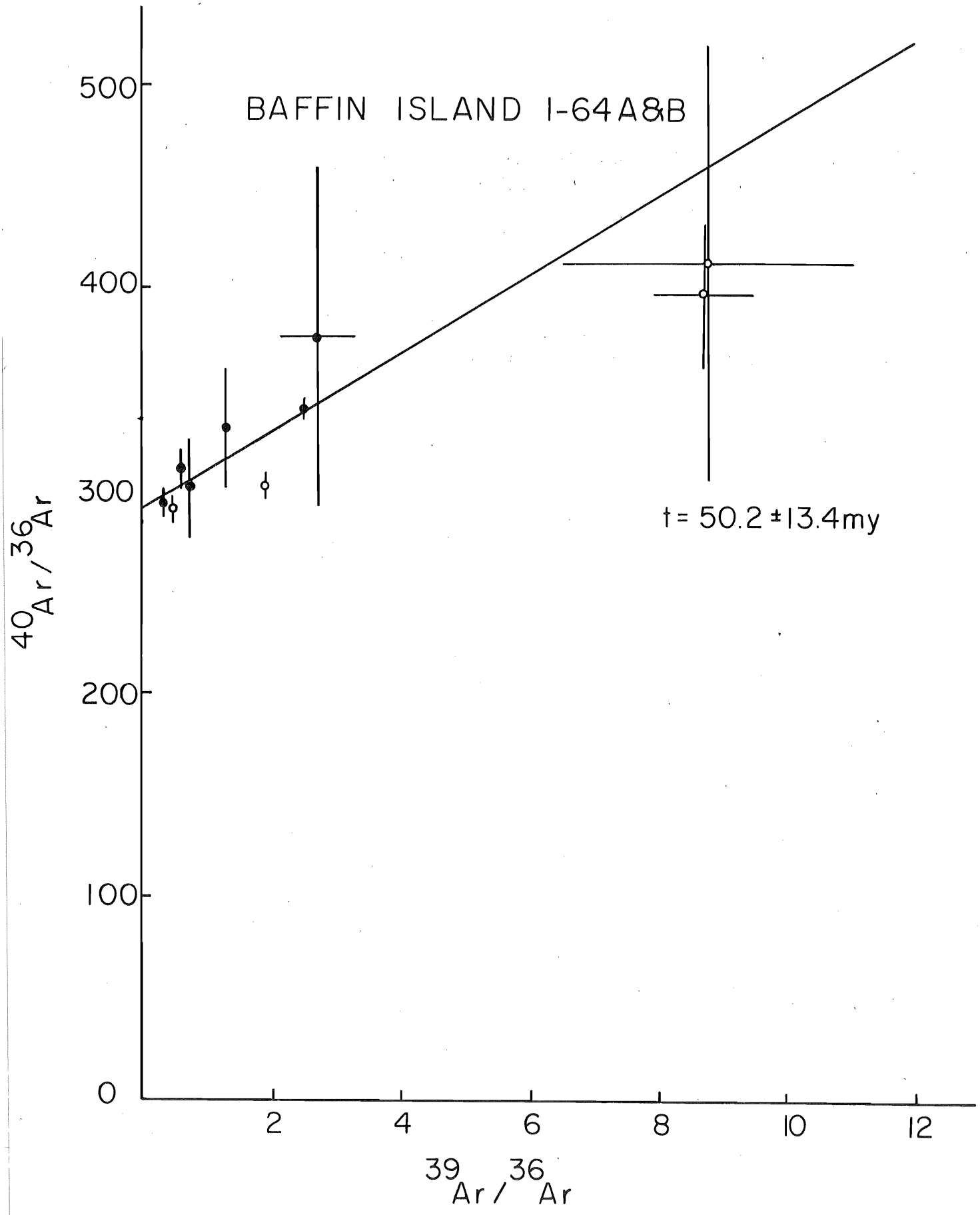
BAFFIN ISLAND I-64A&B
t = 50.2 ±13.4my
500
400
300
200
100
0
2
4
6
8
10
12
40Ar/36Ar
39Ar/36Ar

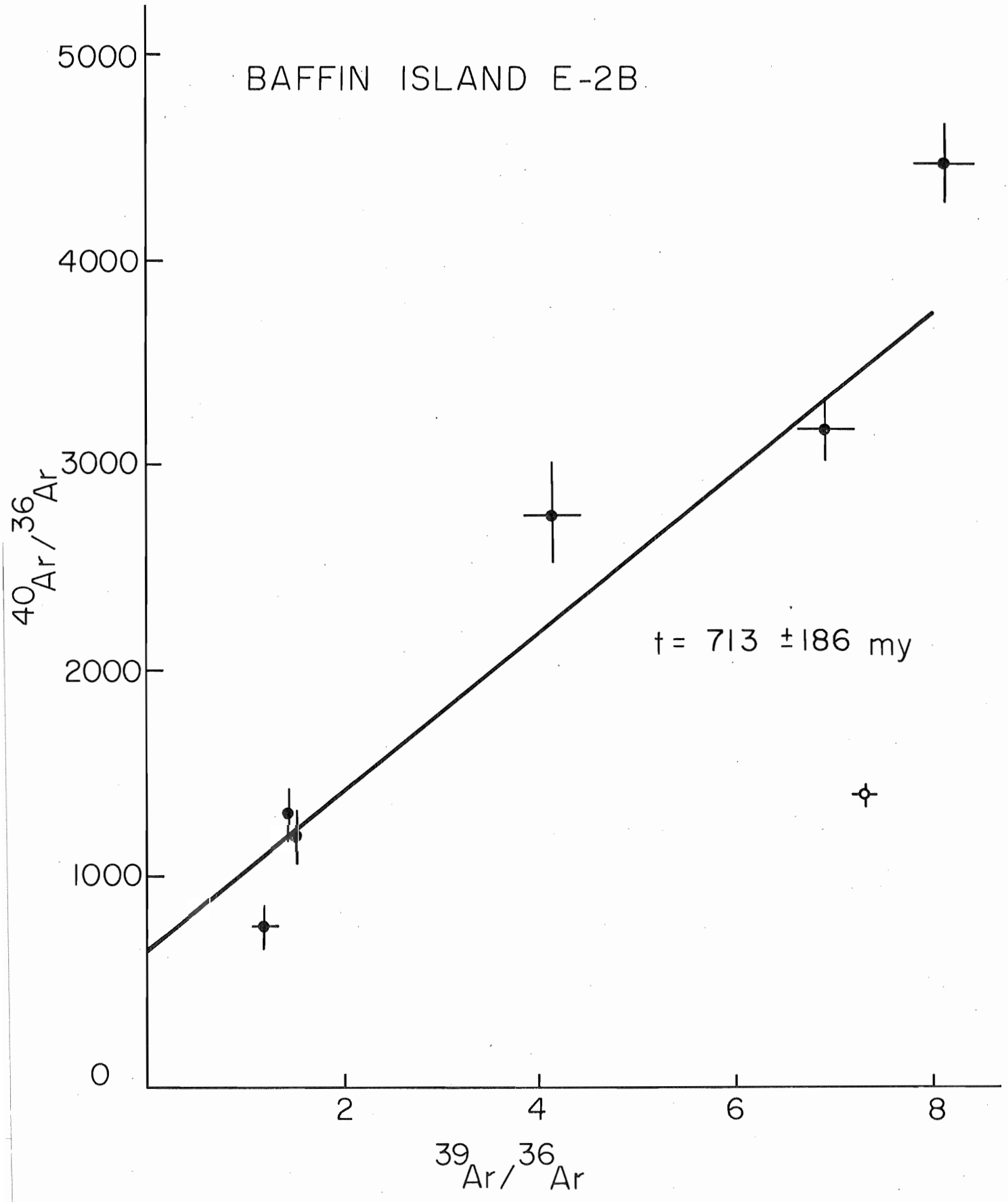
BAFFIN ISLAND E-2B
5000
4000
3000
2000
1000
0
$^{40}Ar/^{36}Ar$
t = 713 ±186 my
2
4
6
8
$^{39}Ar/^{36}Ar$

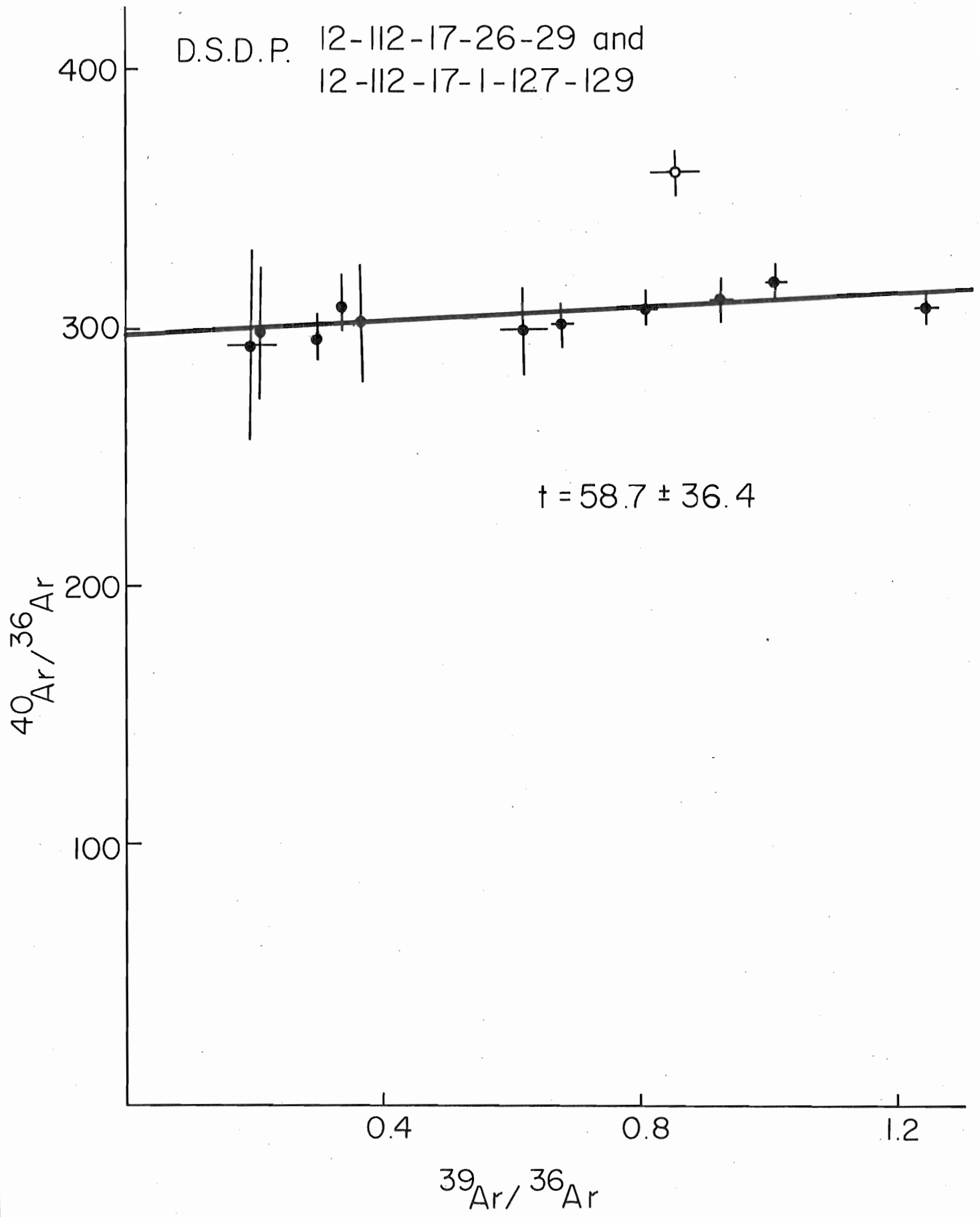
D.S.D.P. 12-112-17-26-29 and
12-112-17-1-127-129
400
300
200
100
t = 58.7 ± 36.4
40Ar/36Ar
0.4
0.8
1.2
39Ar/36Ar

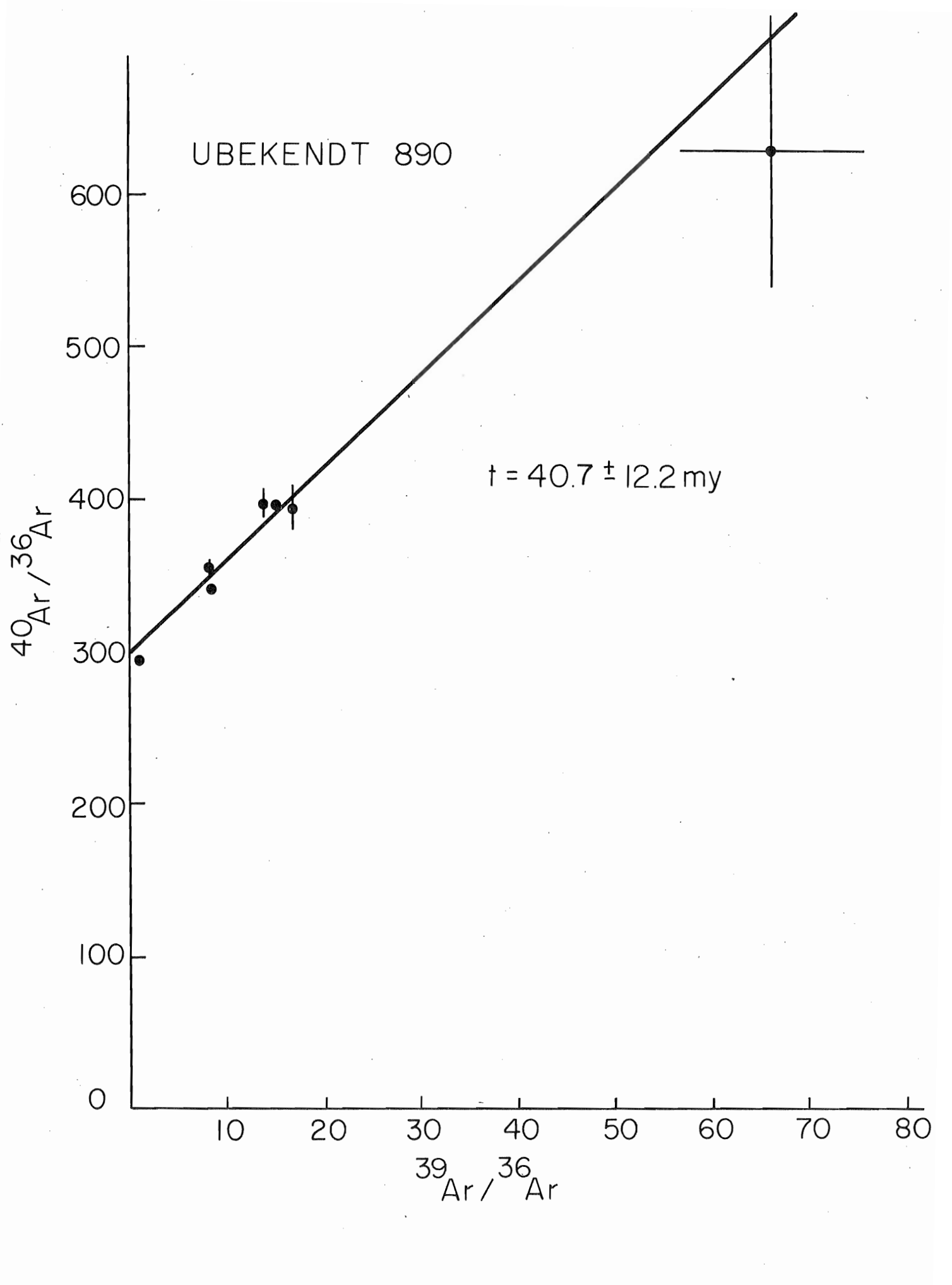
UBEKENDT 890
t = 40.7 ± 12.2 my
600
500
400
300
200
100
0
10
20
30
40
50
60
70
80
40Ar / 36Ar
39Ar / 36Ar

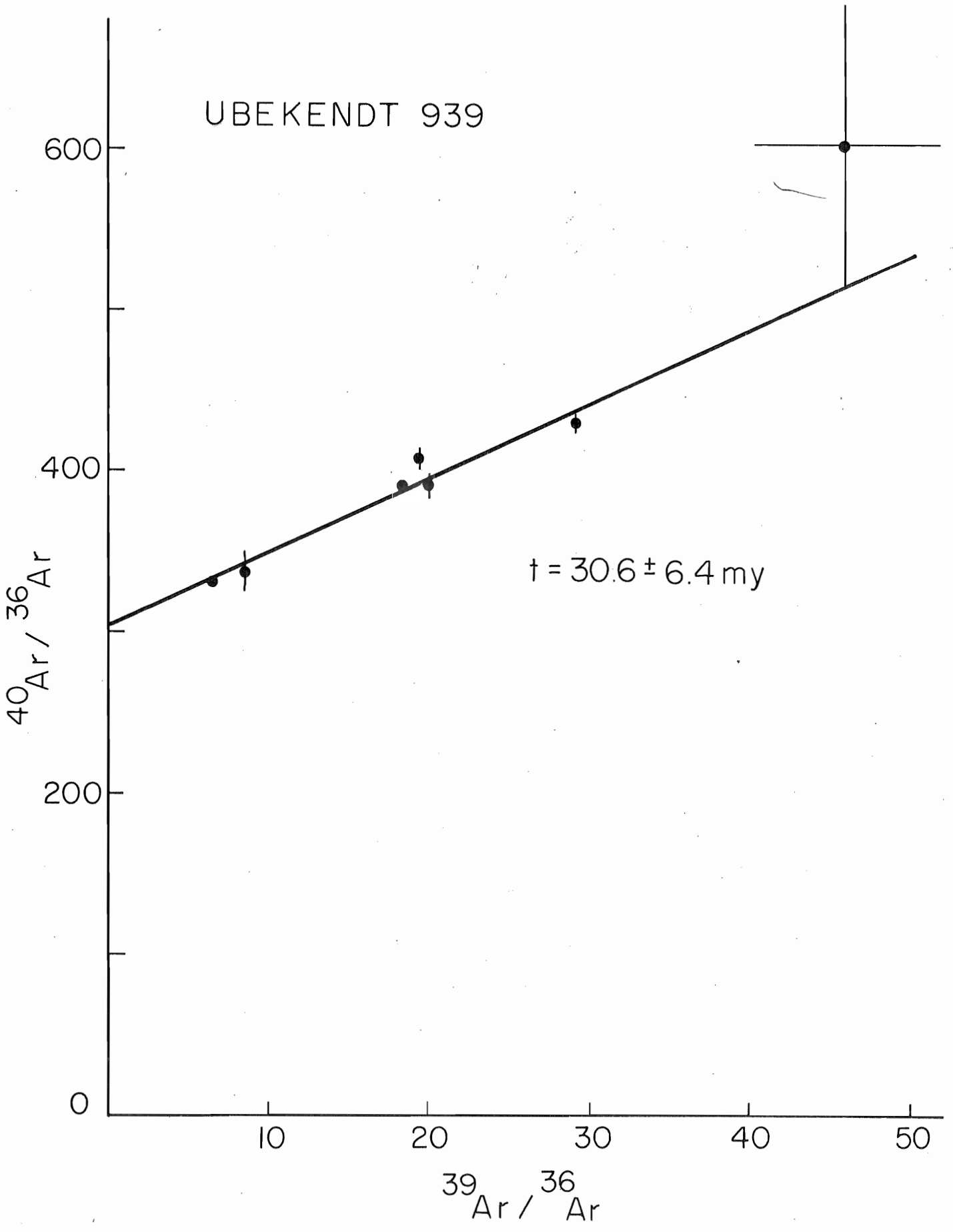
UBEKENDT 939
600
400
200
0
10
20
30
40
50
$^{40}Ar / ^{36}Ar$
$^{39}Ar / ^{36}Ar$
t = 30.6 ± 6.4 my

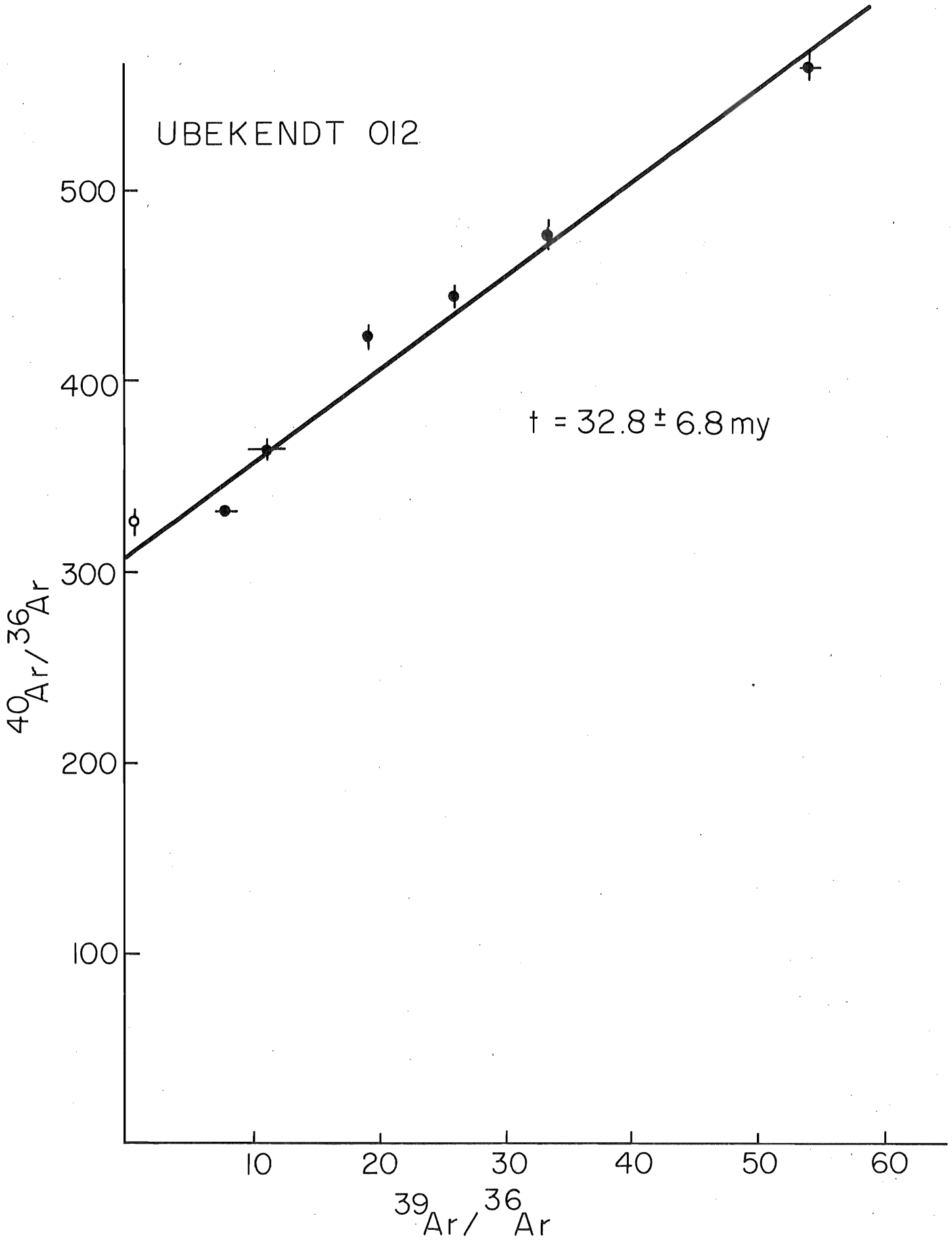
UBEKENDT 012
t = 32.8 ± 6.8 my
500
400
300
200
100
$^{40}Ar/^{36}Ar$
10
20
30
40
50
60
$^{39}Ar/^{36}Ar$

Appendix E. Sample Descriptions and some Chemical Analyses for the Unknown Samples.

SVARTENHUK TRACHYTES (2)

625

anortho + hb(?)

Subaerial very vesicular flow, Arfertuarssuk. Large, partly corroded phenocrysts of alkali feldspar (anorthoclase). Ferromagnesian minerals, possibly hornblende, completely pseudomorphed. Groundmass extremely fine-grained with trachytic texture. Approx. mode: Anortho 20%, Ferromag 5%, Gm 80%.

630

anortho + cpx

Intrusion (?) at least 30 m. thick, Arfertuarssuk. Large euhedral phenocrysts of anorthoclase and a second alkali feldspar (?) apparently undergoing resorption. Also phenocrysts of aegirine augite. Approx. mode: Anortho 15%, Cpx 5%, Cm 80%.

598

oliv + plag + cpx + mt

Subaerial flow, Svartenhavn. Chlorite pseudomorphs after olivine phenocrysts, glomeroporphyritic clusters of oscillatory-zoned plagioclase and small phenocrysts of augite. Likely phenocrysts of magnetite. Groundmass of granular plagioclase, clinopyroxene and magnetite. Vesicles filled with chlorite. Approx. mode: Phenocrysts; Plag 5%, Cpx 3%, Mt 2%. Groundmass; Plag 35%, Cpx 35%, Mt 10%, Chlor 1%.

589

oliv + plag + cpx + mt(?)

Subaerial flow, 3 m. thick, Tasiussap ima. Partly serpentinized phenocrysts of olivine with inclusions of opaque and reddish spinel. Glomeroporphyritic clusters of clinopyroxene. Magnetite phenocrysts (?). Groundmass texture is essentially granular. Groundmass clinopyroxene is zoned outwards to a brown rim (titanaugite ?). Partial breakdown of plagioclase to zoolite. Approx. mode: Oliv 5%, Plag trace, Cpx 2%, Mt 2%, Gm 35%, Zeol 5% Sp trace.

638

oliv + plag + cpx

Boulder, east side of Arfertuarssuk. Phenocrysts of olivine completely altered to carbonate and an unknown mineral. Large phenocrysts of plagioclase showing very strong, mostly normal zoning and a few small augite phenocrysts. Granular groundmass. Approx. mode: Pseudo Oliv 10%, Plag 20%, Cpx 5%, Gm 60%, Mt 5%.

999

ol cpx + plag

Black breccia, location uncertain. Amygdaloidal with fractured and resorped phenocrysts of plagioclase with olivine and clinopyroxene phenocrysts in a glassy matrix. Plagioclase also appears to fill cavities and is altered or accompanied by an unknown brown mineral. Approx. mode: Plag. 25%, Oliv 20%, Cpx 10%, GM 50%.

BAFFIN ISLAND BASALTS (3)

AA-19

Thick flow at radar station, Cape Dyer. Second leucocratic and vesicular band from the top and 1 m. thick. Coarse-grained aggregate of plagioclase and twinned augite, both

of which are strongly zoned. Olivines small, rounded and partly iddingsitized. Interstitial material consists of skeletal magnetite, feathery augite and a wormy intergrowth of plagioclase and quartz (?) resembling a myrmekitic texture. Approx. mode: Oliv 1%, Plag 45%, Cpx 45% Interstit 4%.

I-64 oliv — Basaltic block in orange breccia, Reid's Bay. Generally subhedral to euhedral fresh olivine phenocrysts (Fa_{14}) with some reddish spinel enclosed. Groundmass contains recognizable plagioclase laths, reddish spinels, microlites of augite, fine-grained magnetite and minor glass. Approx. mode: Oliv 35%, Plag 30%, Cpx 30%, Glass 2%, Mt 2%, Sp trace.

E-2 oliv + plag — Black breccia, Cape Searle. Fresh euhedral and skeletal olivine phenocrysts with spinel inclusions and also a few phenocrysts of plagioclase. Unaltered glass (sideromalane) is greenish and completely isotropic. Each fragment of glass has a complete darkened border of palagonite and individual fragments may be separated by a zone of fibropalagonite. Some vesicules are filled with a zeolite (chabazite ?). Approx. mode: Oliv 10%, Plag 10%, Siderom 35%, Palag 20%, Fbpalag 25%, Sp trace.

UBEKENDT EJLAND LAMPROPHYRES (3)

890

cpx + ol

Dyke, Tuperssuarta. Phenocrysts of subhedral zone aegirine-augite and augite and serpentine pseudomorphs of olivine in a cryptocrystalline groundmass of plagioclase laths, clinopyroxene and iron oxides. Plagioclase shows slight lineation. Approx. mode: Cpx 25%, Pseudo Oliv 5%, Plag 20%, Iron Ox 5%, Gm 45%.

939

cpx

Dyke, Itiverna. Phenocrysts of zoned euhedral aegirine and augite in a crystalline groundmass of biotite, carbonate, magnetite and nephiline. Approx. mode: Cpx 45%, Bio 15%, Neph + Plag 20%, Mt 10%, Carb 5%, Pseudo oliv 5%.

012

cpx

Dyke, near Ivna. Euhedral to subhedral zoned augite phenocrysts in a fine-grained groundmass of biotite needles, magnetite crystals, carbonate masses and clinopyroxene crystals. Partially isotropic crypto-crystalline groundmass, olivine pseudomorphed by talc/carbonate. Approx. mode: Cpx 35%, Bio 15%, Mt 5%, Carb 5%, Gm 40%.

D.S.D.P. Site 112

26-29 & 127-129

plag + cpx

Black, hard, porphyritic, variolitic to microlitic basalt, altered in patches and stringers to a soft green, chloritic material. There are some white veinlets of calcite. Approx. mode: Plag 20%, Cpx 5%, Glass 15%, Mt 10%, Cm 50%.

Chemical Analyses: Svartenhuk Peninsula

	598	589	625	630	638
SiO_2	48.3	44.2	64.9	63.8	46.2
TiO_2	3.12	1.51	0.88	0.81	2.90
Al_2O_3	13.6	12.3	17.4	15.8	15.4
Cr_2O_3	0.02	0.09	0.00	0.00	0.02
Fe_2O_3	7.5	3.0	1.6	4.4	3.7
Feo	7.1	7.7	0.3	0.7	7.5
MnO	0.20	0.17	0.2	0.13	0.16
MgO	5.3	11.1	0.2	0.7	4.4
NiO	0.01	0.04	0.00	0.00	0.01
CaO	10.7	13.0	1.0	1.5	11.3
Na_2O	2.64	1.53	5.72	6.15	2.87
K_2O	0.32	0.81	5.64	4.75	0.38
P_2O_5	0.35	0.29	0.27	0.24	0.33
H_2O+	0.77	3.65	1.75	0.57	1.14
CO_2	-	-	-	-	3.28
Total	99.9	99.4	99.8	99.6	99.6

Analysis for sample 999 is unavailable

Chemical analyses: Clarke (1968b)

Sample numbers 598 and 589 in Clarke (1968b) are reversed in this thesis

Chemical Analyses: Baffin Island

	AA-19	E-2	I-64
SiO_2	51.1	45.2	44.2
TiO_2	1.21	0.90	0.84
Al_2O_3	14.8	12.3	10.9
Cr_2O_3	0.15	0.14	0.27
Fe_2O_3	1.6	3.8	2.7
FeO	5.9	6.3	7.4
MnO	0.14	0.16	0.18
MgO	8.5	13.1	19.3
NiO	0.02	0.05	0.12
CaO	14.3	9.0	9.8
Na_2O	2.01	1.64	0.99
K_2O	0.13	0.13	0.12
P_2O_5	0.11	0.08	0.10
H_2O+	0.44	7.60	2.68
CO_2	-	-	-
Total	100.4	100.4	99.6

Chemical analyses; Clarke (1968b)

Chemical Analyses: Ubekendt Ejland

	890	939	012
SiO_2	45.76	43.29	38.62
TiO_2	1.83	1.21	1.22
Al_2O_3	14.18	13.66	14.21
Cr_2O_3	0.00	0.00	0.00
Fe_2O_3	4.06	3.37	3.15
FeO	6.74	4.61	4.40
MnO	.18	.16	.17
MgO	8.08	11.39	8.28
NiO	0.00	0.00	0.00
CaO	11.07	12.50	14.30
Na_2O	2.23	1.69	2.32
K_2O	.96	2.19	2.98
P_2O_5	.54	.50	.46
H_2O+	3.52	3.85	3.91
CO_2	1.09	.85	5.51
Total	100.24	99.27	99.53

Chemical Analyses: Clarke (1975, personal communication)

Appendix F1 Variance of the $^{40}Ar/^{39}Ar^{NK}$ Ratio

For convenience equation (3.1) may be written as:

$$F = \frac{A - xB + (xb + ac)\,D - C}{1 - aD} \qquad \text{(F1.1)}$$

where $A = {}^{40}Ar/{}^{39}Ar$, $B = {}^{36}Ar/{}^{39}Ar$, $D = {}^{37}Ar^{C}/{}^{39}Ar$, $F = {}^{40}Ar^{*}/{}^{39}Ar^{NK}$, $a = {}^{39}Ar^{NCa}/{}^{37}Ar^{NCa}$, $b = {}^{36}Ar^{NCa}/{}^{37}Ar^{NCa}$, $c = {}^{40}Ar^{NK}/{}^{39}Ar^{NK}$ and $x = 295.5$. The estimated error in the $^{40}Ar^{*}/^{39}Ar^{NK}$ ratio, ΔF, may be obtained by differentiating equation (F1.1) to obtain:

$$\Delta F = \left[\left(\frac{\partial F}{\partial A}\right)^{2}\Delta A^{2} + \left(\frac{\partial F}{\partial B}\right)\Delta B^{2} + \left(\frac{\partial F}{\partial D}\right)^{2}\Delta D^{2}\right]^{1/2}$$

$$= \left[\frac{\Delta A^{2}}{(1-aD)^{2}} + \left(\frac{-x}{1-aD}\right)^{2}\Delta B^{2} + \left(\frac{xb + aA - a\,x\,B}{(1-aD)^{2}}\right)^{2}\Delta D^{2}\right]^{1/2} \qquad \text{(F1.2)}$$

In general the quantity aD is small and can be neglected, thus equation (F1.2) reduces to $\Delta F \simeq (\Delta A^{2} + (xb + aA - axB)^{2}\Delta D^{2} + x^{2}\,\Delta B^{2})^{1/2}$. Since $\sigma_{A} \simeq \frac{\Delta A}{A}$, $\sigma_{B} \simeq \frac{\Delta B}{B}$ and $\sigma_{D} \simeq \frac{\Delta D}{D}$, then the variance in the $^{40}Ar^{*}/^{39}Ar^{NK}$ ratio, σ_{F}^{2} can be approximated by:

$$\sigma_{F}^{2} = \frac{A^{2}\sigma_{A}^{2} + x^{2}B^{2}\sigma_{B}^{2} + (aA - xaB + xb)^{2}\,D^{2}\sigma_{D}^{2}}{F^{2}}$$

Appendix F2 Variance of J

The estimated error in the flux monitor, ΔJ, may be obtained by differentiating equation (2.15) to obtain:

$$\Delta J = \left(\frac{\lambda e^{\lambda t_s}}{F}\right)^2 \Delta t_s^2 + \left(\frac{e^{\lambda t_s}-1}{F^2}\right)^2 \Delta F^2 \quad ^{1}/_{2}$$

where Δt_s is the estimated error in the age of the standard and ΔF is the estimated error in the ratio $^{40}Ar^*/^{39}Ar^{NK}$. If the standard deviations $\sigma_J \simeq \frac{\Delta J}{J}$ and $\sigma_{t_s} \simeq \frac{\Delta t_s}{t_s}$ are substituted in the above expression, then the variance in J, σ_J^2 , may be approximated by:

$$J^2\sigma_J^2 = \left(\frac{\lambda^2 t_s^2 e^2\lambda t_s}{F}\right) \sigma_{t_s}^2 + J^2\sigma_F^2$$

Or, upon rearranging terms and using expression (2.15), the above expression becomes

$$\sigma_J^2 = \frac{\lambda^2 t_s^2 \, e^{2\lambda t_s}}{(e^{\lambda t_s}-1)^2} \sigma t_s^2 + \sigma_F^2$$

Appendix F3 Variance of Apparent Age

The estimated error in the apparent age, Δt_u, may be obtained by differentiating equation (2.19) to obtain

$$\Delta t_u = \frac{1}{\lambda} \left(\frac{J^2 \Delta F^2 + F^2 \Delta J^2}{(1 + FJ)^2} \right)^{1/2}$$

where ΔJ is the estimated error in the flux monitor and F is the estimated error in the ratio $^{40}Ar^*/^{39}Ar^{NK}$. If the standard deviations $\sigma_J \simeq \frac{\Delta J}{J}$, $\sigma_{t_u} \simeq \frac{\Delta t_u}{t_u}$ and $_F = \frac{\Delta F}{F}$ are substituted in the above expression, then the variance in the apparent age, σ_{t_s}, may be approximated by the following expression:

$$\sigma_{t_u}^2 = \frac{F^2 J^2}{\lambda^2 t_u^2} \frac{(\sigma_F^2 + \sigma_J^2)}{(1 + FJ)^2}$$

N

0 90 km

SVARTENHUK

NUGSSUAQ

DISCO

72°

71°

70°

69°

55°

53°

51°

589

Svartenhavn

625

630

Arfertuarssuk

638

598

Tasiussap imâ

999

0 20Km

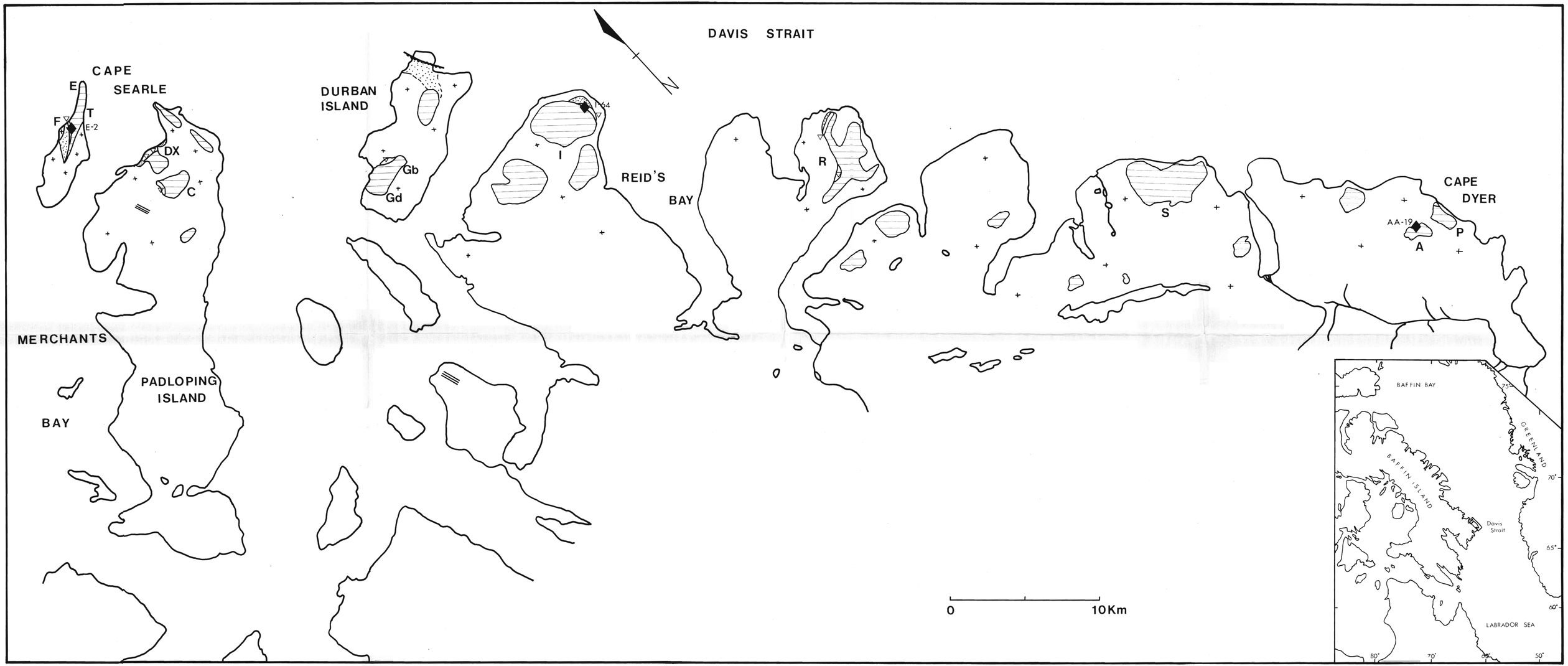
DAVIS STRAIT
N
CAPE SEARLE
E
T
F
E-2
DX
C
DURBAN ISLAND
Gb
Gd
I-64
I
REID'S BAY
R
S
CAPE DYER
AA-19
A
P
MERCHANTS BAY
PADLOPING ISLAND
0
10Km
BAFFIN BAY
GREENLAND
BAFFIN ISLAND
Davis Strait
LABRADOR SEA
75°
70°
65°
60°
80°
70°
60°
50°